

**THIN HORIZONTAL LAYERING AS A
STRATIGRAPHIC FILTER IN ABSORPTION
ESTIMATION AND SEISMIC DECONVOLUTION**

**ARTHUR LAKES LIBRARY
COLORADO SCHOOL OF MINES
GOLDEN, CO 80401**

by

Albena Alexandrova Mateeva

ProQuest Number: 10797007

All rights reserved

INFORMATION TO ALL USERS

The quality of this reproduction is dependent upon the quality of the copy submitted.

In the unlikely event that the author did not send a complete manuscript and there are missing pages, these will be noted. Also, if material had to be removed, a note will indicate the deletion.



ProQuest 10797007

Published by ProQuest LLC (2019). Copyright of the Dissertation is held by the Author.

All rights reserved.

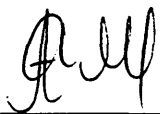
This work is protected against unauthorized copying under Title 17, United States Code
Microform Edition © ProQuest LLC.

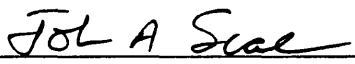
ProQuest LLC.
789 East Eisenhower Parkway
P.O. Box 1346
Ann Arbor, MI 48106 – 1346

A thesis submitted to the Faculty and the Board of Trustees of the Colorado School of Mines in partial fulfillment of the requirements for the degree of Doctor of Philosophy (Geophysics).

Golden, Colorado

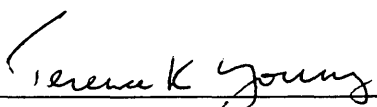
Date 16 June, 2003

Signed: 
Albena Alexandrova Mateeva

Approved: 
Dr. John A. Scales
Professor of Geophysics
Thesis Advisor

Golden, Colorado

Date June 16, 2003


Dr. Terence K. Young
Professor and Head,
Department of Geophysics

ABSTRACT

It has long been recognized that transmission through fine layering is accompanied by apparent attenuation (loss of high frequencies and dispersion) caused by short-period multiples. Thus, attenuation measurements from transmission experiments typically overestimate the intrinsic absorption. However, in exploration seismology, one conducts reflection rather than transmission experiments (even a VSP has a reflection component). That is why, contrary to popular belief, thin layering may cause an underestimate rather than an overestimate of the intrinsic absorption. The true consequences of ignoring small-scale heterogeneities depend both on the acquisition geometry and on the procedure for absorption estimation. In Chapter 2, I consider surface seismic data and show that spectral ratios do not exhibit apparent attenuation in a homogeneously absorbing stationary layered medium. I demonstrate the importance of including the earth's surface in apparent attenuation studies.

Absorption estimation from surface seismic data is very desirable but far from routine yet. Instead, absorption information is usually extracted from Vertical Seismic Profiles (VSP). The influence of thin horizontal layering on VSP spectral ratios is studied in Chapter 3. I show that the largest distortions occur when a strong reflection coefficient series (reflectivity) is overlain or underlain by a weak reflectivity. In such cases, scattering can either cause a high-frequency loss larger than anelasticity, or on the contrary, it can over-compensate the anelastic loss and lead to a spectral ratio with a positive slope (negative effective Q). Scattering introduces the largest but not the only error in absorption measurements. One must know the total uncertainty of absorption data in order to infer reservoir conditions such as saturation and

permeability from them. In Chapter 4, I propose ways of quantifying the absorption errors introduced by different factors. I illustrate the process through a field data example.

Aside from absorption estimation, the presence of thin layering is important in signal processing. Scattering degrades the resolution of seismic data (Chapter 5). In Chapter 6, I show that short-period multiples can be included in the convolutional model of the seismic trace through the operator R_m/R where R_m is the spectrum of the elastic impulse response, and R is that of the reflectivity. When multiples are weak, or even moderately strong, intrinsic and apparent attenuation can be combined into a single effective attenuation operator for the purposes of wavelet estimation and deconvolution. This cannot be done when multiples are strong because R_m/R becomes non-minimum phase. A deconvolution operator derived under the assumption that the stratigraphic filter is minimum phase would underestimate the time delay of the wavelet in a medium with a strong reflectivity.

TABLE OF CONTENTS

ABSTRACT	iii
LIST OF FIGURES	ix
LIST OF TABLES	xviii
ACKNOWLEDGMENTS	xix
Chapter 1 GENERAL INTRODUCTION	1
Chapter 2 SPECTRAL FOOTPRINT OF THIN HORIZONTAL LAYERING IN SURFACE SEISMIC DATA	7
2.1 Introduction	7
2.2 Earth model	9
2.3 Plane waves at normal incidence	10
2.4 Point source, offset receivers	17
2.5 Discussion	19
2.6 Conclusions	20
Chapter 3 DISTORTIONS IN VSP SPECTRAL RATIOS CAUSED BY THIN HORIZONTAL LAYERING	23
3.1 Introduction	23
3.2 Earth reflectivity	24

3.3	Receiver in a layered half-space	25
3.4	Influence of the free surface	28
3.5	End-member examples	29
3.5.1	Strong stationary reflectivity	30
3.5.2	Strong above weak reflectivity	37
3.5.3	Weak above strong reflectivity	44
3.6	Conclusions	45
Chapter 4 UNCERTAINTIES IN ABSORPTION ESTIMATES		47
4.1	Introduction	47
4.2	Data	48
4.3	Model parametrization	49
4.4	Method of estimating Q	49
4.5	Preparations for spectral ratio estimation	52
4.5.1	Choice of receiver pairs	52
4.5.2	Choice of frequency band	55
4.6	Errors	56
4.6.1	Error due to finite time windowing	56
4.6.2	Ambient noise	59
4.6.3	Window positioning and travelttime uncertainties	61
4.6.4	Receiver positioning errors in the synthetic seismograms	61
4.6.5	Fitting uncertainties (local interference)	63
4.7	Estimating attenuation	64
4.7.1	Effective attenuation from VSP data	65
4.7.2	Scattering effects	66

4.7.3	Intrinsic attenuation (absorption)	70
4.7.4	Mean intrinsic Q profile	72
4.8	Discussion	75
4.9	Conclusion	79
Chapter 5 SEISMOGRAMS AND REFLECTIVITY – CAN		
	WE SEE THE SUBSURFACE? (SHORT NOTE)	80
5.1	Introduction	80
5.2	Multiples take over	81
5.3	Correlation between traces and reflectivity	82
5.4	Conclusions	87
Chapter 6 APPARENT AND INTRINSIC ATTENUATION		
	IN THE SEISMIC WAVELET MODEL	89
6.1	Introduction	89
6.2	Convolutional models for the seismic trace	90
6.3	The operator R_m/R	92
6.3.1	Earth model without a free surface	92
6.3.2	Earth model with a free surface	94
6.4	Strong-reflectivity example	95
6.4.1	Synthetic data	95
6.4.2	Spectral properties test	97
6.5	Modeling the phase of the apparent attenuation operator using bore- hole data	100
6.6	Discussion	101
6.7	Conclusion	105

Chapter 7	CONCLUSION	106
	REFERENCES	109
APPENDIX A	WEAK-REFLECTIVITY REFLECTION AND TRANSMISSION RESPONSES	121
APPENDIX B	FROM PLANE WAVES AT NORMAL INCIDENCE TO POINT SOURCE AND OFFSET RECEIVERS	127
APPENDIX C	POWER SPECTRUM OF THE ELASTIC STRATIGRAPHIC FILTER	130
APPENDIX D	GENERATING SYNTHETIC REFLECTIVITIES	132
APPENDIX E	CODES FOR 1-D SEISMOGRAMS GENERATION – <i>sugoupillaud, sugoupillaudpo</i>	135
APPENDIX F	REFLECTIVITY LOG FOR MODELING THE SCATTERING EFFECTS	138
APPENDIX G	COVARIANCE OF SLOPE ESTIMATES FROM PAIRS WITH A COMMON RECEIVER	140

LIST OF FIGURES

1.1	Transmission impulse response of a horizontally layered medium. The direct arrival is quickly weakened by transmission losses at interfaces. Its energy is transferred to short period multiples. When interface reflection coefficients alternate their sign, multiples have the polarity of the direct arrival; thus, they reinforce it through constructive interference at low frequencies [after O'Doherty & Anstey (1971)].	5
2.1	Reflectivity (a) and synthetic seismograms for plane waves at normal incidence (b,c) in a horizontally layered medium. The source (a down-going unit spike) and the receivers are just below the earth surface, which is modeled either as a free surface (b) or as an absorbing surface (c). The seismograms are for a vector-type field, e.g., vertical component of velocity.	11
2.2	Spectral change with time of (a) reflection coefficient series (stationary by construction); (b) impulse response with $r_0 = -1$; (c) impulse response with $r_0 = 0$. Each time series has been divided into 256 ms-long adjacent segments (128 samples per segment). Shown are the spectra of the first eight segments of each series.	14

2.3	Energy at three depths: surface receiver (Figure 2.1b,c), and receivers at 250 ms and 500 ms one-way traveltime (250 and 500 layers in a Goupillaud model) below the surface; the synthetics are for plane waves at normal incidence; the energy measurements are over the 0.5-3.0 s interval, i.e., at times after the ballistic arrival at the deepest receiver. (a) $r_0 = -1$; (b) $r_0 = 0$	21
3.1	Signal in a buried receiver: transmitted train (p_0) and its primary reflections from below (p_0R); multiples of the reflections from below are ignored.	25
3.2	VSP in a non-stationary reflectivity: (a) strong above weak reflectivity; (b) weak above strong reflectivity. Thick arrows indicate arrivals that contribute significantly to the signal coloring; thin arrows represent weak contributions or weak filtering.	26
3.3	Power spectrum of the synthetic reflection coefficient series: Reflectivity 1 is strong and blue; Reflectivity 2 is weak and almost white.	29
3.4	VSP elastic impulse response in a strong stationary reflectivity (Reflectivity 1): (a) with surface-related multiples (as are traces recorded in practice); (b) without surface-related multiples (shown for comparison). The receivers are 200 ms apart (200 layers apart in the Goupillaud model – Appendix E), the first being at 100 ms (100 layers) below the earth surface.	31
3.5	Zoom from Fig. 3.4a: The transmitted train disperses and loses high frequencies with depth.	32

3.6	Power spectra at three receiver depths with and without surface-related multiples: (a) At early times, surface-related multiples have negligible influence on trace spectra, except at high frequencies, which are rarely used in absorption estimation. (b) At late times, surface-related multiples make spectra of down-hole traces steeper, amplifying the loss of high frequencies with depth.	34
3.7	Spectral ratio between Receiver 3 and Receiver 1 (400 ms apart): (a) at early times; (b) at late times. Note that the slope of the solid lines is essentially same in (a) and (b).	35
3.8	Slope of the spectral ratio between Receiver 3 and a number of shallower receivers, normalized by the one-way traveltime between the receivers in a strong stationary reflectivity. The time window for spectral estimation is 256 samples long. The spectra on all traces were smoothed by a 20%-of-series-length median filter before computing the spectral ratios. The error bars represent the uncertainty of each slope estimate (least-squares fit). The data are compatible with a constant apparent attenuation (thick gray line – computed by weighted least-squares).	37
3.9	VSP elastic impulse response with surface-related multiples in (a) strong-above-weak reflectivity; (b) weak-above-strong reflectivity. The receiver placement and numeration is as in Fig. 3.2. The receiver depths are the same as in the stationary case – 100 ms and 500 ms below the earth surface, respectively.	39

3.10	Elastic spectra at early times (Window 1: 200 samples after the first arrival) in (a) strong-above-weak reflectivity; (b) weak-above-strong reflectivity.	40
3.11	Spectral ratio in (a) strong-above-weak reflectivity; (b) weak-above-strong reflectivity.	41
3.12	Analogous to Fig. 3.8 but for the strong-above-weak reflectivity case. The thick gray line is the best weighted-least-squares fit and actually consists of two independently estimated segments – one for large receiver separation such that the time-window on the shallow trace does not sense the weak reflectivity below the deeper receiver, and another for smaller separation. The two segments give virtually identical estimates for the trend in the apparent attenuation. The thin dashed line indicates the slope produced by intrinsic absorption in a medium with $Q_{int} = 50$	42
3.13	Analogous to Fig. 3.8 but for the weak-above-strong reflectivity case. The thin dashed line indicates the absolute value of the slope produced by intrinsic absorption in a medium with $Q_{int} = 50$	43
4.1	Well-logs used to identify the main subsurface intervals, the mean quality factors $Q_1 - Q_4$ of which are to be determined. Shown on the left is the span of the VSP; dots represent the first seven VSP receivers (with large non-uniform spacing; the rest of the receivers are close and uniformly spaced). The existence of a sandstone layer in the near surface is known <i>a priori</i> – its base with a reflection coefficient r is drawn approximately.	50

4.2	Cartoon: (a) Pairing the receivers in Layer i . Pairs containing the bottom-most receiver will be presented by a light color throughout the paper. Pairs containing the top-most receiver will be presented by a dark color. The distinction is made because the two sets sample different parts of the layer. (b) Indication for significant and systematic absorption variations in Layer i : small-separation pairs that sample predominantly the top or bottom halves of the layer (e.g., 3 and 4) give different estimates of the intrinsic attenuation, while pairs that span most of the layer (e.g., pairs 1, 2 and 6) show similar values for the intrinsic attenuation.	53
4.3	Power spectra of signal (source function filtered through receiver and instrumentation, and scaled to the peak amplitude of a typical VSP trace) and ambient noise.	55
4.4	Tapering effects in the absence of noise: (a) slope bias measured over the 15-85 Hz band for three window lengths; the data for the 64-sample window are fit by a linear regression. (b) variability of the bias estimate for a 64-point taper – measured (circles) and fit (solid line) by a quadratic function of the measured slope magnitude.	59
4.5	Analogous to Fig. 4.4 but in the presence of ambient noise: (a) bias for three window lengths; the data for 64-sample taper are fit by a quadratic model. (b) variability of the bias estimate for a 64-point taper – measured (circles) and fit (solid line) quadratic model.	60
4.6	Linear fit in the presence of scattering – the estimated spectral slope depends on the frequency band used.	65

4.7	Attenuation estimators: (left) S_{eff} measured from VSP data, (center) S_{sc} measured from synthetic traces in a horizontally layered non-absorbing medium, (right) computed intrinsic attenuation: $S = S_{\text{eff}} - S_{\text{sc}}$. Dark and light data points correspond to receiver pairs that contain, respectively, the top and bottom receiver in a layer. All plots are on the same scale.	67
4.8	Reflectivity log used to predict scattering effects. Its construction is described in Appendix F. Shown on the right is the length of the taper used for first-arrival windowing.	68
4.9	Scattering attenuation estimates in Layer 2 – local fit (left) versus global fit (right). The behavior of the global fit is in an excellent agreement with the theoretical predictions in Chapter 3. The local fit is quite erratic.	69
4.10	Subdivision of Layer 3 (plots analogous to those in Fig. 4.7).	71
4.11	Attenuation estimates in Layer 4 from the top 10 receivers in it, which do not feel the padding of the reflection coefficient log below the borehole bottom; (plots analogous to those in Fig. 4.7).	72
4.12	Mean intrinsic Q profile. The background shades visualize the layers, characterized by the mean Q. Circles indicate estimates derived from all available pairs. Crosses indicate conditional estimates, obtained by excluding outliers.	74

5.1	Share of primaries and multiples on the trace, computed as (from top to bottom of legend): $\text{std}(y)/\text{std}(x)$, $\text{std}(x_0 - y)/\text{std}(x)$, $\text{std}(x - x_0)/\text{std}(x)$, $\text{std}(x - y)/\text{std}(x)$. The sum of shares may exceed 100% because it does not take into account interference. (a) weak-reflectivity example; (b) strong-reflectivity example.	83
5.2	Zero-lag correlation between synthetic seismograms (x, x_0, y) and reflectivity (r) . Each data point is for a time window centered at that time, with length (a) 200 samples for the weak reflectivity, (b) 50 samples for the strong reflectivity.	84
5.3	Zero-lag correlation between narrow band-pass filtered traces and reflectivity. The three curves are for time windows centered at 100, 300, and 500 ms, respectively. The picture is virtually the same in weak reflectivity for four-times later windows (0.4, 1.2, 2 s). In the absence of surface-related multiples, the trends are similar but the correlation is a bit higher at early times.	85
5.4	The decay in the correlation between trace and reflectivity (solid black line) is slower when: only low-frequencies are considered (dashed gray line), their lower effective velocity is taken into account (solid gray line), and free-surface multiples are removed (dotted black line). . . .	86
6.1	The reflection impulse response R_m of a layered half-space without a free surface: a weak-reflectivity approximation ignoring raypaths trapped in the shallow subsurface.	93

6.2	Power spectrum of the synthetic reflection coefficient series (average estimate over 100 realizations).	96
6.3	Power spectrum of R_m/R with (solid) and without (dashed) surface-related multiples.	97
6.4	Phase spectrum of R_m/R with (solid) and without (dashed) surface-related multiples (reflection coefficient of the earth's surface, r_0 , set to -1 and 0 , respectively).	98
6.5	Phase spectrum of $(R_m/R)_0$ (solid) and minimum-phase spectrum (dashed) computed from $ R_m/R _0$	99
6.6	Phase spectrum of $(R_m/R)_1$ (solid) and minimum-phase spectrum (dashed) computed from $ R_m/R _1$	101
6.7	Phase spectrum of $(R_m/R)_1$ (solid) and minimum-phase spectrum (dashed) computed from $ R_m/R _0$	102
6.8	Typical phase properties of R_m/R as a function of reflectivity standard deviation: (solid) minimum-phase property in the presence of surface-related multiples; (dash-dot) minimum-phase property in the absence of surface-related multiples; (thick dash) modeling the phase of $(R_m/R)_1$ by the minimum-phase equivalent of $ R_m/R _0$; (thin dash) influence of surface related multiples on the phase of R_m/R . All phase-error estimates are median over the low one-third of the spectrum ($f < \text{Nyquist}/3$), for a time window of 0.5 s centered at 0.5 s.	104

6.9	Minimum-phase property of $(R_m/R)_1$ in time windows centered at approximately 0.5 s (solid line; identical to that in Figure 6.8) and 1 s (dashed).	105
A.1	Transmission through a stack of layers	122
A.2	Two-way transmission through a stack of layers: raypaths trapped in the shallow subsurface (dash-line) are ignored.	122
A.3	Signal in a buried receiver shortly after the first arrival: direct arrival and primary reflections from below; multiples of the reflections from below (dash-line) are ignored, as well as changes in the downgoing pulse over the considered short time interval.	123
A.4	Signal in a surface receiver (earth surface omitted)	125
A.5	Signal in a surface receiver (earth surface accounted for)	126

LIST OF TABLES

2.1	Synthetic reflectivity used throughout the examples – similar to that of Well 8 from the papers of Walden and Hosken (1985, 1986). It is modeled as an ARMA(1,1) process with autoregressive parameter θ and moving average parameter ϕ ; the amplitudes of the reflection coefficients are drawn from a Laplace distribution with a scale parameter λ (Appendix D).	10
3.1	The two synthetic reflectivities used throughout the examples are modeled as ARMA(1,1) processes with autoregressive parameter θ and moving average parameter ϕ . The amplitudes of the reflection coefficients are drawn from a mixture of two Laplace distributions with a mixing proportion parameter p and scale parameters λ_1 and λ_2 , respectively (Appendix D).	30
3.2	Effective versus intrinsic Q for end-member reflectivity examples. Shown are estimates of Q_{eff} from receiver pairs with large and small separation (e.g., $dz = 500$ m and $dz = 50$ m in a medium with velocity 2500 m/s).	45
4.1	Scattering versus intrinsic attenuation – a median estimate over all receiver pairs in a given layer.	78

ACKNOWLEDGMENTS

The field data used in this thesis were kindly provided by WesternGeco. I picked up the apparent attenuation topic during a summer job with WesternGeco in 2000. In a fortunate turn of events, that same year, my advisor Dr. John Scales came back from a sabbatical in France with some exciting new ideas about scattering. Our inversion team swiftly transformed into a scattering team. I learned a lot and had great fun at our formal and informal seminars. My very special thanks to my fellow-scatterheads Kasper van Wijk, Matt Haney, Alex Grêt, and Alison Malcolm for their friendship and moral support. I am deeply grateful to Dr. John Scales for his trust in me. Also, I sincerely thank Dr. Roel Snieder for his guidance at difficult times, Dr. Alex Kaufman for his frank advice and letting me practice \LaTeX on his book, Dr. Luis Tenorio for being so patient with all my questions, Dr. Ken Lerner for his help and encouragement, Dr. Ilya Tsvankin for inviting me as a teaching assistant to the Introductory Seismology class, which I greatly enjoyed. I am infinitely grateful to all my teachers. Also, I feel very fortunate to have had wonderful fellow-students at CWP. My special thanks go to my friends and colleagues Jérôme Le Rousseau and Petr Jílek for always been there and showing the way. I am in debt to Jo Ann Fink, Barbara McLenon, Michelle Szobody, Lela Webber, and Sara Summers whose care, kindness, and help throughout the years went much beyond their job. Finally, I would like to thank my family for almost writing my dissertation by cheering my every step.

To my family

Chapter 1

GENERAL INTRODUCTION

During propagation, seismic signals lose energy to anelastic processes such as fluid motion, friction, and eventually, heat. This irreversible loss is called intrinsic attenuation, or, absorption. The amplitude decay caused by absorption can be modeled by an exponential function of frequency and time, i.e.,

$$A = A_0 e^{-\frac{\omega t}{2Q}} \quad (1.1)$$

The quality factor Q is generally frequency-dependent. However, over the limited frequency band of exploration seismology, it can be well approximated by a frequency-independent constant (e.g., Kjartansson, 1979; Raikes & White, 1984). Finding this constant is of significant interest to seismic exploration for three main reasons. First, it carries information about lithology and reservoir conditions such as saturation, permeability, porosity, and pore pressure (e.g., Mavko *et al.*, 1979; Winkler & Nur, 1979; Mavko & Nur, 1979; Klimentos & McCann, 1990; Batzle *et al.*, 1996). Second, if we knew the absorption properties of the subsurface, we could include them in seismic data processing (deconvolution, stacking, migration, inverse Q filtering, etc.) and get much sharper images of the subsurface (Widmaier *et al.*, 1994; Sollie *et al.*, 1994; Sollie & Mittet, 1994; Pramanik *et al.*, 2000). Third, amplitude-versus-offset (AVO) and anisotropy analysis need to be corrected for absorption which has

an offset-dependent signature and may cause a non-hyperbolic moveout (Swan, 1991; Hampson, 1991; Luh, 1993; Haase, 2000, 2001). All of these applications require absorption estimates at seismic frequencies. Laboratory measurements of Q are typically done at much higher frequencies. A notable exception is the method of Batzle *et al.* (1996) in which rock samples are subjected to a low-frequency deformation and their quality factor is estimated from the phase shift between the applied stress and the resulting strain. Measurements of Q from field seismic data have a long history but are still quite crude. One of the main difficulties is to distinguish absorption from other frequency-dependent phenomena, and particularly, scattering from small-scale heterogeneities. Since the usual targets of seismic exploration are in sedimentary basins, thin horizontal layering is the simplest and most important cause of scattering. *Thin* layering here means smaller but comparable to a seismic wavelength; i.e., with a thickness on the order of 10 m, or a time-thickness on the order of the sampling interval in seismic data. Much thinner layers would give rise to anisotropy but not to frequency-dependent amplitude behavior (Folstad & Schoenberg, 1992) because they look the same – infinitely thin – to all seismic frequencies. Much thicker layers do not filter the seismic wavelet; they only scale it through geometrical spreading and reflection/transmission at their boundaries.

The filtering action of the thin horizontal layering defined above is the focus of this thesis. The filtering is governed by the statistical properties of the reflection coefficient series describing the thin layering (I call it “reflectivity” series for short). If the earth’s reflectivity was white (as often assumed for convenience in deconvolution), its impulse response would be frequency-independent and would not interfere with absorption estimation. However, well-log studies have established that the earth reflectivity is “blue”, i.e., its amplitude spectrum increases with frequency over the

seismic frequency band (Walden & Hosken, 1985; Saggaf & Robinson, 2000). In the time domain, that corresponds to consecutive reflection coefficients tending to have the opposite sign¹, i.e., one can think of the earth as built of thinly interlaced lithologies with alternating high and low impedances. If the impedance contrasts are large, the reflection coefficient series can be very energetic, giving rise to strong short-period multiples. The importance of these multiples to the seismic wavelet was first demonstrated by O’Doherty & Anstey (1971). They noticed that a seismic signal usually decays much more slowly than it should if it was losing a $(1 - r^2)$ fraction of its energy at every interface with a reflection coefficient r , even if $r \ll 1$. They reasoned that short-period multiples must reinforce the signal through constructive interference at low frequencies (Fig. 1.1). When consecutive reflection coefficients tend to have the opposite sign, multiples tend to have the same polarity as the incident pulse. Thus, they interfere constructively with the direct arrival at wave periods that are large compared to the multiples delay, i.e., at low frequencies. O’Doherty & Anstey (1971) provided a formula connecting the power spectrum of the reflection coefficient series $|R(f)|^2$ to the amplitude spectrum of the normal-incidence transmission impulse response $T(f)$,

$$T(f) = e^{-|R(f)|^2 \Delta t}, \quad (1.2)$$

where Δt is the one-way time thickness of the stack of layers in dimensionless units (i.e., normalized by the one-way time thickness of an individual layer). This formula is a weak-reflectivity approximation for a small time window after the first arrival. It

¹After removing the mean of the reflectivity series. This mean describes the impedance trend with depth. It does not alter the frequency content of the wavelet, only scales it through geometrical spreading (e.g., Asch *et al.*, 1991).

has become quite famous and has been re-derived and generalized a number of times (e.g., Banik *et al.*, 1985; Resnick *et al.*, 1986; Görich & Müller, 1987; Burridge *et al.*, 1988; Papanicolaou & Lewicki, 1994; Shapiro & Zien, 1993; Shapiro & Hubral, 1996; Haney *et al.*, 2003). Besides frequency content changes, the progressive transfer of energy to higher order multiples causes dispersion – low frequencies are slower than high frequencies (e.g., Shapiro *et al.*, 1994a,b). Thus, the signal transmitted through a stack of thin layers is dispersive and high-frequency deficient; it is minimum-phase, too (Sherwood & Trorey, 1965; Robinson & Treitel, 1977, 1978; Banik *et al.*, 1985). In this sense, it is similar to the signal transmitted through a homogeneous but absorbing slab. That is how the famous statement that “multiples cause apparent attenuation” originated. As simple and basic as it is, it seems to cause confusion in the context of seismic exploration. The problem is that, in exploration, we do not have a transmission experiment through a finite scattering region; instead, we have a reflection experiment conducted over a layered half-space bounded by a free surface. The first implication is that we do not record isolated transmission signals. Thus, unlike in earthquake seismology, we cannot rely on coda waves to separate intrinsic from scattering attenuation (Aki & Chouet, 1975; Roecker *et al.*, 1982; Richards & Menke, 1983; Sato, 1984; Frankel & Wennerberg, 1987; Wu & Aki, 1988; Bianco *et al.*, 1999). The second implication is that scattering does not necessarily cause “attenuation” (high-frequency loss). The high frequencies it removes from the transmitted signal, are not lost, only redirected in space. They boost the high-frequency content of surface seismic data. The bottom line is, scattering and absorption are physically different, and their action on the seismic trace is not identical. Detailed understanding of the elastic stratigraphic filter may give us clues to separating intrinsic from scattering attenuation, as well as help in the design of efficient signal

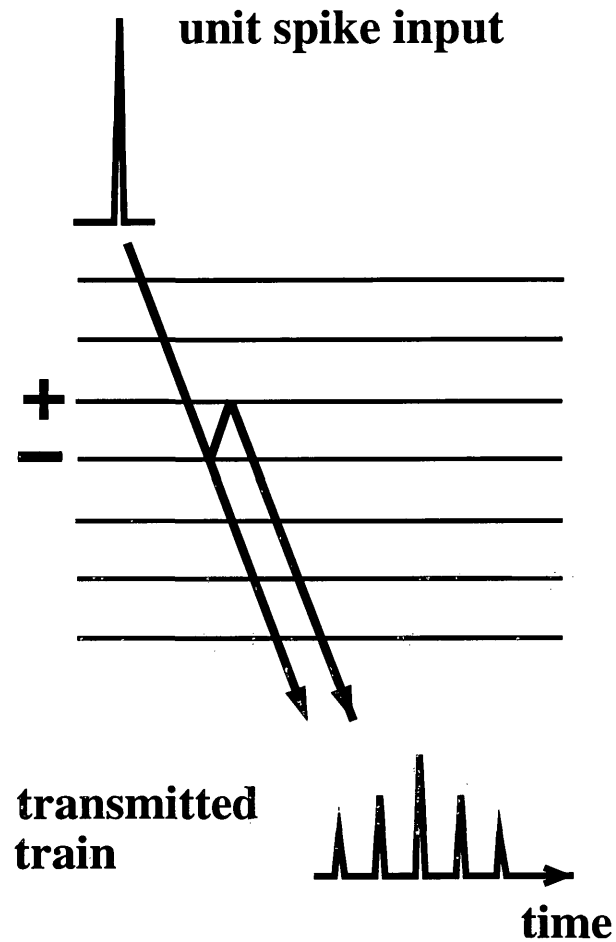


Figure 1.1. Transmission impulse response of a horizontally layered medium. The direct arrival is quickly weakened by transmission losses at interfaces. Its energy is transferred to short period multiples. When interface reflection coefficients alternate their sign, multiples have the polarity of the direct arrival; thus, they reinforce it through constructive interference at low frequencies [after O'Doherty & Anstey (1971)].

processing tools. That is why, it is the main objective of this thesis.

The thesis consists of five individual papers. The first three concern absorption estimation, while the last two are related to signal processing. More specifically, Chapters 1 and 2 study the bias that can be introduced by ignored scattering in absorption measurements from surface seismic and VSP data, respectively. Chapter 3 quantifies the total uncertainty caused by scattering and other factors in absorption estimates from VSP data. It is based on a real data example. Chapter 4 shows how short-period multiples destroy the correlation between the reflection coefficient series of the subsurface and seismograms. It demonstrates the need for adequate compensation of the filtering action of small-scale heterogeneities. An operator accounting for short-period multiples in the convolutional model of the seismic trace is derived in Chapter 5. Its properties are compared with those of intrinsic absorption to determine whether the two can be combined into a single effective attenuation operator for the purposes of wavelet estimation and deconvolution. This last paper is co-authored by Douglas Hart (Regis University) and Scott MacKay (WesternGeco). Since each paper is self-contained, some basic explanations and earth model descriptions may be repeated. All paper appendices have been put at the end of the thesis. They are arranged in a logical sequence that occasionally deviates from the order of citation in the main text.

Chapter 2

SPECTRAL FOOTPRINT OF THIN HORIZONTAL LAYERING IN SURFACE SEISMIC DATA

2.1 Introduction

Thirty years ago O'Doherty & Anstey suggested that short-period multiples can cause apparent attenuation (dispersion and loss of high-frequencies) in signals transmitted through a “cyclic” layered sequence. Since then, their famous formula connecting the amplitude spectrum of the transmitted signal to that of the reflection coefficient series has been re-derived and generalized a number of times (e.g., Banik *et al.*, 1985; Burridge *et al.*, 1988; Papanicolaou & Lewicki, 1994; Görich & Müller, 1987; Resnick *et al.*, 1986; Shapiro & Zien, 1993; Shapiro & Hubral, 1996; Haney *et al.*, 2003). A major implication of O'Doherty & Anstey's idea is that the effective attenuation measured from transmission-type experiments, such as VSP and cross-hole seismic, is typically an over-estimate of the intrinsic attenuation (absorption). However, one must remember that this is a purely transmissional effect. The high frequencies that have been removed from the transmitted signal by fine layering, are not lost, only redirected in space (reflected). That is why, in a reflection experiment (surface seismic data), the notion of “apparent attenuation” may be confusing. One of the first studies of apparent attenuation in the context of reflection seismology was that of Schoenberger & Levin (1974) who compared spectra of synthetic seismograms with and without internal multiples and showed that the presence of multiples causes

apparent loss of high frequencies. This is a new twist to the apparent attenuation definition – it compares the primaries-only seismogram to a seismogram with multiples rather than input to output signal (e.g., seismic source to reflections). Schoenberger & Levin’s finding has a direct bearing to wavelet modeling and deconvolution (Chapter 6, Appendix C) but does not imply that the effective attenuation measured from surface seismic data will be larger than the true absorption. The goal of this paper is to clarify the influence of thin layering on absorption estimates from surface seismic data. Contrary to popular belief, scattering may cause an underestimate rather than an overestimate of the intrinsic attenuation. Better understanding of the trace spectrum is urgently needed, given the increased interest in measuring Q from surface seismic data in pursuit of spatial coverage. Such measurements are far from routine yet. Most commercial procedures track spectral changes along stacked traces, and thus cannot give a valid absorption estimate, only an attenuation-related attribute (e.g., Dasgupta & Clark, 1998). A few techniques for measuring absorption from prestack gathers have been proposed in recent years. Zhang & Ulrych (2002) determined Q from the shift of the peak frequency of the signal with offset and time. Hicks & Pratt (2001) obtained Q through a full-waveform inversion for the complex-velocity structure of the subsurface. Dasgupta & Clark (1998) devised a simple spectral-ratio-like technique, extrapolating attenuation measurements at far offsets to zero-offset. None of these studies attempted to separate the intrinsic attenuation (absorption), which carries information about lithology and reservoir conditions, from thin-layering (scattering) effects. In a follow-up of Dasgupta & Clark (1998), Clark *et al.* (2001) showed that effective attenuation measurements can give useful estimates of absorption changes in comparative circumstances, e.g. time-lapse. They also mentioned the possibility of using well-logs to account for scattering, but that was a marginal point

in their study and the details remained unclear.

The present study of the spectral coloring introduced in surface seismic data by thin layering aims at providing basic understanding. I show some simple synthetic examples and relate them to the analytical results of White *et al.* (1990) and Asch *et al.* (1991) for the spectrum of the reflection impulse response of a layered medium. This analysis is most relevant to absorption isolation in studies similar to Dasgupta & Clark (1998) that measure the frequency content of traces at different times and offsets. I first consider plane waves at normal incidence, and then, a point source and offset receivers.

2.2 Earth model

Suppose a medium is finely layered but homogeneous on the macro-scale, i.e., its absorption properties and the statistics of the reflection coefficient series do not change with depth. In such a homogeneously absorbing medium, anelasticity and scattering contribute cumulatively to the effective attenuation, because arrivals with equal traveltimes have suffered the same amount of absorption regardless of their trajectory. Therefore, to understand how the effective attenuation would differ from the intrinsic attenuation, it is sufficient to compute the impulse response of the non-absorbing layered earth. For that purpose, the earth model can be defined by a series of reflection coefficients (“reflectivity” for short), sampled at the rate of seismic data¹. It is well known that earth reflectivity is “blue”, i.e., its power spectrum increases with frequency over the seismic frequency band (Walden & Hosken, 1985; Saggaf & Robinson, 2000). In the time domain this corresponds to a negative correlation between

¹Such sampling is acceptable because finer layering would cause anisotropy but not apparent attenuation (Folstad & Schoenberg, 1992).

θ	ϕ	mean	std	λ
0.9	0.3	-0.0002	0.11	0.09

Table 2.1. Synthetic reflectivity used throughout the examples – similar to that of Well 8 from the papers of Walden and Hosken (1985, 1986). It is modeled as an ARMA(1,1) process with autoregressive parameter θ and moving average parameter ϕ ; the amplitudes of the reflection coefficients are drawn from a Laplace distribution with a scale parameter λ (Appendix D).

close samples; i.e., consecutive reflection coefficients tend to have the opposite sign, for example, due to finely interlaced lithologies. If those lithologies have contrasting impedances, the reflection coefficient series contains many large reflection coefficients and gives rise to significant apparent attenuation during transmission. Such strong, blue reflectivities are of primary interest to our study.

Besides a realistic subsurface, the reflectivity model should include the earth surface. It is often omitted in apparent attenuation studies but, as we will see, it makes a big difference to the trace spectrum. Not modeling the earth surface is equivalent to assuming that all surface-related multiples have been fully suppressed, which is hardly achievable, especially in land data acquired over a finely layered medium. Partial multiple suppression would only introduce unknown spectral distortions. That is why it is important to understand the spectral behavior of the trace with and without surface-related multiples (i.e., surface reflection coefficient r_0 equal to -1 and 0, respectively).

2.3 Plane waves at normal incidence

A reflection coefficient series that would produce large apparent attenuation is shown in Figure 2.1a. It is synthetic but realistic, similar to that of Well 8 from

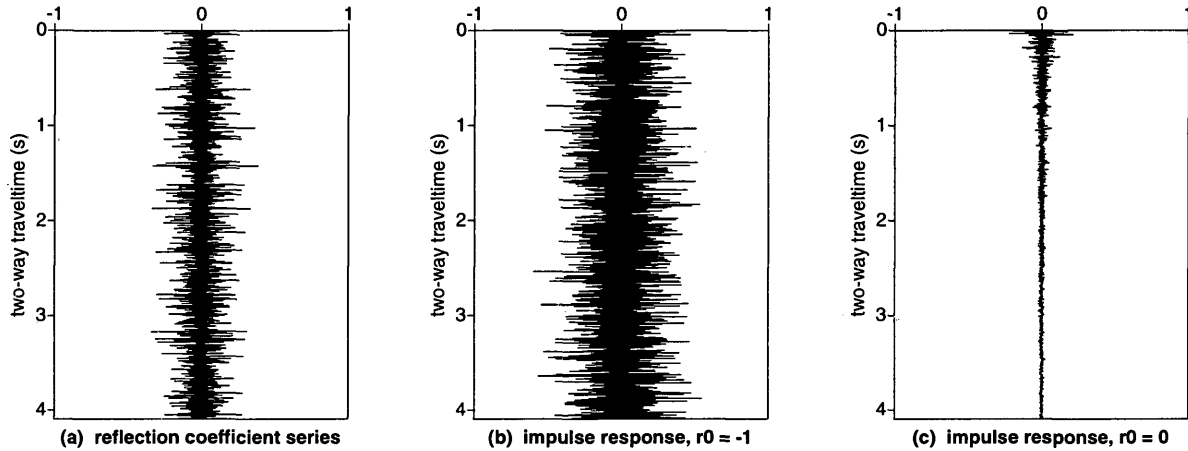


Figure 2.1. Reflectivity (a) and synthetic seismograms for plane waves at normal incidence (b,c) in a horizontally layered medium. The source (a downgoing unit spike) and the receivers are just below the earth surface, which is modeled either as a free surface (b) or as an absorbing surface (c). The seismograms are for a vector-type field, e.g., vertical component of velocity.

the papers of Walden and Hosken (1985; 1986). Its statistical properties are given in Table 2.1. Figures 2.1b, 2.1c show its normal-incidence reflection impulse response with and without a free surface, respectively. Surface-related multiples make a striking contribution – not only is the energy level with $r_0 = -1$ much higher than that with $r_0 = 0$, but the energy decay with time is very different, too. It is quite fast for $r_0 = 0$ and virtually absent for the model with a free surface. This means that the bulk of energy, especially at late times, comes from different parts of the medium, namely, from some depth for $r_0 = 0$, and from the near-surface (via surface-related multiples) for $r_0 = -1$. The significance of this to absorption estimation will be discussed further.

To explore spectral changes with time, I divided each trace into time segments, 256 ms (128 samples) in length. Figure 2.2 shows the estimated spectra of the first eight segments of each time series. Again, the presence of a free surface makes a

large difference. The spectrum for $r_0 = -1$ (Fig. 2.2b) has the same character as the reflectivity spectrum (Fig. 2.2a), i.e, it is “blue”. This is remarkable since the trace is comprised of pulses that have been transmitted to a certain depth and back up, experiencing loss of high frequencies along the way (O’Doherty & Anstey, 1971). Yet, the superposition of reflections emerging at a given time is rich in high frequencies, because the primary reflectivity is. This has a direct bearing on source-to-reflector absorption estimates as those in Dasgupta & Clark (1998). Suppose the source and receiver signatures for a zero-offset seismic trace are known and can be removed to get the impulse response. If we attributed all of the spectral coloring to anelasticity, we would *underestimate* the intrinsic attenuation because the loss of high frequencies has been partially offset by back-scattering from the thin layers. In our example, the apparent gain of high frequencies is about 0.12 dB/Hz (Fig. 2.2b), so the “source-to-reflector at 1 s” intrinsic quality factor would be overestimated² by 10% in a medium with $Q_{int} = 25$, and by 35% in a medium with $Q_{int} = 80$ (the higher the intrinsic Q , and the shallower the target reflector, the larger the error). Such a direct estimate of absorption from the trace spectrum is sensitive to uncertainties in the source and receiver signatures, and to frequency-dependent coupling. That is why, *spectral ratios* between different time windows are more likely to be used. Spectral ratios can estimate the intrinsic Q of a homogeneously absorbing medium accurately because the spectrum of the elastic impulse response is constant with time. The problem is that, if the quality factor of the near surface differs substantially from that at depth (as it often does), spectral ratios will be heavily weighted by the absorption properties of

²The amplitude loss caused by absorption over time t in a constant- Q medium can be described by

$$A = A_0 e^{-\alpha z} = A_0 e^{-\frac{\omega t}{2Q}}, \quad (2.1)$$

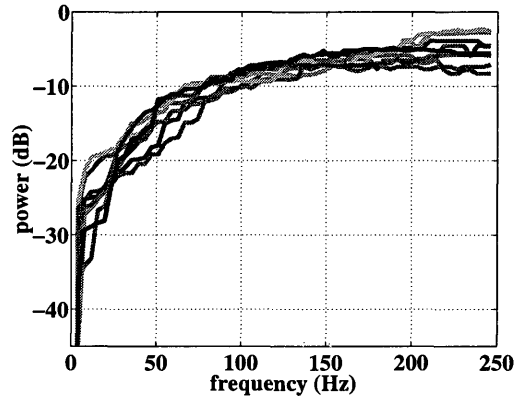
where ω is angular frequency. Therefore, the spectral ratio slope caused by absorption is $-20\pi \log_{10} e/Q \approx -27/Q$ dB/Hz/s.

the near surface, because a large portion of the energy emerging at late times consists of shallow-sampling surface-related multiples. Thus, it may seem beneficial to suppress surface-related multiples before absorption estimation. However, for the trace without any surface-related multiples the elastic impulse response is not stationary (Fig. 2.2c) – it loses predominantly high frequencies over time, and therefore, spectral ratios would overestimate the intrinsic absorption. In our example, the apparent loss of high frequencies for $r_0 = 0$ occurs at a rate of -0.075 dB/Hz/s, which is 7% of the rate due to intrinsic attenuation in a medium with $Q_{int} = 25$, and 22% in a medium with $Q_{int} = 80$. While the spectral ratios for $r_0 = 0$ exhibits apparent attenuation, the trace spectrum itself does not, until late times. At early times, it is blue, as that for $r_0 = -1$ (in fact, at early times, the traces with and without surface-related are similar because it takes time for the surface-related multiples to build up). The energy that has reached the earth surface for the model with $r_0 = 0$ is not available for further bouncing in the layered medium. In a blue reflectivity, predominantly high frequencies are reflected. That is why they are the first to come back to the surface and are removed from the system at the highest rate; hence, the phenomenon in Fig. 2.2c.

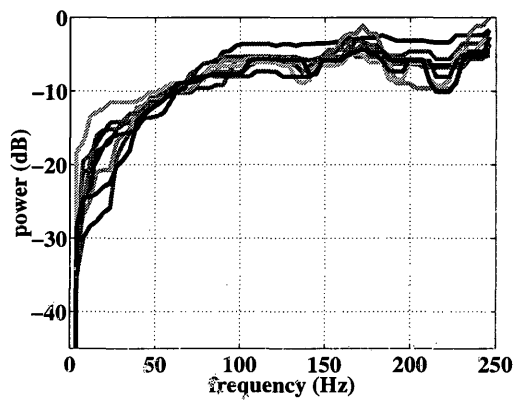
The spectral behavior illustrated through the above example could have been deduced from the analytical results of White *et al.* (1987, 1990). They found that the (expected) power spectrum $P(t, f)$ of the reflected signal in a window centered at two-way time t is

$$P(t, f) = |S(f)|^2 \frac{1}{t} \mu \left[\frac{tv}{l(f)} \right] \quad (2.2)$$

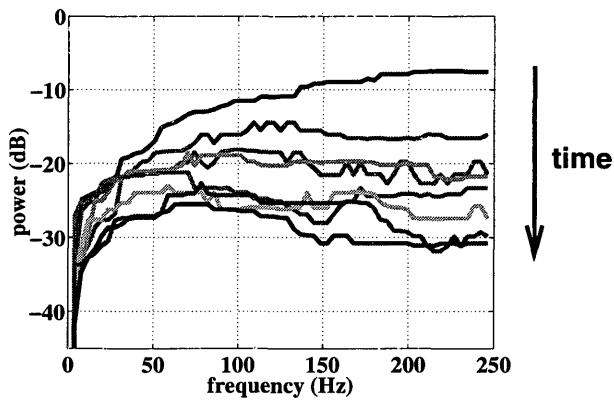
where $|S(f)|^2$ denotes the input power spectrum ($|S(f)|$ is constant with frequency



(a) reflection coefficient series



(b) trace with a free surface



(c) trace with an absorbing surface

Figure 2.2. Spectral change with time of (a) reflection coefficient series (stationary by construction); (b) impulse response with $r_0 = -1$; (c) impulse response with $r_0 = 0$. Each time series has been divided into 256 ms-long adjacent segments (128 samples per segment). Shown are the spectra of the first eight segments of each series.

for a spike source); v is the effective medium velocity; $l(f)$ is the localization length (distance at which the amplitude, transmitted across the layers, has diminished by the factor of e) – its frequency dependence can be often described by

$$l(f) = c_1 + \frac{c_2}{f^2}, \quad (2.3)$$

where c_1 and c_2 are constants (White *et al.*, 1990; Shapiro & Zien, 1993); the function μ in eq. (2.2) is of the form

$$\mu(\chi) = \begin{cases} \frac{\chi}{(1+\chi)^2} & \text{without a free surface} \\ 4\chi & \text{with a free surface} \end{cases} \quad (2.4)$$

$\chi = tv/l$ has the meaning of distance traveled in localization length units.

Let P_1, P_0 denote the spectrum P for $r_0 = -1$ and $r_0 = 0$ respectively. Then,

$$P_1(t, f) = |S(f)|^2 \frac{4v}{l(f)} = \frac{\text{const}}{l(f)}; \quad (2.5)$$

i.e., the elastic impulse response in the presence of a free surface is

- *Stationary.* Therefore, thin layering does not bias absorption measurements from spectral ratios.
- *Blue.* Therefore, attenuation measurements from the trace spectrum itself underestimate the absorption.

This is a theoretical explanation of the observations from Figure 2.2b.

For the hypothetical model without a free surface, White *et al.* (1990) give

$$P_0(t, f) = |S(f)|^2 \frac{\frac{v}{l(f)}}{\left(1 + \frac{tv}{l(f)}\right)^2} \quad (2.6)$$

According to eqs. (2.5) and (2.6), $P_1(f) \approx 4P_0(f)$ at $t \rightarrow 0$. The similarity between the early portions of the traces with and without surface-related multiples has been already mentioned. The scaling factor of 4 is simply due to the displacement doubling at the free surface³. Over time, P_0 decreases (as $1/t^2$ at late times), the drop being faster when $l(f)$ is smaller, i.e., at high frequencies. In summary, the elastic impulse response in the absence of surface-related multiples is

- *Losing high frequencies over time.* Thus, ignored thin layering would lead to an overestimate of the intrinsic attenuation by spectral ratio methods.
- *Blue or red.* Thus, attenuation measurements from the trace spectrum itself can either underestimate, or overestimate absorption, depending on the time window used for spectral analysis.

All conclusions so far were based on plane waves at normal incidence. The next section extends them to a point source and offset receivers, which is the case most relevant to seismic exploration.

³The total wavefield recorded just below the earth surface has only an up-going component for $r_0 = 0$, and both up- and down-going components (identical) for $r_0 = -1$. The two-fold increase in amplitude translates into a four-fold increase in power.

2.4 Point source, offset receivers

A rigorous mathematical description of the scattering in a stationary layered acoustic medium for a point source (vertical force) and offset receivers (vertical component of velocity) has been given by Asch *et al.* (1991). They derive a low-frequency constant-density approximation to the reflection impulse response, with and without a free surface. Up to a frequency-independent geometrical spreading factor, their results are identical to eqs. (2.2)-(2.4) (Appendix B) with

$$\chi = \frac{t v \sin \theta}{l(f, \theta)}, \quad (2.7)$$

where

$$\sin \theta = \sqrt{1 - \left(\frac{x}{vt}\right)^2}, \quad (2.8)$$

x being offset, and $l(f, \theta)$ the (vertical) localization length for a plane wave traveling at angle θ across the layering:

$$l(f, \theta) \approx l(f) \sin^2 \theta \quad \text{with} \quad l(f) \approx \frac{c_2}{f^2} \quad (2.9)$$

As before, χ can be interpreted as distance traveled in localization length units, though now the travel direction θ is time-dependent for a given trace.

The findings of Asch *et al.* (1991) can be recapped as follows. For times after the first arrival ($t > x/v$), the spectrum of the reflection impulse response, with and without surface-related multiples, is

$$P_1^*(t, f, x) \sim \frac{f^2}{t^2} \sqrt{1 - \left(\frac{x}{vt}\right)^2} \quad (2.10)$$

and

$$P_0^*(t, f, x) \sim \frac{f^2}{t^2} \left[1 + \frac{v t f^2}{c_2 \sqrt{1 - \left(\frac{x}{vt}\right)^2}} \right]^{-2} \quad (2.11)$$

where the star denotes a point source. The only difference between the plane wave and the point source cases at normal incidence ($x = 0$) is the t^{-2} decay due to geometrical spreading. At non-zero offsets, the spectral behavior for a point source is more complicated, but the conclusions from the previous section are still valid, namely:

- For $r_0 = -1$, the elastic impulse response is

Blue, though decreasingly so with offset;

Spectral ratios are frequency-independent, although not stationary anymore.

- For $r_0 = 0$, the elastic impulse response is

Blue or red, depending on the time window;

Losing high frequencies over time, though more slowly than at normal incidence.

The derivation of Asch *et al.* (1991) on which the above conclusions are based is for an acoustic medium. However, as Shapiro *et al.* (1994b) and Kerner & Harris

(1994) found out, the acoustic approximation works well for apparent attenuation estimates at angles up to 25-30 degrees.

2.5 Discussion

For the more realistic model with a free surface, spectral ratios between different time windows offer a simple and accurate measure of absorption, as long as the medium is stationary with depth. If the reflection coefficient series changes with depth, spectral ratios that capture different reflectivities can be significantly distorted, i.e., part of the frequency change in them can be due to scattering rather than absorption. Whether that would lead to an under- or over-estimate of the absorption depends on the geological setting, namely, whether the strong blue reflectivity lies above or below a weaker one. To predict spectral ratio distortions caused by non-stationary layering, we need well logs. In contrast, the *spectrum* of the elastic impulse response for $r_0 = -1$ is always blue, only the strength of the coloring may change when the reflectivity changes with depth.

It may seem strange that the simplest absorption measurements can be done from the more complicated trace containing surface related multiples. The reason is that surface-related multiples serve as additional probes in the medium, and the absorption information they carry is consistent with that carried by deep reflections in a homogeneously absorbing medium. Of course, this advantage is lost when the quality factor of the near surface is very different from that at depth. If the near surface is extremely absorbing, surface related multiples are weakened faster than deep reflections, almost⁴ as if $|r_0| < 1$, in which case spectral ratios may exhibit

⁴The difference between near-surface absorption and a reduced $|r_0|$ is that the former is frequency-dependent, and the latter is not.

some apparent attenuation, similar to that in Figure 2.2c. Separating absorption from scattering effects in a medium that varies with depth is beyond the scope of this paper. However, the above excursion gives us a flavor of the difficulties involved in mapping absorption variations in the presence of strong scattering – spectral coloring is only one of the problems introduced by thin layering; another is that scattering redistributes the wavefield in space, so that a significant portion of the energy emerging at a given time may not come from the depth of the primary reflection. Thus, the attenuation measured from a given time window is a weighted average of that of the regions from which the energy comes. Figure 2.3 shows the energy distribution with depth for our reflectivity example. For $r_0 = -1$, the energy is concentrated near the surface and monotonically decreases with depth at all times (Figure 2.3a). For $r_0 = 0$, energy is trapped in a certain depth interval, long after the direct arrival has passed through it; this interval will contribute to the surface seismic trace more than a deeper reflector. Because of this complicated energy distribution, intrinsic and apparent attenuation are coupled in strongly scattering media. Thus, a reflectivity log would not be sufficient to predict the apparent attenuation in surface seismic data; a preliminary absorption model (e.g., from a VSP) would be necessary, too.

2.6 Conclusions

In a homogeneously absorbing, stationary layered medium, spectral-ratio methods applied to surface seismic data give accurate Q estimates. In contrast, absorption measurements directly from the trace spectrum would underestimate the intrinsic absorption unless the blue color of the elastic impulse response is taken into account. The underestimate would be largest at small offsets and for shallow targets.

Suppressing surface-related multiples would not benefit absorption estimation

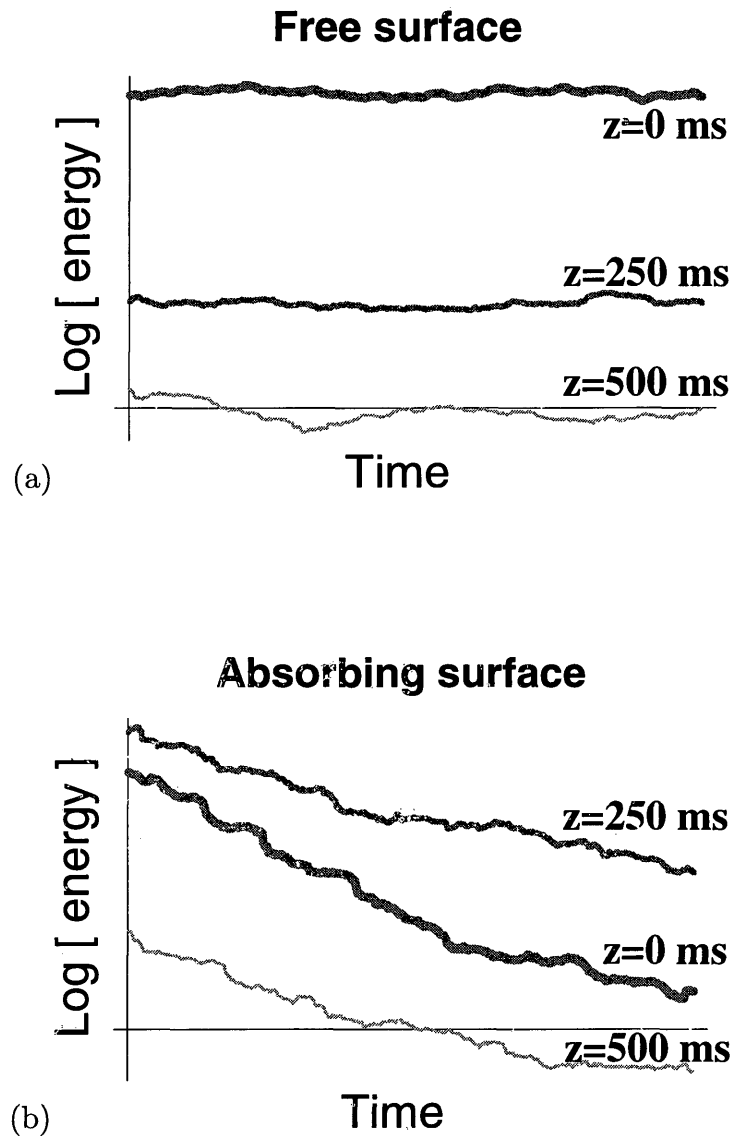


Figure 2.3. Energy at three depths: surface receiver (Figure 2.1b,c), and receivers at 250 ms and 500 ms one-way traveltime (250 and 500 layers in a Goupillaud model) below the surface; the synthetics are for plane waves at normal incidence; the energy measurements are over the 0.5-3.0 s interval, i.e., at times after the ballistic arrival at the deepest receiver. (a) $r_0 = -1$; (b) $r_0 = 0$.

in a constant-Q medium. However, if the quality factor of the near surface is very different from that at depth, removing the surface-related multiples would lessen the influence of the shallow zone at the expense of inducing apparent attenuation in the spectral ratios. The apparent attenuation would be largest at small offsets, and in strong reflectivities, i.e., finely interlaced lithologies with contrast impedances.

Chapter 3

DISTORTIONS IN VSP SPECTRAL RATIOS CAUSED BY THIN HORIZONTAL LAYERING¹

3.1 Introduction

In exploration seismology, absorption estimates come largely from Vertical Seismic Profile (VSP) experiments. The most commonly used techniques are based on spectral ratios, i.e., comparing the frequency content of the first arrival at successive receiver locations [different VSP methods for absorption estimation are discussed in Tonn (1991); for a more recent development see, for example, Sun & Castagna (2000)].

Unfortunately, VSP spectral ratios can be contaminated by frequency-dependent scattering from small-scale heterogeneities in the medium (e.g., thin layers). Thus, these ratios measure the effective attenuation, which is a biased estimate of the intrinsic absorption. The goal of this paper is to assess the maximum share of apparent attenuation that can be introduced in the effective attenuation estimates by thin horizontal layering. I assume that the effective attenuation is derived from noise-free VSP spectral ratios (no background noise, timing and positioning errors, instrumentation artifacts, etc.).

I start by reviewing some properties of the earth reflection coefficient series (which I call “reflectivity” for short) that determine the spectral coloring of the im-

¹Submitted to JGI.

pulse response in the absence of absorption. Then I explain the frequency content of the elastic² spectral ratios. Contrary to popular belief, they are not necessarily high-frequency deficient in the presence of thin layering; i.e., ignoring scattering does not necessarily lead to an overestimate of the intrinsic absorption. I take into account the presence of the earth surface, which magnifies the thin-layering effects. After having identified the most unfavorable geological settings for absorption estimation, I quantify the bias (the apparent attenuation, or the difference between effective and intrinsic attenuation) that can be expected in such settings through a couple of synthetic, yet realistic examples. I show that when the subsurface is characterized by a strong and stationary reflection coefficient series, the elastic VSP spectral ratios exhibit apparent attenuation comparable to that caused by absorption in a medium with $Q_{int} = 70$. The largest bias, though, is likely to occur when geology changes with depth. In a non-stationary reflectivity, scattering can either cause an even greater high-frequency loss than intrinsic absorption or, on the contrary, it can over-compensate for the anelastic loss and lead to spectral ratios with a positive slope (negative effective Q , the quality factor being defined as $Q = -20\pi \log e/\text{slope} \approx -27/\text{slope}$).

3.2 Earth reflectivity

Two characteristics of a reflectivity series govern the spectrum of a seismic trace. The first is the magnitude of the reflection coefficients, which determines how energetic the multiples will be compared to the primaries. The second is the frequency content of the reflection coefficient series. Typical earth reflectivities are approximately frequency-independent (pseudo-white) only above a corner frequency, below which their power spectra fall as f^β , $\beta \in [0.5; 1.5]$ (Walden & Hosken, 1985; Saggaf

²Throughout this paper *elastic* refers to the lack of absorption, not to the presence of shear-waves.

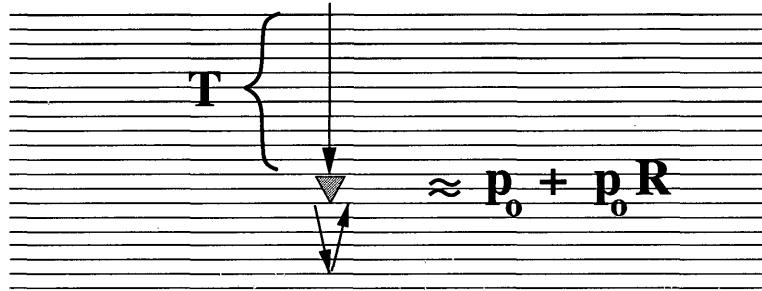


Figure 3.1. Signal in a buried receiver: transmitted train (p_0) and its primary reflections from below ($p_0 R$); multiples of the reflections from below are ignored.

& Robinson, 2000). The stronger the deviation of a reflectivity from whiteness, the stronger the coloring (the frequency-dependance) in its impulse response.

The magnitude and frequency content of a reflection coefficient series are not completely independent characteristics because the acoustic impedance of the sub-surface can vary only within certain limits. Strong reflectivities have markedly blue spectra, i.e., spectra whose power increases with frequency over most of the seismic frequency band. In such blue sequences, closely spaced samples are negatively correlated; i.e., consecutive reflection coefficients tend to have opposite signs. This is the only way to have a large number of large reflection coefficients while the acoustic impedance stays within certain geological bounds.

3.3 Receiver in a layered half-space

Strong reflectivities are of primary interest to this study because they are likely to cause problems with absorption estimation. However, to understand how thin layering acts on the signal in a down-hole receiver, it is instructive to look first at a simple weak-reflectivity approximation.

Suppose $R(\omega)$ is the Fourier transform of the time-domain reflection coefficient

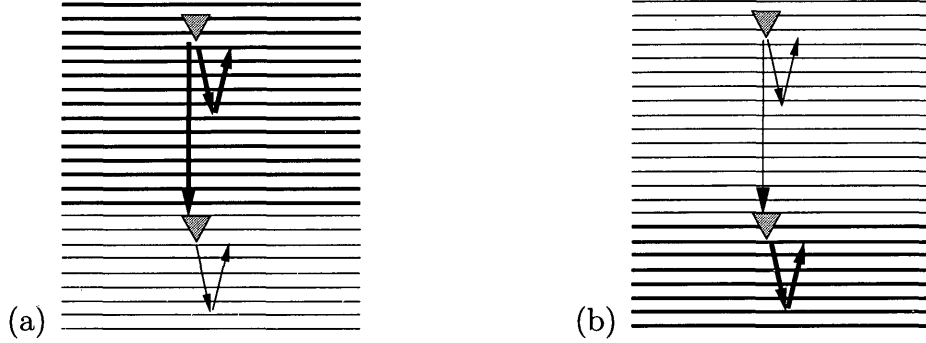


Figure 3.2. VSP in a non-stationary reflectivity: (a) strong above weak reflectivity; (b) weak above strong reflectivity. Thick arrows indicate arrivals that contribute significantly to the signal coloring; thin arrows represent weak contributions or weak filtering.

series (reflectivity log). As discussed in the previous section, $R(\omega)$ is an increasing function of frequency. For now assume that the thin layering is stationary, so that $R(\omega)$ does not change with depth (the non-stationary case will be considered later). Using the results of Banik *et al.* (1985) one can show (Appendix A) that near the time T of the direct arrival the impulse response p at a buried receiver is

$$p(\omega) \approx p_0(\omega) (1 + R(\omega)), \quad (3.1)$$

where p_0 is the transmission impulse response of a stack of layers with a (one-way) traveltime thickness T . The transmission impulse response p_0 is minimum-phase, with an amplitude spectrum given by O'Doherty & Anstey's formula (O'Doherty & Anstey, 1971)

$$|p_0(\omega)| = e^{-|R(\omega)|^2 T}, \quad (3.2)$$

where T is dimensionless (normalized by the time-thickness of an individual thin layer, i.e., the sampling interval of the time-domain reflection coefficient series).

Equation (3.1) tells us that in a small window after the first break, the main contributions to the trace come from the transmitted impulse (filtered by the overburden) and its primary reflections from the interfaces immediately below the receiver location (Fig. 3.1). This is a weak-reflectivity approximation because it ignores multiples of the reflections from below the receiver as well as changes, over the considered time window, in the down-going pulse that generates them. Equations (3.1) and (3.2) might be numerically inaccurate for strong reflectivities but they capture the most important facts (remember $R(\omega)$ is blue):

- the transmission through the layered overburden causes apparent loss of high frequencies (apparent attenuation);
- the reflections from immediately below the receiver boost the high-frequency content of the trace near the first arrival.

These counter-actions determine the final color of the trace at the early times typically used in VSP spectral ratios for absorption estimation. In a stationary reflectivity, the reflections from below have the same relative contribution at any receiver. Thus, the elastic spectral ratios exhibit apparent attenuation purely due to the transmission through the stack of layers between the receivers.

In practice, reflectivities are often non-stationary and the reflections from below play an important role in the spectral ratios. We can consider two basic situations: weak reflectivity above strong reflectivity and vice versa. First, suppose the shallower receiver is in a strong reflectivity zone and the deeper receiver is underlain by a weak reflectivity (Fig. 3.2a). The signal in the deeper receiver has not only been depleted

of high frequencies during transmission, it also lacks the high-frequency boost that would have been provided by reflections from below. Therefore, the spectral ratio between the two receivers will exhibit an even larger apparent attenuation than that in a strong but stationary reflectivity. Now let the geometry be reversed (Fig. 3.2b); in this case the high-frequency boost by reflections from below in the deep receiver is much larger than that in the shallow one and can even overcome the (small) high-frequency loss along the path between the receivers. Thus, the signal may appear to enrich in high-frequencies with depth. If the absorption of the medium is too small to overturn the slope of the elastic spectral ratio, we may observe a negative effective Q . Negative effective Q values have been reported in the literature (De *et al.*, 1994; Hackert & Parra, 2002).

3.4. Influence of the free surface

The previous section was devoted to the spectral coloring caused by thin layering alone. The presence of the earth surface was not taken into account.

The main role of the earth surface (a free surface) is to retain in the medium whatever frequencies have reached it and put them back in circulation. How much a trace would be influenced by these re-introduced frequencies depends on the receiver depth. A shallow receiver would feel the surface-related multiples at all frequencies. Since in a blue reflectivity sequence the depth of penetration (the localization length) decreases with frequency, only a small portion of the high frequencies bounced back by the earth surface would reach a down-hole receiver. Thus, the deeper the receiver, the narrower (lower) the frequency band over which surface-related multiples add to the trace. This, combined with the fact that a low enough frequency contributes equally to all traces (all receivers become shallow compared to the localization depth

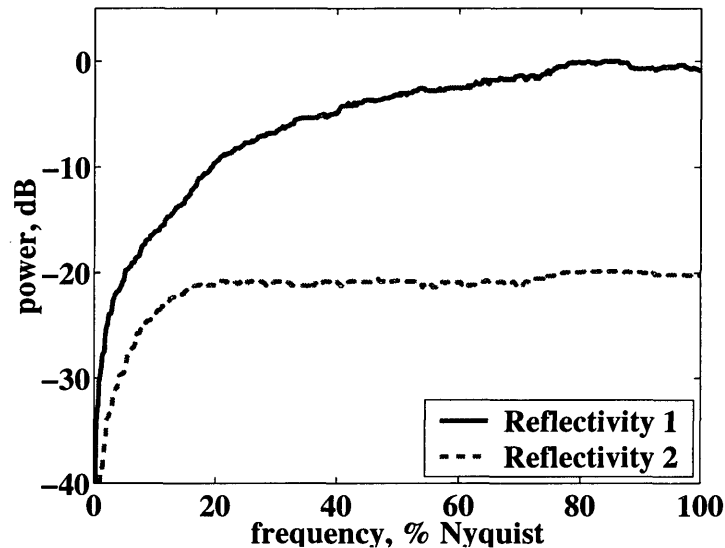


Figure 3.3. Power spectrum of the synthetic reflection coefficient series: Reflectivity 1 is strong and blue; Reflectivity 2 is weak and almost white.

as $\omega \rightarrow 0$), may cause additional apparent attenuation in VSP spectral ratios. The effect is stronger at later times when surface-related multiples make a larger difference on the trace than they do at early times (see the example below).

3.5 End-member examples

The purpose of this section is to illustrate the above concepts and to put an upper bound on the bias of the absorption estimates derived from VSP spectral ratios in finely layered media. I compute VSP spectral ratios for horizontally layered, perfectly elastic earth models and compare them to the ratios expected in a homogeneous but anelastic space. In media with spatially-invariant absorption properties, the total attenuation is a simple superposition of scattering effects and intrinsic absorption, so the comparison between their individual values makes sense. My computations (by a time-domain reflectivity code with a Goupillaud model – Appendix E) are for

	Reflectivity 1 (strong, blue)	Reflectivity 2 (weak, almost white)
θ	0.9	0.98
ϕ	0.3	0.8
mean	-0.0002	-0.0002
std	0.11	0.02
p	1.0	0.23
λ_1	0.09	0.007
λ_2	—	0.017

Table 3.1. The two synthetic reflectivities used throughout the examples are modeled as ARMA(1,1) processes with autoregressive parameter θ and moving average parameter ϕ . The amplitudes of the reflection coefficients are drawn from a mixture of two Laplace distributions with a mixing proportion parameter p and scale parameters λ_1 and λ_2 , respectively (Appendix D).

plane waves at normal incidence but the results are directly applicable to a zero-offset VSP with a point source because the geometrical spreading will introduce only a frequency-independent scaling factor in the spectral ratios (e.g., Asch *et al.*, 1991).

I first consider the case of a stationary, strong reflectivity. Then I append the strong reflectivity, above or below, with a much weaker one to create extreme examples of non-stationary layering. My reflection coefficient series are synthetic but realistic, similar to those of Well 8 and Well 5 from the papers of Walden and Hosken (1985, 1986). Their properties are given in Table 3.1, and their power spectra are depicted in Fig. 3.3. The generation of the reflectivities is described in Appendix D.

3.5.1 Strong stationary reflectivity

The normal-incidence elastic impulse response of Reflectivity 1 is shown in Fig. 3.4 for three down-hole receivers. The loss of high frequencies with depth is clearly seen in the first-arrival zoom in Fig. 3.5 and in the spectra in Fig. 3.6. The spectral ratio

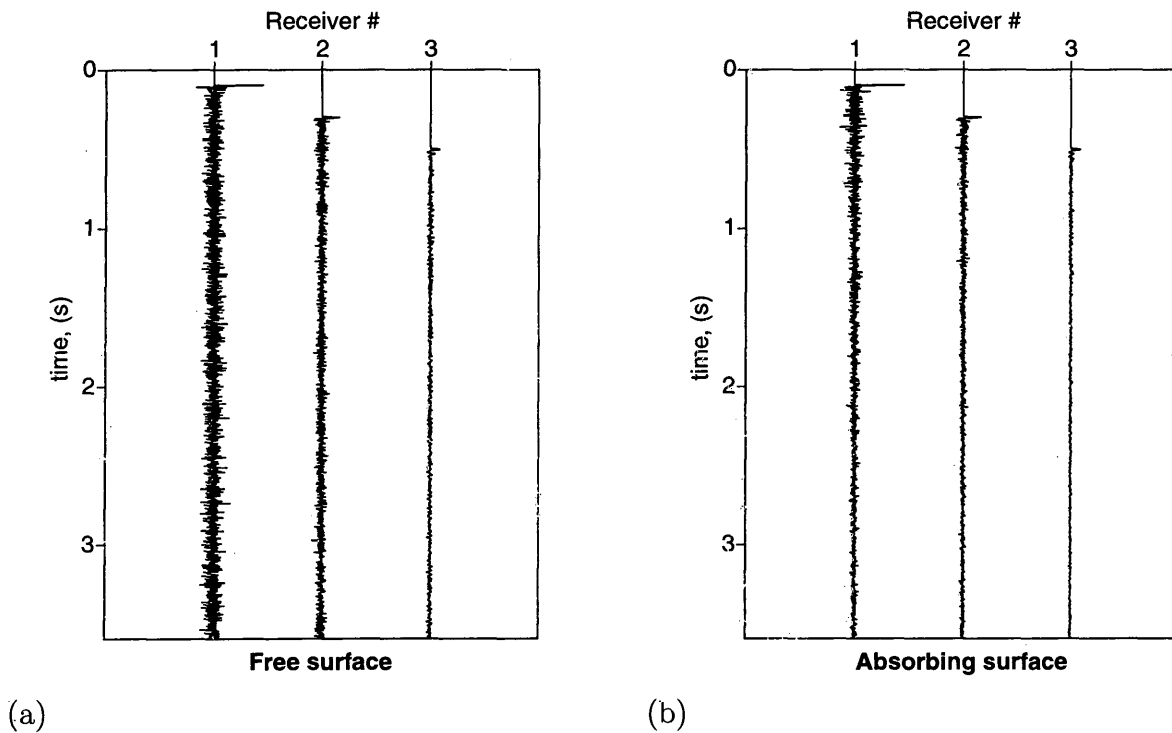


Figure 3.4. VSP elastic impulse response in a strong stationary reflectivity (Reflectivity 1): (a) with surface-related multiples (as are traces recorded in practice); (b) without surface-related multiples (shown for comparison). The receivers are 200 ms apart (200 layers apart in the Goupillaud model – Appendix E), the first being at 100 ms (100 layers) below the earth surface.

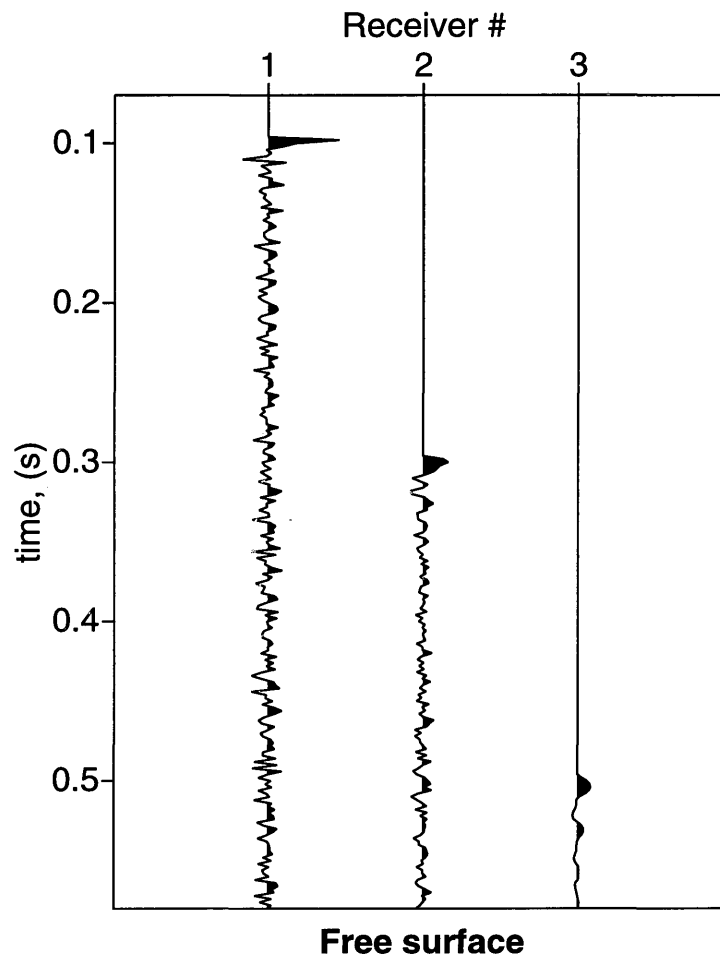


Figure 3.5. Zoom from Fig. 3.4a: The transmitted train disperses and loses high frequencies with depth.

between the early events on the deepest and the shallowest trace (Fig. 3.7a, solid line) has a slope of -0.4 dB/Hz/s. It is comparable³ to the slope produced by absorption in a homogeneous medium with intrinsic quality factor $Q_{int} = 70$, which is in the typical range for Q_{int} in the upper crust. Therefore, in a stationary reflectivity, about half of the observed spectral ratio slope (absorption and apparent attenuation together) may come from apparent attenuation. It is due mainly to the thin layering between the receivers – the additional apparent attenuation caused by surface-related multiples is insignificant at early times (Figs. 3.6a, 3.7a). Surface-related multiples become important later on the trace (Fig. 3.6b, 3.7b). This is easy to understand if we compare the traces with and without surface-related multiples in the time domain (Fig. 3.4a,b). In the presence of a free surface, down-hole traces become stationary after the transmission train has passed. Without the free surface, traces decay with time. Thus, at late times, the traces that we record in the field consist largely of surface-related multiples, even though the early portions of the traces with and without a free surface are quite similar. This means that while spectral ratios obtained from early windows carry information about the medium between the receivers, ratios based on late windows would be strongly influenced by the properties of the near surface. It should be pointed out that regardless of the dominant mechanism, the apparent attenuation does not change with time in a stationary reflectivity (Fig. 3.7), at least over the lower half of the trace spectrum, typically used for absorption estimation for its high signal-to-noise ratio.

³The comparison between scattering and intrinsic attenuation is based on the following. The amplitude loss caused by absorption over time t in a constant-Q medium can be described by

$$A = A_0 e^{-\alpha z} = A_0 e^{-\frac{\omega t}{2Q}}, \quad (3.3)$$

where ω is angular frequency. Therefore, the spectral ratio slope caused by absorption is $-20\pi \log_{10} e/Q \approx -27/Q$ dB/Hz/s. A slope of -0.4 dB/Hz/s corresponds to $Q \approx 70$.

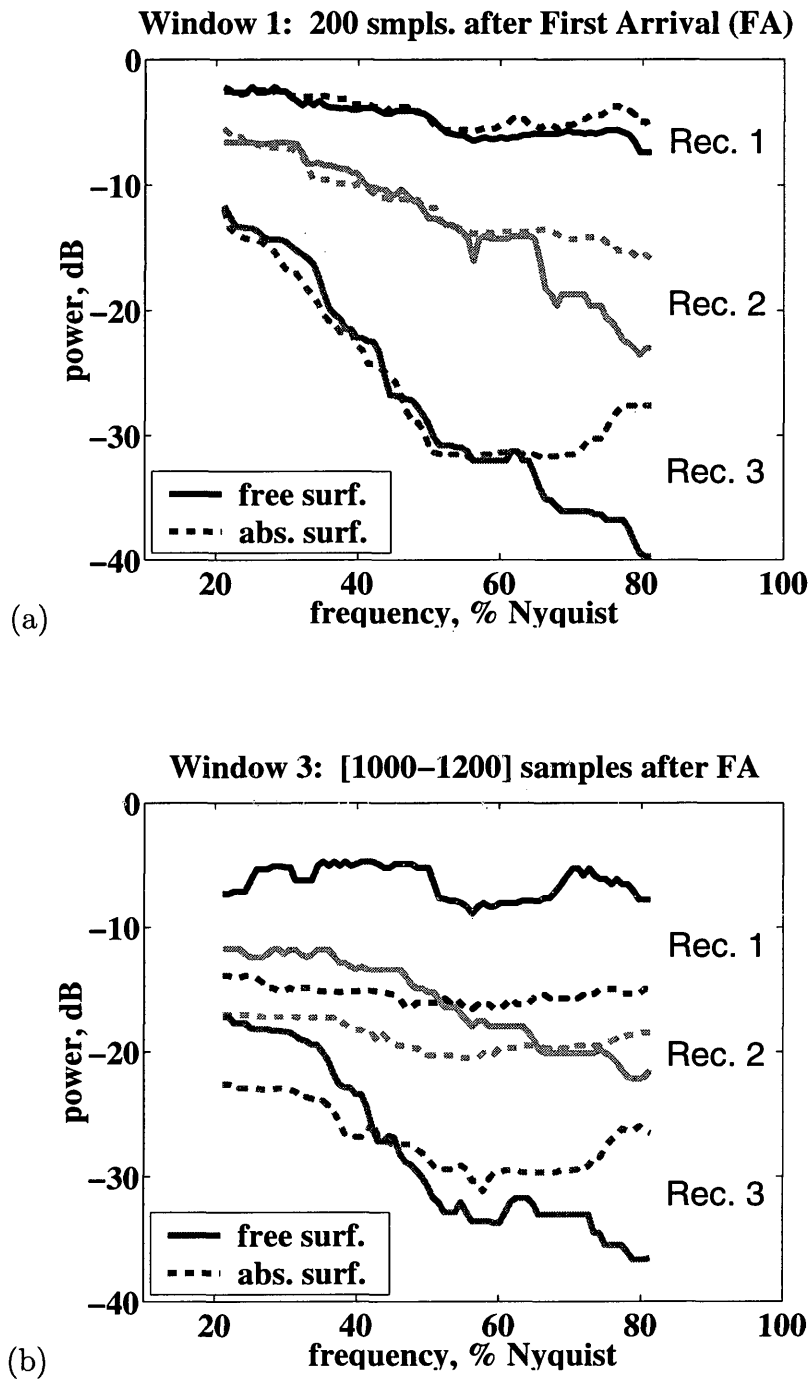


Figure 3.6. Power spectra at three receiver depths with and without surface-related multiples: (a) At early times, surface-related multiples have negligible influence on trace spectra, except at high frequencies, which are rarely used in absorption estimation. (b) At late times, surface-related multiples make spectra of down-hole traces steeper, amplifying the loss of high frequencies with depth.

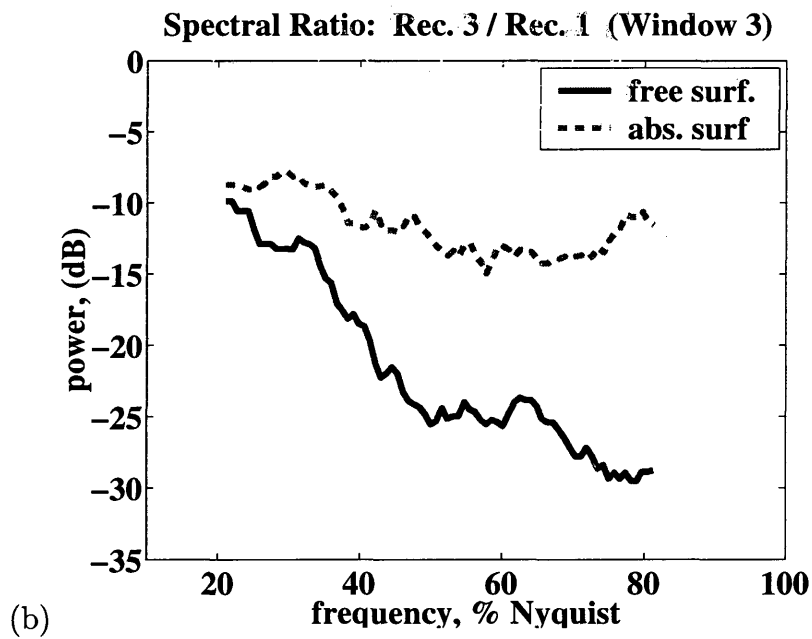
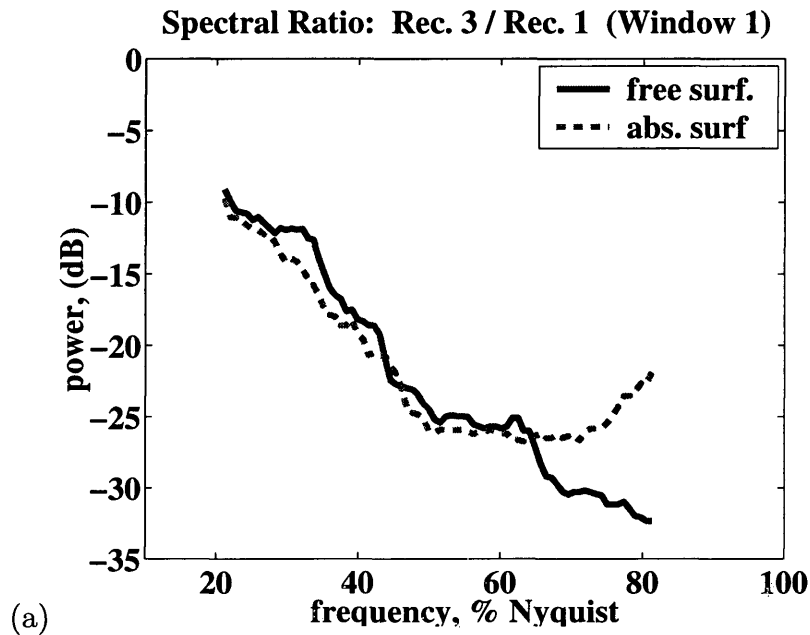


Figure 3.7. Spectral ratio between Receiver 3 and Receiver 1 (400 ms apart): (a) at early times; (b) at late times. Note that the slope of the solid lines is essentially same in (a) and (b).

Another feature of the apparent attenuation in a stationary reflectivity is that it does not depend on the receiver separation – only the uncertainty of its estimate increases as the receivers get closer (Fig. 3.8). As we will see, this is not the case in a non-stationary reflectivity, where an elastic spectral ratio depends on the contrast in the reflectivity properties beneath each of the two receivers, which is a factor not proportional to receiver separation.

The increased variability of the slope estimates from close receivers in Fig. 3.8 is caused by the inability of the down-going pulse to stabilize (self-average while propagating through the scattering medium) over the short path of propagation between the receivers. Shapiro & Zien (1992) showed that, for a purely transmissional experiment (no reflections from below a receiver), the standard deviation of the estimated apparent attenuation α is

$$\sigma_{\alpha} \propto \sqrt{\frac{\alpha}{L}}, \quad (3.4)$$

where L is the distance traveled, i.e., the distance between the receivers. The closer the receivers, the larger the uncertainty σ_{α} . In our experiment, reflections from below the receivers also contribute to the variability of the attenuation estimate, and their contribution does not diminish as the receiver separation increases (they do not self-average). That is why, the apparent attenuation uncertainty does not vanish for large receiver separations. The data in Fig. 3.8 are consistent with the observation of Spencer *et al.* (1982) that there is an optimal receiver separation for attenuation estimation – below it the variability of the estimates is too large; beyond it the variability does not decrease substantially with distance.

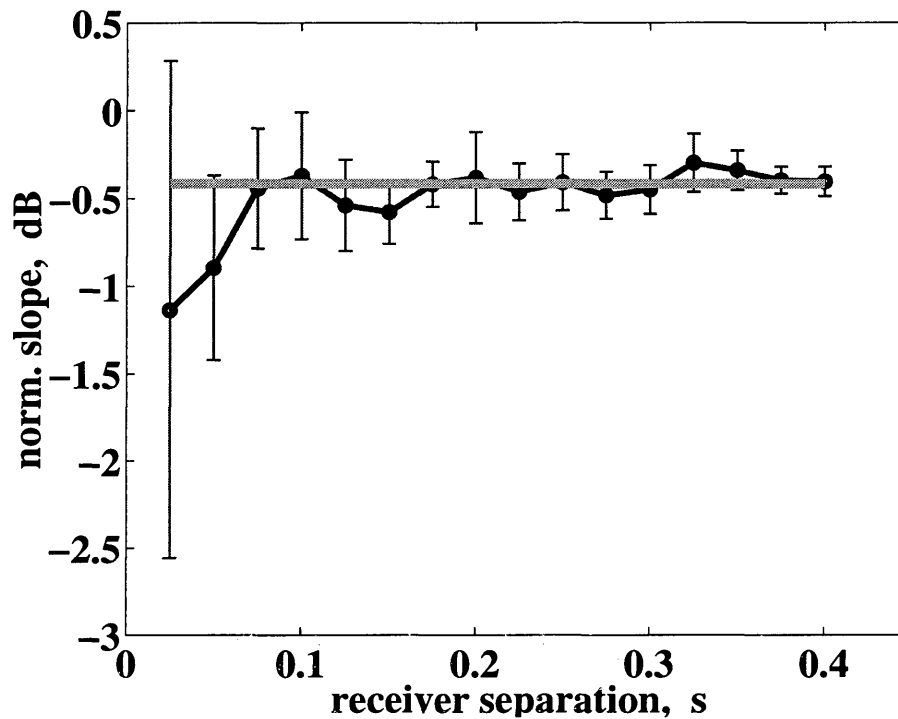


Figure 3.8. Slope of the spectral ratio between Receiver 3 and a number of shallower receivers, normalized by the one-way traveltime between the receivers in a strong stationary reflectivity. The time window for spectral estimation is 256 samples long. The spectra on all traces were smoothed by a 20%-of-series-length median filter before computing the spectral ratios. The error bars represent the uncertainty of each slope estimate (least-squares fit). The data are compatible with a constant apparent attenuation (thick gray line – computed by weighted least-squares).

3.5.2 Strong above weak reflectivity

The largest apparent attenuation occurs in a non-stationary reflectivity when the deeper receiver is underlain by a weak reflectivity. To simulate such a case, I appended the strong, blue Reflectivity 1 by the weak, almost white Reflectivity 2 at the level of Receiver 3 (500 layers below the earth surface). The elastic impulse responses in Receiver 1 (in the strong reflectivity zone) and Receiver 3 (just below the strong reflectivity) are shown in Fig. 3.9a, and their spectra at early times are shown in

Fig. 3.10a. The spectra do not look much different from those in the stationary case, just their ratio (Fig. 3.11a) is about -0.02 dB/Hz steeper than before⁴. This increase in slope, however, occurs “instantly” across the reflectivity jump; it is determined purely by the contrast in the reflectivity properties below the two receivers, and does not depend on the receiver separation (given that Receiver 3 stays in place, so that the path between the receivers is entirely in Reflectivity 1). Thus, while this additional apparent attenuation caused by change in geology will be small compared to the total attenuation accumulated along the path between distant receivers, it can contribute significantly to absorption estimates⁵ extracted from close receivers. Of course, in practice, the slope of the spectral ratio is not discontinuous at the depth of the reflectivity change because of the finite time-window used for spectral estimation; as the receivers get closer together, the window around the first arrival on the shallow trace starts to sample the weak reflectivity zone. Despite this smearing though, the total apparent attenuation can exceed the attenuation due to absorption for $Q_{int} = 50$ when the receiver separation is less than 220 ms. This is illustrated in Fig. 3.12, which shows the spectral ratio between Receiver 3 and a number of shallower receivers, normalized by the traveltimes between the receivers in a pair. Now, unlike in the stationary reflectivity case in Fig. 3.8, the data are incompatible with a constant apparent attenuation but are consistent with a linear model, i.e., apparent attenuation linearly dependent on receiver separation. As the receiver offset decreases, the apparent attenuation increases.

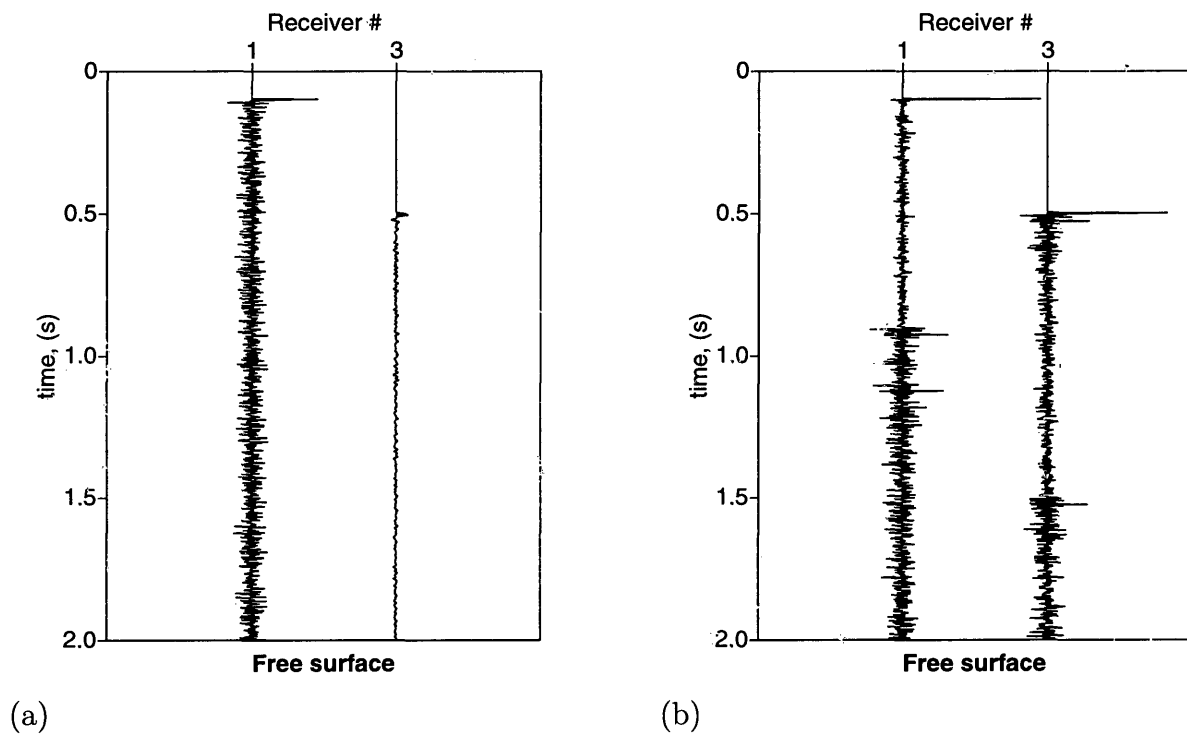


Figure 3.9. VSP elastic impulse response with surface-related multiples in (a) strong-above-weak reflectivity; (b) weak-above-strong reflectivity. The receiver placement and numeration is as in Fig. 3.2. The receiver depths are the same as in the stationary case – 100 ms and 500 ms below the earth surface, respectively.

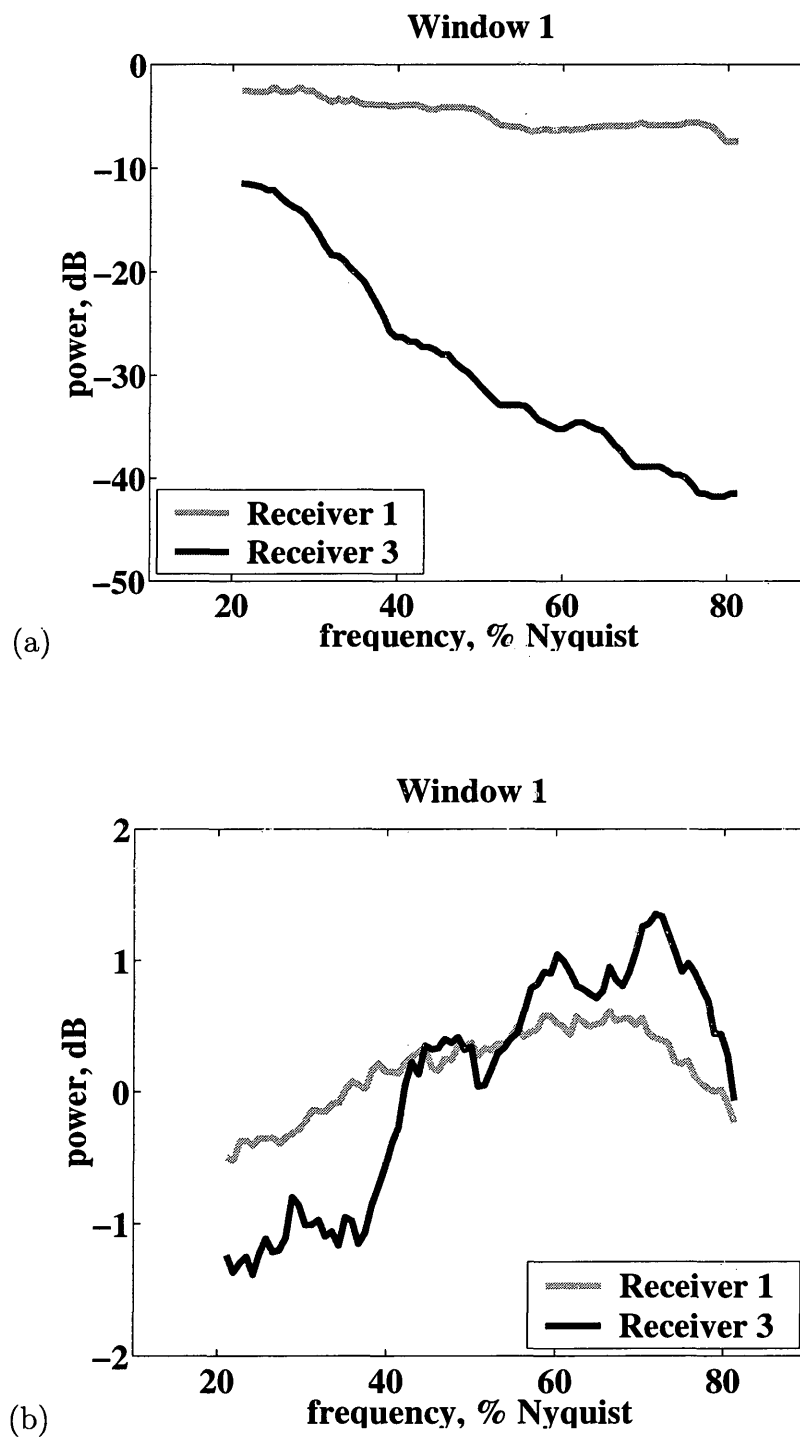


Figure 3.10. Elastic spectra at early times (Window 1: 200 samples after the first arrival) in (a) strong-above-weak reflectivity; (b) weak-above-strong reflectivity.

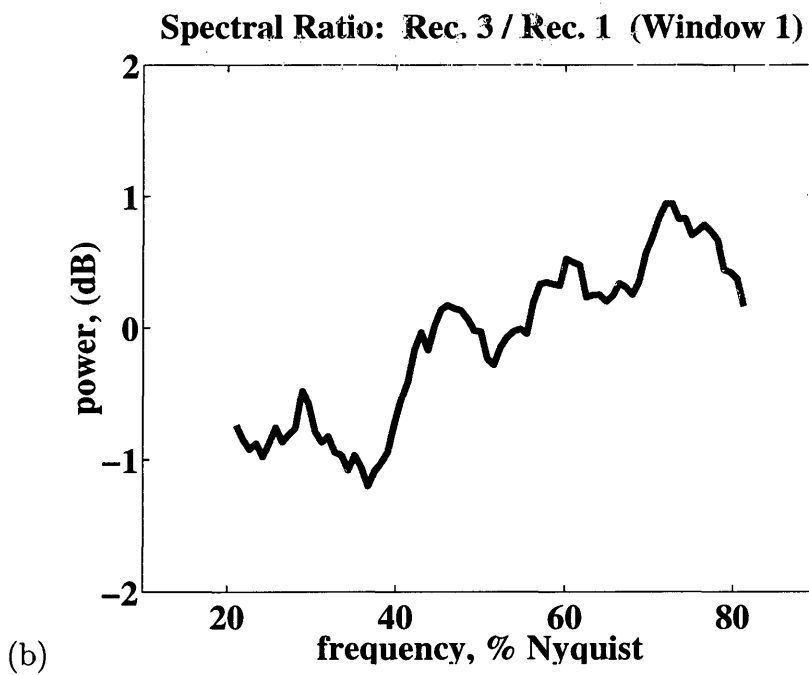
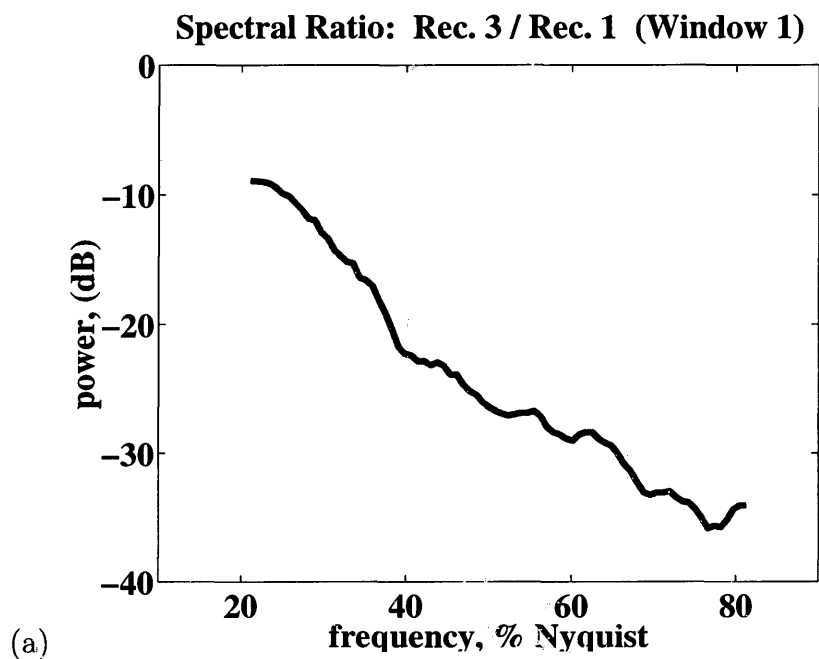


Figure 3.11. Spectral ratio in (a) strong-above-weak reflectivity; (b) weak-above-strong reflectivity.

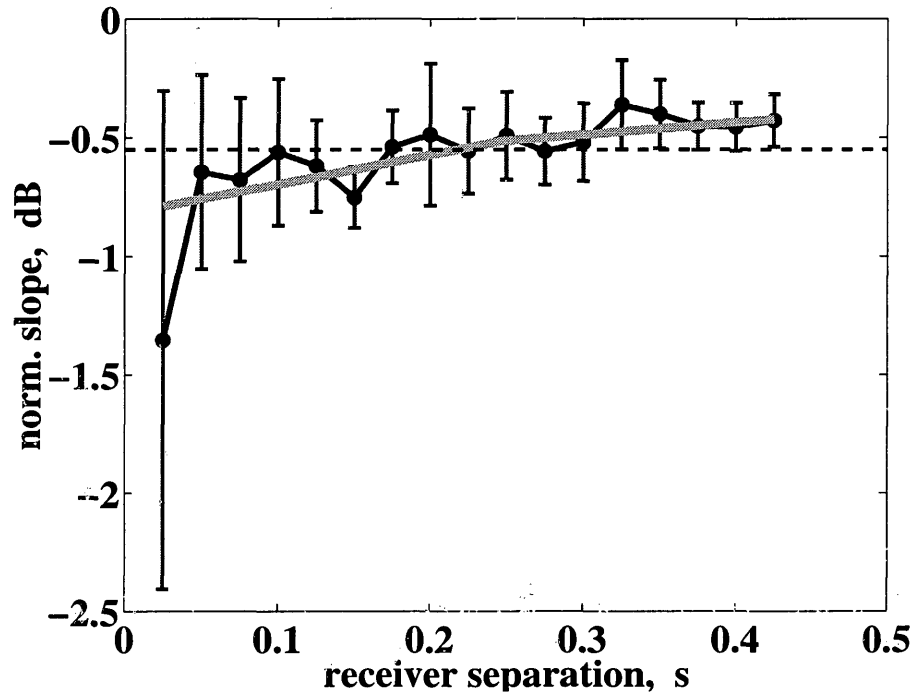


Figure 3.12. Analogous to Fig. 3.8 but for the strong-above-weak reflectivity case. The thick gray line is the best weighted-least-squares fit and actually consists of two independently estimated segments – one for large receiver separation such that the time-window on the shallow trace does not sense the weak reflectivity below the deeper receiver, and another for smaller separation. The two segments give virtually identical estimates for the trend in the apparent attenuation. The thin dashed line indicates the slope produced by intrinsic absorption in a medium with $Q_{int} = 50$.

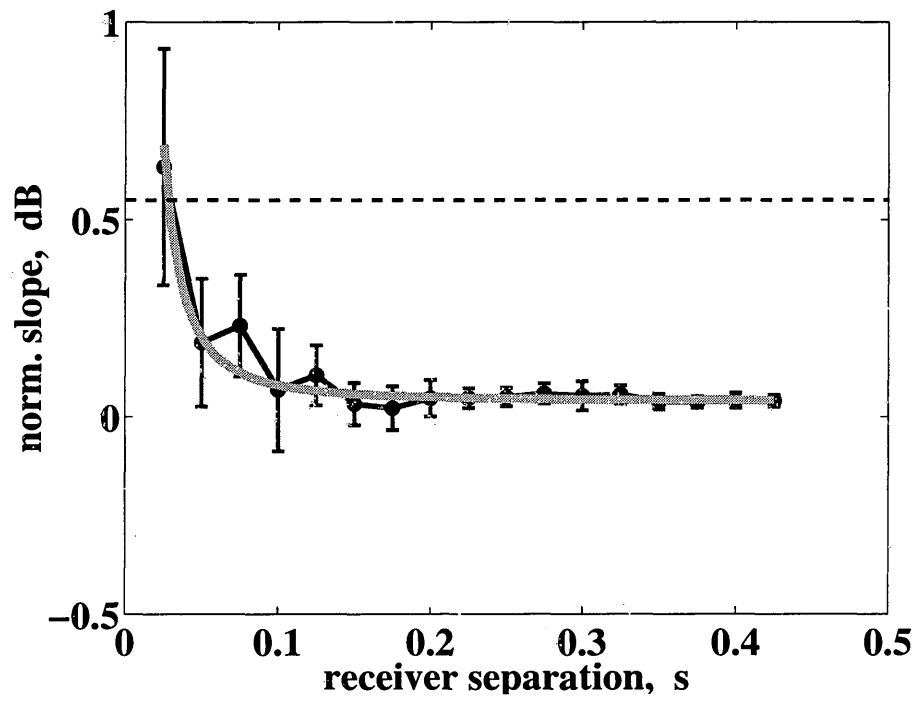


Figure 3.13. Analogous to Fig. 3.8 but for the weak-above-strong reflectivity case. The thin dashed line indicates the absolute value of the slope produced by intrinsic absorption in a medium with $Q_{int} = 50$.

3.5.3 Weak above strong reflectivity

Now let the weak Reflectivity 2 be underlain by the strong Reflectivity 1, and again let the change occur at the depth of Receiver 3. The elastic impulse response, shown in Fig. 3.9b, is more dynamic than in the previous case. The weak scattering in the overburden leaves the transmitted signal much stronger and more compact (compare with Fig. 3.9a; all traces are plotted on the same scale). The reflection from the top of the strong-reflectivity zone is seen in Receiver 1 at 0.9 s. The event at 1.1 s is its free-surface multiple. This free-surface multiple is also seen at 1.5 s in Receiver 3. Before that, the trace decays with time as it would in the absence of a free surface because the surface-related multiples of the reflections generated in the overburden are too weak to compensate for the transmission losses in the strong reflectivity below the receiver. The surface-related multiples of the reflections from the strong reflectivity zone noticeably boost the energy in Receiver 3 after 1.5 s.

The early-time spectra of the two traces are shown in Fig. 3.10b. The spectrum of the shallow trace is slightly blue because the reflections from below, even though weak, outweigh the filtering in the overburden, i.e., the $(1 + R)$ term in eq. (3.1) over-compensates the high-frequency deficit in $p_0 = \exp(-T|R|^2)$ at the depth of Receiver 1. The over-compensation is even more dramatic in Receiver 3 for which the former term, $(1 + R)$, contains the strong and blue Reflectivity 1 and the later term, $\exp(-T|R|^2)$, contains the weak, almost white Reflectivity 2. Thus, the signal in the deep receiver is richer in high frequencies than the signal in the shallower receiver. This leads to a spectral ratio with a positive slope (Fig. 3.11b). The slope is only

⁴Note that the change of slope here is given in dB/Hz; it is not normalized by the time-separation between Receivers 1 and 3.

⁵Absorption estimates are based on spectral ratios slopes, normalized by receiver separation, e.g., dB/Hz/s=dB.


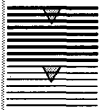

	Q_{int}	Q_{eff}	Q_{eff}
	50	30	30
	50	25	20
	50	55	negative

Table 3.2. Effective versus intrinsic Q for end-member reflectivity examples. Shown are estimates of Q_{eff} from receiver pairs with large and small separation (e.g., $dz = 500$ m and $dz = 50$ m in a medium with velocity 2500 m/s).

about 0.015 dB/Hz but since it occurs instantly across the reflectivity change (as explained in the previous section) it can be large compared to that attributable to intrinsic absorption when the receivers are close. This is illustrated in Fig. 3.13, which shows the spectral ratio between Receiver 3 and a number of shallower receivers, normalized by the receiver pair separation. The apparent gain of high frequencies with depth increases inversely proportional to the square of the receiver separation (that is the lowest-order polynomial that fits the trend). For a receiver separation of less than 30 ms, scattering can over-compensate for the high-frequency loss caused by anelasticity in a medium with $Q_{int} = 50$ and produce a negative effective Q .

A comparison between the intrinsic and effective Q , summarizing the examples from this section is given in Table 3.2.

3.6 Conclusions

Based on the above most unfavorable, yet realistic examples, we can conclude the following:

- To characterize the medium between two receivers, one can use the ratio between early windows on the VSP traces. Late windows are influenced by the absorption properties of the near surface.
- In a stationary reflectivity, VSP spectral ratios exhibit apparent attenuation comparable to that caused by absorption in a homogeneous medium with $Q_{int} = 70$.
- The largest apparent attenuation occurs when the shallow receiver is in a strong reflectivity zone and the deep receiver is underlain by a weak reflectivity. In such cases the apparent attenuation dominates the VSP spectral ratio, unless the receiver separation is large (e.g., more than 220 ms in a medium with an intrinsic $Q_{int} = 50$).
- A negative effective Q (spectral ratio with a positive slope) can be observed when the shallow receiver is in a weak reflectivity and the deep receiver is underlain by a strong reflectivity, and the receiver separation is small (e.g., less than 30 ms in a medium with an intrinsic $Q_{int} = 50$).

Common wisdom tells us that absorption cannot be reliably assessed from spectral ratios between closely spaced receivers because the variability of the slope estimate is large compared to the slope itself. The fact that scattering tends to bias absorption estimates more when the receivers are close is an additional reason not to use close pairs.

To assess intrinsic absorption (anelasticity) from VSP spectral ratios in a horizontally layered medium, we need sonic and density logs from which to predict the scattering effects.

Chapter 4

QUANTIFYING THE UNCERTAINTIES IN ABSORPTION ESTIMATES FROM VSP SPECTRAL RATIOS

4.1 Introduction

Absorption carries valuable information about lithology and reservoir conditions, such as saturation and permeability (Winkler & Nur, 1979; Batzle *et al.*, 1996), but to infer them, we must know how accurate the absorption measurements are. In seismic exploration, most absorption estimates come from Vertical Seismic Profiles (VSP). Geophysicists typically quantify the reliability of the derived estimates by simply quoting the errors determined when fitting a straight line to the logarithmic spectral ratio between the first arrivals at two depths. At best, this is an optimistic estimate for the uncertainty of the *effective* attenuation caused by both stratigraphic filtering and absorption. The existence of apparent “attenuation” caused by scattering, and particularly by thin layering, is well known (O’Doherty & Anstey, 1971; Schoenberger & Levin, 1974). The quotation marks around attenuation are put because, as I showed in Chapter 3, non-stationary reflectivity may cause apparent gain rather than loss of high frequencies through backscattering (reflections from the thin layers immediately beneath a VSP receiver). Using the VSP spectral ratios as an estimator of absorption is acceptable only when the scattering attenuation is small compared to the intrinsic attenuation. Often this is not the case, and the scattering effects must be subtracted from the effective attenuation to get a physically plausible absorption estimate (e.g.,

a positive Q). In doing so, the bias in the attenuation estimate is removed, but its variability is increased. Characterizing the bias and variability caused by thin layering is part of the goal of this paper, which is to quantify the total uncertainty in the absorption estimates. Other factors to consider are: uncertainty of the measured traveltime between two VSP receivers, receiver positioning errors when modeling the scattering, spectral distortions due to windowing, and ambient noise. I propose simple ways of quantifying the different uncertainties in the context of a field data example. Eventually, an absorption profile with fair error estimates is obtained.

4.2 Data

The data for this study are a VSP with known source and receiving instrumentation signatures, and well-logs acquired in the same borehole. The VSP is used to profile the effective absorption, i.e., the combined action of anelasticity and scattering. Sonic and density logs are used to compute synthetic seismograms from which to assess the share of scattering in the effective attenuation. The known signatures of the VSP source and receiving instrumentation allow us to find the frequency band for most reliable absorption estimation, as well as to evaluate the errors caused by the windowing of first arrivals and ambient noise.

The VSP consists of 175 traces, starting at 150 m below the surface. The depth-coverage is not uniform. The first six receivers are 150 m apart, spanning the first kilometer of the section. The rest of the receivers are 15 m apart and span the 1-3.5 km interval. The source for the VSP is a vibrator, 70 m from the borehole head. This offset is negligible compared to the receiver depths. The well-logs start at about 600 m depth and stop at the same depth as the VSP (Fig. 4.1).

4.3 Model parametrization

Surface seismic images suggest the investigated area is horizontally layered. Thus, we can consider a 1D earth model and invert for the average intrinsic Q of the major geological units. Four main intervals with thicknesses on the order of a kilometer are evident on the well-logs (Fig. 4.1). It is *a priori* known that there is a thin sandstone layer in the near surface, not captured by the well-logs. I assume that the top interval present in the well logs (600-1000 m) extends up to the base of the thin sandstone layer (the interval appears quite uniform on the VSP data, which start above the well logs). Thus, the preliminary earth model consists of five layers: a thin near-surface sandstone with a quality factor Q_0 , and four thick subsurface layers, characterized by mean quality factors Q_1 - Q_4 . Only the deep layer parameters Q_1 - Q_4 can be constrained by VSP spectral ratios because the VSP starts below the sandstone. In principle, Q_0 can be assessed from the signal in the shallowest VSP receiver if the source and receiving instrumentation signatures are known and if the source and receiver coupling with the ground is frequency-independent or known.

Initial estimates of $Q_1 - Q_4$ indicated that the quality factor of the top part of Layer 3 is substantially different from that of its lower part. Indeed, a closer inspection of the well logs reveals a thin layer at about 2500 m depth that may separate the interval into two zones with different fluid contents that result in different Q -values. Thus, I denote them by Q_{3a} and Q_{3b} and assess them separately.

4.4 Method of estimating Q

There are a number of approaches to estimating absorption from VSP experiments (Tonn, 1991). The most commonly used techniques are variations of the spectral-ratio method, developed by Hauge (1981) and Kan (1981). To make this

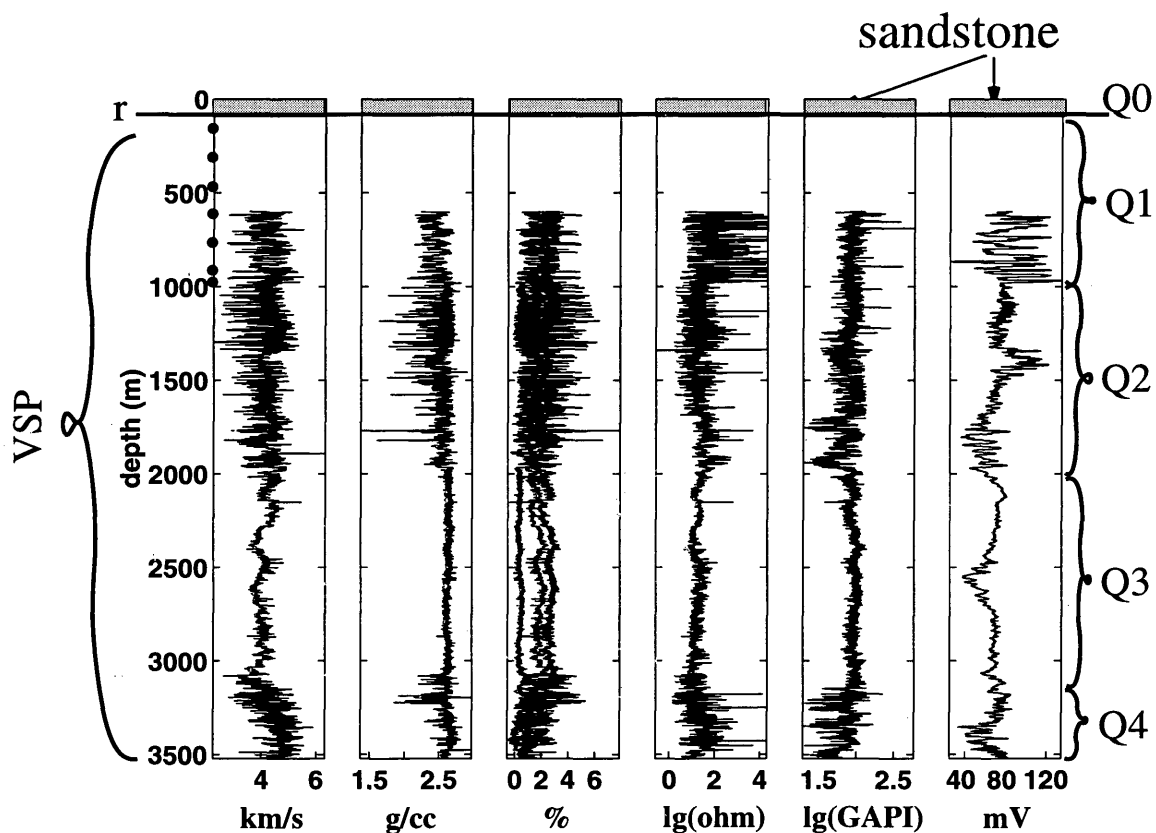


Figure 4.1. Well-logs used to identify the main subsurface intervals, the mean quality factors $Q_1 - Q_4$ of which are to be determined. Shown on the left is the span of the VSP; dots represent the first seven VSP receivers (with large non-uniform spacing; the rest of the receivers are close and uniformly spaced). The existence of a sandstone layer in the near surface is known *a priori* – its base with a reflection coefficient r is drawn approximately.

study relevant to as many users as possible, I consider a generic spectral-ratio approach, in which the effective attenuation of a given depth interval $[z_1; z_2]$ is measured by the slope S_{eff} of the log-amplitude spectral ratio between the first arrivals at depths z_1 and z_2 ,

$$\frac{20}{t_2 - t_1} \log \frac{A(f, z_2)}{A(f, z_1)} = \text{const}_f + S_{\text{eff}} f, \quad (4.1)$$

where t_1 and t_2 are the first-arrival traveltimes at the respective receivers, and f is frequency. The left hand side of eq. (4.1) is measurable from VSP data. The slope S_{eff} can be found by a linear regression and is related to the effective quality factor Q_{eff} by $S_{\text{eff}} \approx -27/Q_{\text{eff}}$. In a homogeneously absorbing medium, anelasticity and scattering contribute cumulatively to the effective attenuation, because arrivals with equal traveltimes have suffered the same amount of absorption regardless of their trajectory. Therefore,

$$S_{\text{eff}} = S + S_{\text{sc}}, \quad (4.2)$$

where $S \approx -27/Q$ characterizes the loss of high frequencies caused by absorption (i.e., Q is the intrinsic quality factor) and $S_{\text{sc}} \approx -27/Q_{\text{sc}}$ characterizes the spectral change due to scattering (Q_{sc} is the apparent quality factor). After S_{eff} has been assessed from VSP data (eq. 4.1), the intrinsic attenuation S , can be isolated by modeling and subtracting the scattering attenuation S_{sc} from S_{eff} . Given a reflection coefficient \log , and assuming the medium is horizontally layered, we can compute synthetic seismograms (absorption-free synthetic VSP) from which to get S_{sc} by fitting a line to the spectral ratio between the same two receivers from which S_{eff} was extracted.

Note that, while the intrinsic Q is assumed to be frequency-independent, we do not have to assume that Q_{sc} is frequency independent (even though, over the narrow frequency band of the seismic source, it arguably is); by fitting the spectral ratio between synthetic traces by a straight line we do not aim at estimating the total scattering attenuation. We only aim to get its linear component S_{sc} that causes the bias in the effective attenuation (S_{eff} being fit by a linear regression, too).

The intrinsic slope S is always negative (the intrinsic Q is positive). In contrast, the slope S_{sc} can be positive if reflections from below make the signal in the deeper receiver relatively richer of high frequencies than the signal in the shallower receiver (Chapter 3). In other words, contrary to common belief, scattering does not necessarily lead to an overestimate of the intrinsic absorption. Ignored scattering (thin layering) is the most probable cause for the unphysical, negative Q -factors reported sometimes in VSP studies.

Eq. (4.2) is strictly valid in homogeneously absorbing media. In reality, the thin beds responsible for the scattering are likely to have different quality factors. Thus, the medium is not homogeneously absorbing. However, as long as the absorption is constant on the macro-scale (e.g., within each thick layer of our model), eq. (4.2) can still be used, with S being an average characteristic of the region.

4.5 Preparations for spectral ratio estimation

4.5.1 Choice of receiver pairs

Suppose a VSP is acquired at n different depths in a given subsurface interval. The n traces can be combined into $n - 1$ non-redundant spectral ratios. There are many possible ways to pair the receivers. A reliable absorption estimate is obtained when the slope of the spectral ratio is large compared to its variability. Thus, I chose

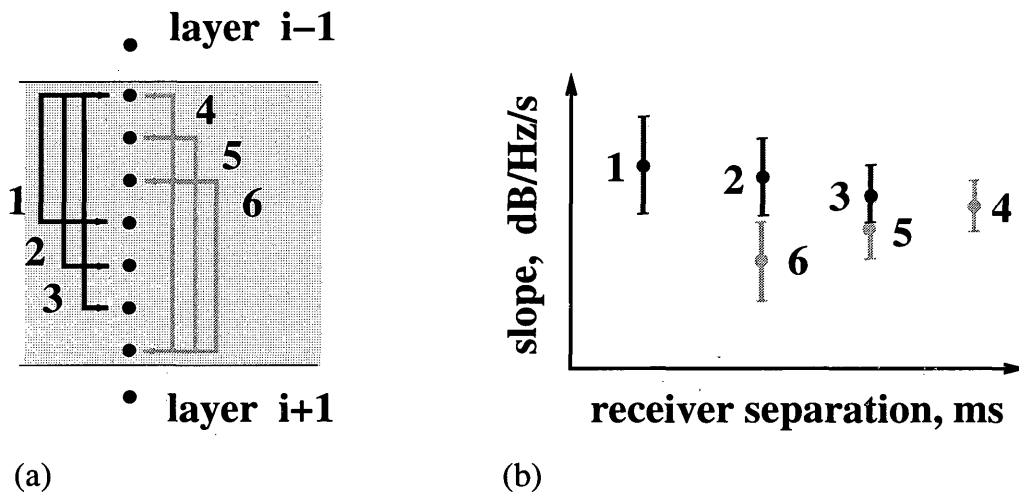


Figure 4.2. Cartoon: (a) Pairing the receivers in Layer i . Pairs containing the bottom-most receiver will be presented by a light color throughout the paper. Pairs containing the top-most receiver will be presented by a dark color. The distinction is made because the two sets sample different parts of the layer. (b) Indication for significant and systematic absorption variations in Layer i : small-separation pairs that sample predominantly the top or bottom halves of the layer (e.g., 3 and 4) give different estimates of the intrinsic attenuation, while pairs that span most of the layer (e.g., pairs 1, 2 and 6) show similar values for the intrinsic attenuation.

to maximize receiver separation. In every layer of the model, I paired the receivers from the top half of the layer with the receiver at the bottom of the layer, and the receivers from the bottom half of the layer with the receiver at the top of the layer (Fig. 4.2a). In this way all traces are used in a non-redundant manner, with minimum receiver separation of about half of the layer thickness.

As a bi-product of the chosen pairing scheme, we get an indication of whether the model discretization is reasonable. For the mean quality factor to be a representative characteristic of a layer, it should not vary too much throughout the layer. One definition of “varying too much” would be the estimated intrinsic Q of the top half of the layer to be substantially different from the intrinsic Q of the lower half. Such instances are easy to spot if we plot a measure of absorption versus receiver separation, as in the cartoon in Fig. 4.2b. This is how Layer 3 was identified as a candidate for splitting into two sub-layers, as already mentioned in Section 4.3.

A potential drawback of the proposed scheme for receiver pairing is that anomalies¹ in the top or bottom receiver would propagate into many spectral ratios and cause systematic errors. Severe problems may be identified in advance by looking at how typical the top- or bottom-trace spectra are, but milder abnormalities would be hard to find.

The existence of a correlation between the spectral ratios obtained from receiver pairs with a common receiver must be taken into account when computing the mean attenuation in a layer. Failing to do so would give an erroneous uncertainty estimate for the mean attenuation, even though the mean attenuation itself would not suffer much because the individual spectral ratios are consistent estimators of it. The covariance matrix needed for fair uncertainty analysis is derived in Appendix G.

¹An anomaly may be caused by coupling, source variations, noise outbursts, or inadequate scattering simulations (e.g., the source offset not being negligible for a shallow trace).

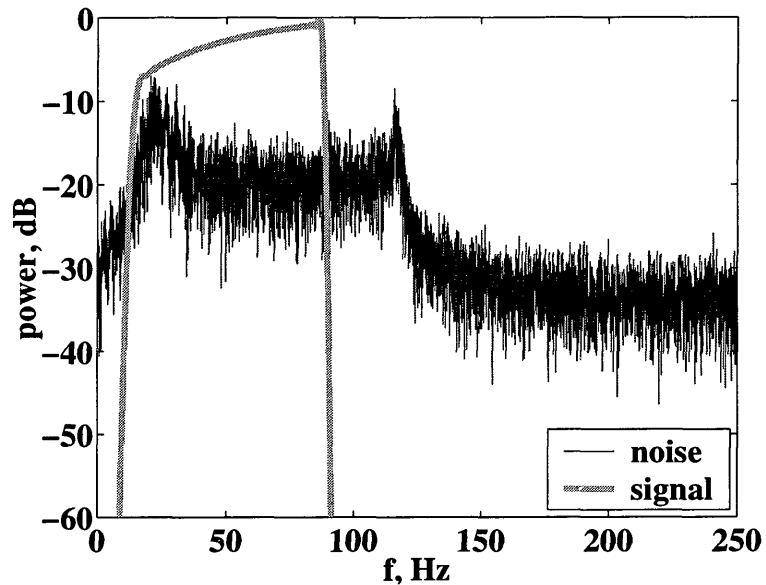


Figure 4.3. Power spectra of signal (source function filtered through receiver and instrumentation, and scaled to the peak amplitude of a typical VSP trace) and ambient noise.

4.5.2 Choice of frequency band

To get meaningful absorption estimates, it is important to identify the frequency band over which the signal-to-noise ratio is sufficiently high. Since scattering from thin layers will be explicitly taken into account in the absorption estimates, it does not represent noise (when not taken into account, this source-generated noise is a dominant cause of bias and uncertainty). The noise in our data is the ambient background that can be seen on the VSP traces before the first arrivals. Fig. 4.3 shows the power spectrum of the noise assessed from windows before the first arrivals together with a model of the signal spectrum, consisting of the known source function (Klauder wavelet), filtered by the known receiving instrumentation responses, and scaled to the first arrival amplitude of a representative VSP trace (a trace in the middle of the profile). As is seen from Fig. 4.3, only frequencies between 15 and 85 Hz can be used

for absorption estimation; the rest of the spectrum is dominated by noise. On most traces the signal-to-noise ratio in the usable frequency band is about 20 dB.

4.6 Errors

A basic assumption in the spectral-ratio method is that the source function and receiver coupling to the ground are identical at all VSP traces. I will assume it is true in our experiment; i.e., I assume that spectral ratios do not suffer from instrumentation artifacts. Spencer *et al.* (1982) proposed a way of relaxing this assumption by using the spectral ratio between upgoing events (reflections) in addition to the spectral ratio between downgoing events (first arrivals), presuming that both ratios characterize the attenuation of the same interval. However, I showed in Chapter 3 that while the spectral ratios between early time-windows are affected mainly by the medium between the receivers, spectral ratios between later time-windows are influenced by the properties of the near surface, because surface-related multiples make up a large portion of the trace at late times. Since in the present study the near surface is expected to have a significantly lower quality factor than the deeper layers, the approach of Spencer *et al.* (1982) would corrupt rather than improve the results. That is why, I assume that the source signature and receiver coupling do not vary from trace to trace. Since our VSP is of high quality, such assumption is reasonable. Some of the remaining causes of error in the effective and scattering attenuation estimates are discussed below together with strategies for quantifying them.

4.6.1 Error due to finite time windowing

Spectral-ratios are based on a time window around the first arrival. Suppose $A_2(f)/A_1(f)$ is the true amplitude ratio between the early portions of two traces.

What we measure is

$$\frac{W * A_2}{W * A_1} \neq \frac{A_2}{A_1}, \quad (4.3)$$

where $W(f)$ is the amplitude spectrum of the taper (the time window). The taper influence depends on the smoothness of A_1 , A_2 . A simplistic model of $A_1(f)$ is the signal model in Fig. 4.3, multiplied by the spectrum of the transmission impulse response of the shallow sandstone². The latter is needed because the reverberations in the sandstone are strong – they roughen the trace spectra (introduce notches). To assess the tapering effects, we can construct “true” spectra $A_2(f)$ by imposing an exponential decay with different Q values on $A_1(f)$, and compare the true slope of A_2/A_1 to the slope fitted to $W * A_2/W * A_1$ for a given taper. Unlike A_2/A_1 , the tapered ratio does not fall on a perfect straight line; i.e., tapering not only biases the absorption estimates, it induces some uncertainty in the slope estimates as well. I call the difference between the slope fitted to $W * A_2/W * A_1$ and the true slope the *tapering bias*. The residuals of the fit determine the *variability of the bias*, which is in fact the variability of the estimated attenuation introduced by the finite time window.

The tapering bias and its variability were measured for a 20% cosine taper with length 64, 128, or 256 samples. Qualitatively, the following was observed (Fig. 4.4):

- The bias is positive, i.e., negative slopes appear less negative (Q appears higher), while positive slopes corresponding to fictitious negative Q-factors appear even more positive.

²Here the sandstone layer is modeled as a homogeneous slab with one-way time-thickness of 15 ms (Appendix F), bounded by reflection coefficients -1 (top) and -0.45 (bottom).

- The bias decreases as the true Q increases.
- Longer windows reduce both the bias and the variability of absorption estimates. The bias is reduced because the biases of the individual amplitude spectra in the spectral ratio are reduced. The variability is reduced mainly because of the larger number of frequency samples in the usable frequency band. A longer taper also preserves better the exponential relationship between A_1 and A_2 and allows less leakage of noise from outside the useful frequency band (next section). The increased stability of the spectral ratio slopes estimated from long time windows has been noted by Goldberg *et al.* (1984) and Ingram *et al.* (1985) when studying spectral ratios between sonic log waveforms.
- For all windows and Q -values tested, the tapering bias was small compared to the other uncertainties in the absorption estimates (quantified later).

Given the latter, I decided to use the shortest 64-sample (128 ms) taper in order to localize the attenuation estimates as much as possible (a long time window would carry information about regions far away from a receiver pair, especially in a high-velocity medium).

The ordinate values in Fig. 4.4a and 4.4b show that the bias and its uncertainty are comparable. Thus, the true slope falls within the error bars of the measured slope. Moreover, the bias for the 64-point taper is only 1% of the measured slope (compare the vertical to the horizontal scale in the Fig. 4.4a). Thus, the windowing effect is negligible, despite that the trace spectra are rough. This seems to contradict earlier findings (e.g., Sams & Goldberg, 1990)³ and permits us to use relatively simple spec-

³A likely explanation is that the notches in our trace spectra occur at the same frequencies at all receivers, and the spectral ratios near them do not fluctuate much more than at other frequencies. This is true even in the presence of noise, when tapering may stabilize the spectra near the notches by “leaking signal” into them from the neighboring regions.

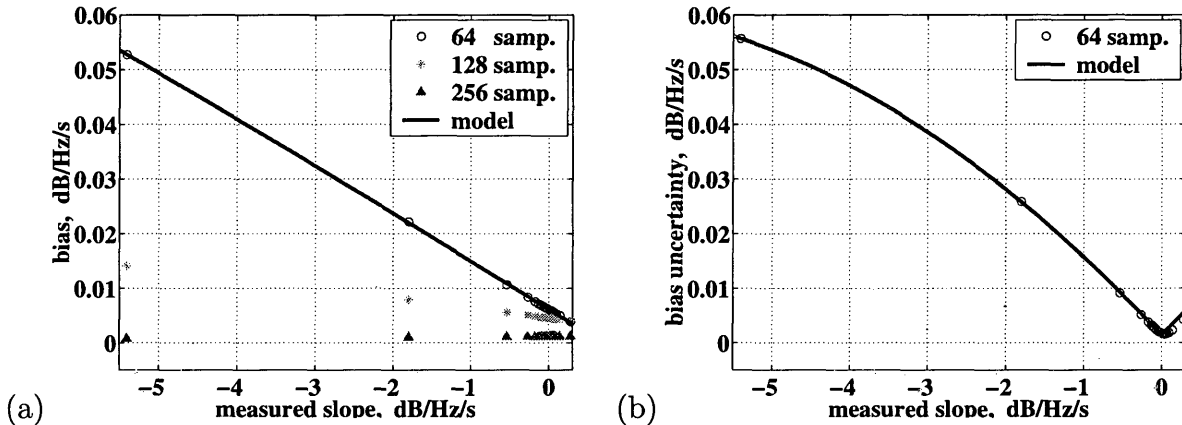


Figure 4.4. Tapering effects in the absence of noise: (a) slope bias measured over the 15-85 Hz band for three window lengths; the data for the 64-sample window are fit by a linear regression. (b) variability of the bias estimate for a 64-point taper – measured (circles) and fit (solid line) by a quadratic function of the measured slope magnitude.

tral estimation techniques (e.g., tapering) instead of, say, multi-tapering (Thomson, 1982; Walden, 1990) or data flipping (Pan, 1998). Such more sophisticated methods are needed when attenuation is estimated “point-wise” from individual frequency samples (e.g., Patton, 1988) rather than from the slope fit over many frequencies.

4.6.2 Ambient noise

Since background noise is time-windowed together with the signal, it makes sense to consider the combined effect of tapering and ambient noise on the absorption estimates. The bias estimation procedure from the previous section was repeated after adding ambient noise (assessed from windows before the first arrivals) to the time-series corresponding to A_1 and A_2 (Fig. 4.5). Now the bias is larger than in the noise-free case; namely, it is about 4% of the measured slope for $Q = 5$, 13% of the measured slope for $Q = 50$, etc. (Fig. 4.5a). As the true Q increases, the relative value of the bias increases, even-though its absolute value decreases. The absolute

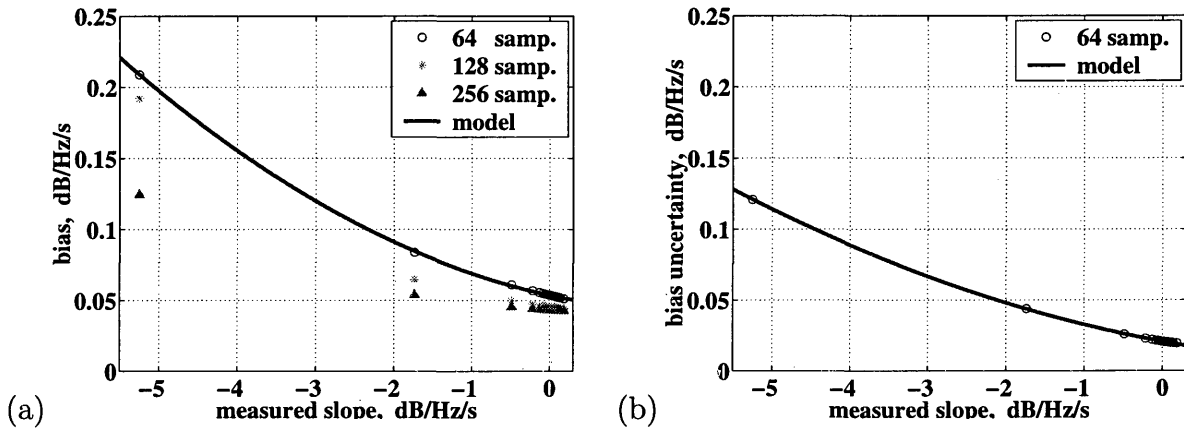


Figure 4.5. Analogous to Fig. 4.4 but in the presence of ambient noise: (a) bias for three window lengths; the data for 64-sample taper are fit by a quadratic model. (b) variability of the bias estimate for a 64-point taper – measured (circles) and fit (solid line) quadratic model.

bias decrease is slower than in the noise-free case, because noise makes the records in two receivers different even if the medium is non-absorbing. Also, unlike in the noise-free case, the true slope is outside the error bars of the measured slope (compare the ordinates in Fig. 4.5a, 4.5b).

To quantify the combined effect of background noise and windowing on attenuation estimates, numerical models were derived from the data in Fig. 4.5. Now both the bias and its variability can be fit by quadratic functions of \hat{S} , i.e.,

$$b_S = \alpha_0 + \alpha_1 \hat{S} + \alpha_2 \hat{S}^2 \quad (4.4)$$

and

$$\text{Var}(b_S) = \beta_0 + \beta_1 \hat{S} + \beta_2 \hat{S}^2 \quad (4.5)$$

The estimated coefficients $\alpha_{0,1,2}$, $\beta_{0,1,2}$ for the 64-point taper are used later to predict the tapering and ambient noise errors in S_{eff} and S_{sc} .

4.6.3 Window positioning and traveltimes uncertainties

Near the first arrival, seismic traces are not stationary, so the frequency content of an early window is sensitive to its exact position. For spectral ratios to measure the earth filtering, care should be taken to window the same signal on all traces. In the absence of significant dispersion (as in our data set), this can be done by adjusting the window position so that the first-arrival peaks at the same instant relative to the beginning of the window on every trace. This is an important detail in the preparation for absorption estimation. Inconsistent windowing causes erratic behavior of the spectral ratios.

The time separation Δt between the receivers in a given pair [$\Delta t = t_2 - t_1$ in eq. (4.1)] can be measured from the first-arrival peaks with a precision on the order of the sampling interval, e.g., $\sigma_{\Delta t} \approx \pm 2$ ms. This uncertainty propagates in the spectral ratio slope as

$$\sigma = \frac{\sigma_{\Delta t}}{\Delta t} \hat{S}, \quad (4.6)$$

where $\hat{S} = S_{\text{eff}}$, for example.

4.6.4 Receiver positioning errors in the synthetic seismograms

The timing uncertainty described by eq. (4.6) is present only in ratios between real VSP traces, not in synthetic traces (the time separation between them is known).

However, since the receiver positions for the synthetic traces are determined by the first-arrival traveltimes measured on the VSP traces⁴, errors in VSP traveltimes translate into positioning errors in the synthetic data – the receivers in the scattering simulations and those in the real VSP are not identically positioned with respect to the fine structure of the subsurface. As a consequence, the spectra of the synthetic traces do not match wiggle-by-wiggle the VSP spectra. The *slope* of a spectral ratio is less sensitive to such positioning errors than the spectral ratio itself. That is why I chose to compensate for the scattering by first fitting the slopes of the synthetic ratios and then subtracting them from the slopes of the real VSP ratios, rather than first subtracting the synthetic ratios from the VSP ratios and then fitting a slope. The sensitivity of S_{sc} to local interference (which changes with receiver position) depends strongly on the usable frequency band. In our case of a 64-point taper and 2 ms sampling, the usable frequency band has only 11 samples, and the slope uncertainty can be significant.

Suppose t is the first-arrival traveltime measured on a real VSP trace. Let σ_t denote its uncertainty. This traveltime uncertainty translates into a receiver positioning error in the synthetic VSP, which in turn, leads to a variability σ_{pos}^2 in S_{sc} . According to the error-propagation method,

$$\sigma_{pos}^2 = \left(\frac{d S_{sc}}{d t} \right)^2 2 \sigma_t^2 \quad (4.7)$$

The coefficient 2 is there because each of the two receivers in the pair from which S_{sc} was estimated has a positioning uncertainty σ_t . For this particular data set I assume

⁴A Goupillaud model is used to generate the synthetic seismograms; thus, receiver positions are specified in terms of traveltime from the earth surface.

$\sigma_t = \pm 1$ ms. The squared derivative in eq. (4.7) can be assessed by differencing the estimated slopes S_{sc} for each set of receiver pairs with a common receiver (only one receiver is moving), and taking the mean of the squared results, i.e.,

$$\left(\frac{d S_{sc}}{d t}\right)^2 = \text{mean}_i \left(\frac{S_{sc}^{(i)} - S_{sc}^{(i-1)}}{t^{(i)} - t^{(i-1)}}\right)^2, \quad (4.8)$$

where $t^{(i)}$ is the first arrival travelttime at the moving receiver from pair i . I assign the same σ_{pos}^2 to all pairs with a common receiver.

4.6.5 Fitting uncertainties (local interference)

Now let us concentrate on the uncertainties that are inherent to the problem rather than caused by imperfect measurements.

Unlike the intrinsic attenuation, which can be described by an exponential law at seismic frequencies, scattering attenuation can be described by a certain law only in a statistical sense. For a given realization of the medium, each frequency is modulated by local interference so that a spectral ratio never falls on a straight line even if the statistical average does. This has several implications to absorption estimation in heterogeneous media:

- A spectral ratio slope estimated from an error-free experiment has a finite uncertainty.
- Effective-attenuation estimates should be corrected for the scattering measured over the *same frequency band*; it can be quite different from that measured over a larger frequency band (Fig. 4.6). The stronger the scatterers, the larger the deviation of the locally fitted slope from the average can be.

- If S_{eff} and S_{sc} are assessed from the same frequency band, the additional linear trend in S_{eff} caused by the *particular realization* of scattering over the target frequency band is modeled and removed; it is not noise. Only the residuals of the fit constitute noise in the spectral ratios (both in the real and synthetic VSP). Assuming those residuals are independent and normally⁵ distributed, the uncertainty of a spectral-ratio slope is well known (e.g., Johnson & Wichern, 2002):

$$\sigma_{fit} = \frac{\sigma_e}{\sqrt{n_f} \sigma_f}, \quad (4.9)$$

where σ_e is the standard deviation of the residuals of the least-square fit, n_f is the number of the data points (frequency samples) in the usable frequency band and σ_f is the standard deviation of the frequency samples (i.e., σ_f characterizes the width of the usable frequency band). In a perfect world, the residuals of the fit for a given receiver pair would be the same for the real and the synthetic VSP. In reality, they are only on the same order of magnitude but are not identical mainly because of positioning errors in the synthetic VSP.

4.7 Estimating attenuation

Now we are ready to derive some attenuation estimates. First, the effective attenuation is evaluated from the VSP data. Then, thin-layering contributions are assessed and subtracted to isolate absorption. Finally, the absorption estimates from

⁵In fact, the residual distribution seems sharper than a Gaussian, so eq. (4.9) may overestimate the slope uncertainty.

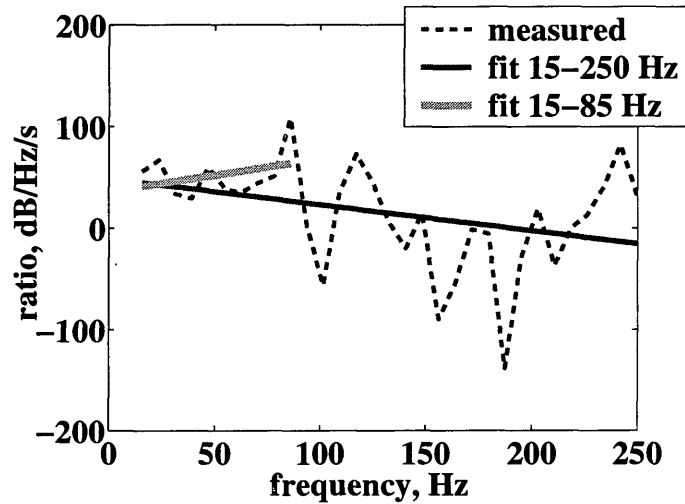


Figure 4.6. Linear fit in the presence of scattering – the estimated spectral slope depends on the frequency band used.

different receiver pairs are appropriately weighted and averaged to get the mean absorption (mean intrinsic Q) in each layer.

4.7.1 Effective attenuation from VSP data

The first arrivals on all traces were windowed by a 64-point 20% cosine taper, positioned so that the main event was not degraded⁶. The receivers were paired as illustrated in Fig. 4.2, and a linear regression was used to fit the spectral ratios on a log-linear scale (eq. 4.1) over the 15-85 Hz band. The uncertainty of the obtained slope S_{eff} has two main components. One comes from interference [fitting error – eq. (4.9)], the other comes from measuring the time-separation between the receivers (eq. 4.6). Thus,

⁶Since the first-arrival waveform is acausal (distorted Klauder wavelet), the early part of it is inevitably cut by the taper. The “main event” which I tried to preserve starts with the trough before the main peak, and carries most of the energy of the arrival.

$$\text{Var}(S_{\text{eff}}) = \frac{\sigma_e^2}{n_f \sigma_f^2} + \frac{\sigma_{\Delta t}^2}{\Delta t^2} S_{\text{eff}}^2 \quad (4.10)$$

Typically, the first term is an order of magnitude larger than the second one.

The error caused by tapering and ambient noise, albeit small compared to the uncertainty (4.10), is also taken into account. For each receiver pair, the predicted bias (eq. 4.4) is subtracted from the estimated slope S_{eff} and the slope uncertainty is adjusted according to

$$\text{Var}(S_{\text{eff}} - b_S) = (1 - 2\alpha_1)\text{Var}(S_{\text{eff}}) + \text{Var}(b_S), \quad (4.11)$$

where $\text{Var}(b_S)$ is predicted from S_{eff} by eq. (4.5), and α_1 is the coefficient from the bias model (eq. 4.4). This is a very minor adjustment compared to the total uncertainty of S_{eff} . The so obtained effective slope estimates are shown in the left column of Fig. 4.7.

4.7.2 Scattering effects

The synthetic VSP for assessing S_{sc} was computed from the reflection coefficient log in Fig. 4.8 by a time-domain reflectivity code (Appendix E), assuming the medium is horizontally layered and non-absorbing. Spectral ratio slopes were estimated in the same manner as from the real VSP. The only difference is that the slopes S_{sc} contain positioning errors instead of timing errors, i.e., the equivalent of eq. (4.10) is

$$\text{Var}(S_{\text{sc}}) \approx \frac{\sigma_e^2}{n_f \sigma_f^2} + \sigma_{\text{pos}}^2, \quad (4.12)$$

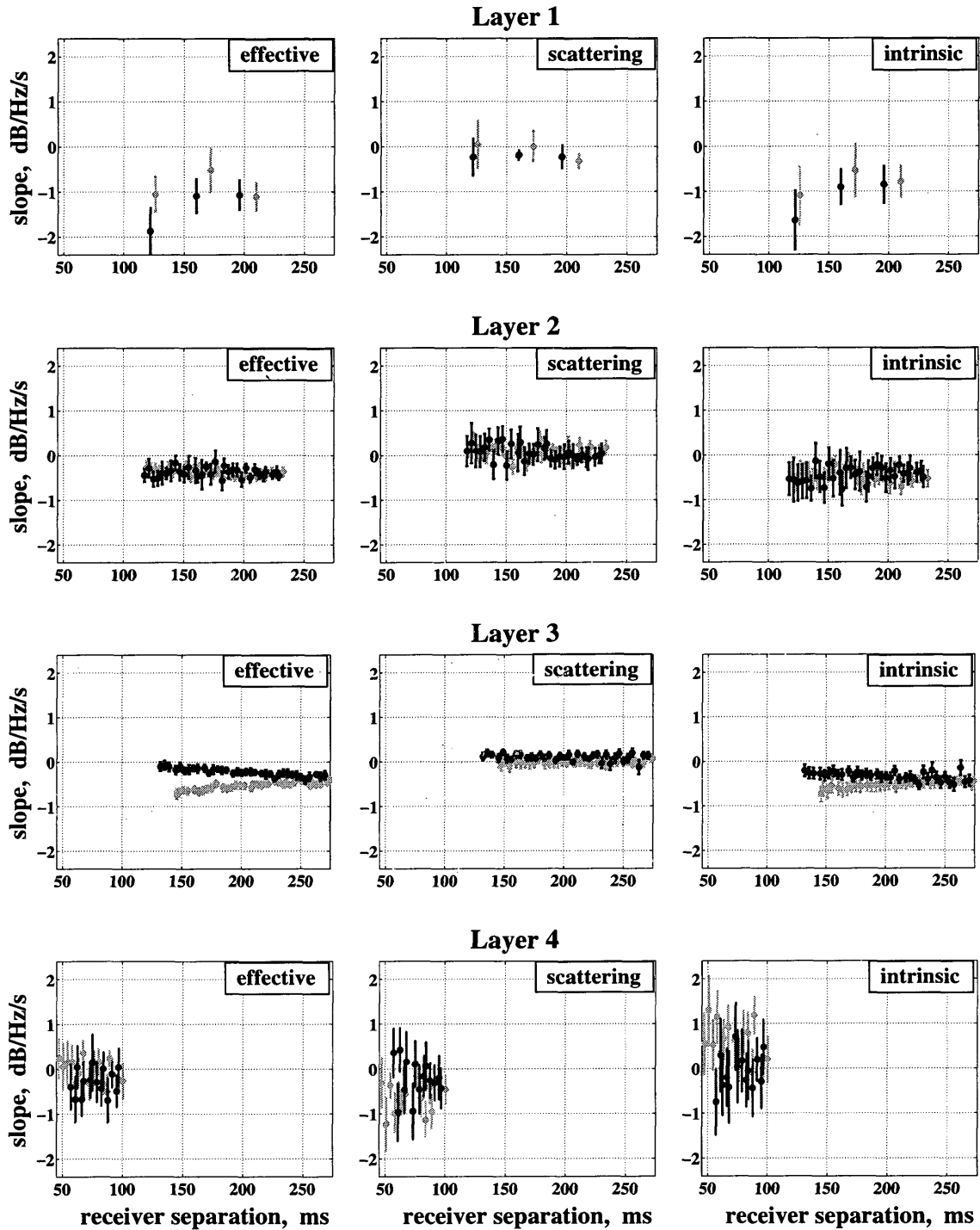


Figure 4.7. Attenuation estimators: (left) S_{eff} measured from VSP data, (center) S_{sc} measured from synthetic traces in a horizontally layered non-absorbing medium, (right) computed intrinsic attenuation: $S = S_{\text{eff}} - S_{\text{sc}}$. Dark and light data points correspond to receiver pairs that contain, respectively, the top and bottom receiver in a layer. All plots are on the same scale.

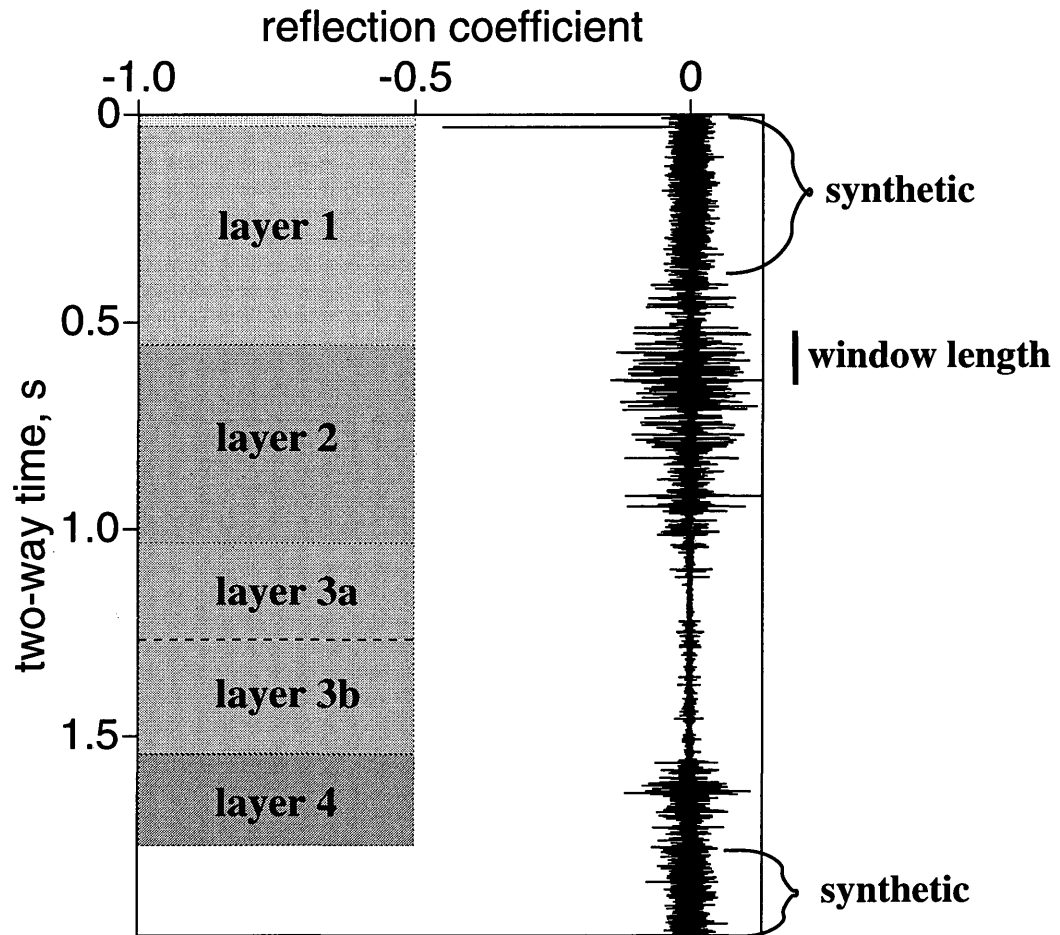


Figure 4.8. Reflectivity log used to predict scattering effects. Its construction is described in Appendix F. Shown on the right is the length of the taper used for first-arrival windowing.

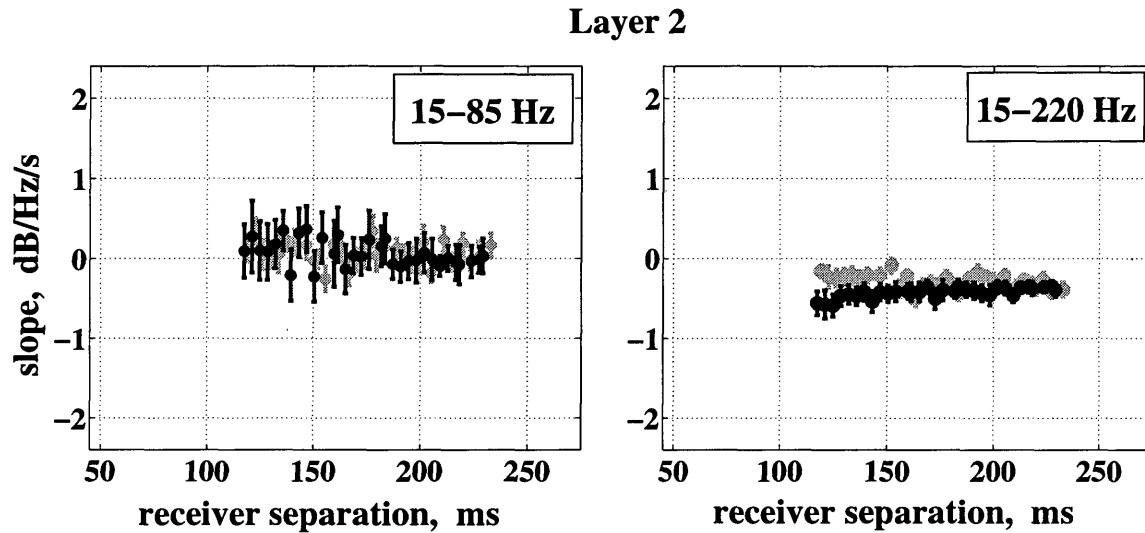


Figure 4.9. Scattering attenuation estimates in Layer 2 – local fit (left) versus global fit (right). The behavior of the global fit is in an excellent agreement with the theoretical predictions in Chapter 3. The local fit is quite erratic.

where σ_{pos}^2 is given by eq. (4.7). Usually the positioning error σ_{pos}^2 is smaller than the fitting uncertainty (the first term), but larger than the timing error in eq. (4.10).

The results for S_{sc} are shown in the central column of Fig. 4.7. Note that these are estimates from the narrow frequency band 15-85 Hz – they quantify the scattering effects as seen by the real VSP, not the scattering effects that would be measured over many realizations of the fine layering or over a larger frequency band. Being strongly influenced by local interference, these values of S_{sc} are hard to predict even qualitatively by looking at the reflectivity log in Fig. 4.8. For example, S_{sc} tends to be positive in Layer 2, while one would expect it to be negative, given the non-increasing reflection coefficient series in that layer (Chapter 3). Such negative values are readily observable if the spectral ratio slope is fit over a larger frequency band (Fig. 4.9).

4.7.3 Intrinsic attenuation (absorption)

Finally, the intrinsic attenuation for each receiver pair is found as $S = S_{\text{eff}} - S_{\text{sc}}$.

Its variance is

$$\text{Var}(S) = \text{Var}(S_{\text{eff}}) + \text{Var}(S_{\text{sc}}), \quad (4.13)$$

because the effective and scattering attenuation estimators are independent. Since both $\text{Var}(S_{\text{eff}})$ and $\text{Var}(S_{\text{sc}})$ are dominated by fitting errors (local interference), and the fitting errors are on the same order of magnitude for the VSP and synthetic spectral ratios, the uncertainty of the intrinsic attenuation estimate is about twice as large as that of the effective attenuation (Fig. 4.7 right).

The results for Layers 3 and 4 call for a comment. The effective attenuation in Layer 3 is clearly larger in the bottom part of the layer than in the top part. The scattering correction has reduced, but not eliminated the trend. This is why I divided the layer in two sub-layers (3a and 3b). The attenuation estimates for these sub-layers are shown in Fig. 4.10. The intrinsic attenuation in them turns out to be substantially different, indeed.

In Layer 4, a number of receiver pairs (especially among those containing the deepest receiver) give positive S_{eff} ; i.e., the signal appears to gain high frequencies with depth. This must be caused by reflections from the fine layering below the deepest receiver and indicates that the reflection coefficient series becomes substantially stronger beneath the borehole (Chapter 3). Unfortunately, this reflectivity change is not observable on the well logs, and thus, is not present in the reflection coefficient log used to predict the scattering effects (Fig. 4.8). Therefore, scattering and intrinsic attenuation cannot be separated for the deepest VSP receivers which feel the medium

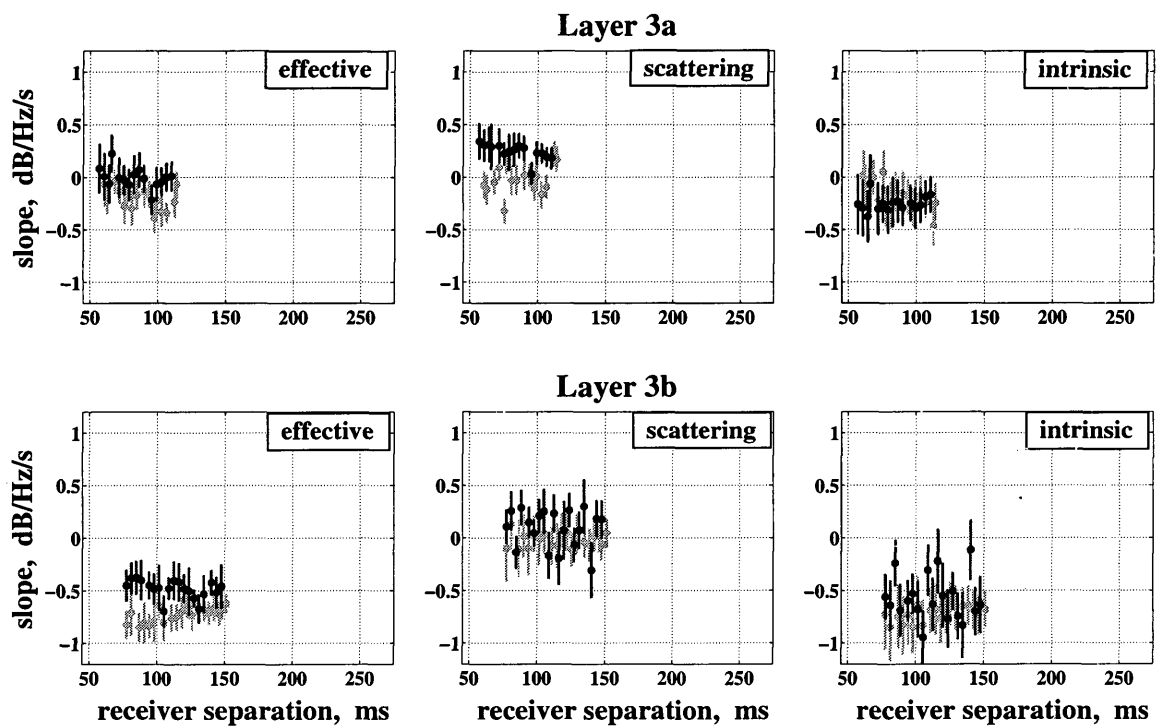


Figure 4.10. Subdivision of Layer 3 (plots analogous to those in Fig. 4.7).

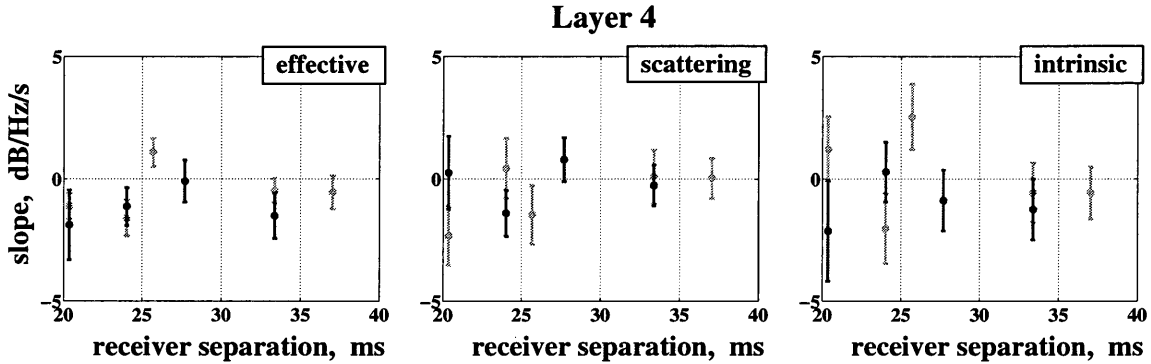


Figure 4.11. Attenuation estimates in Layer 4 from the top 10 receivers in it, which do not feel the padding of the reflection coefficient log below the borehole bottom; (plots analogous to those in Fig. 4.7).

beneath the borehole bottom. The intrinsic attenuation can be only assessed from the receivers that feel the “correct” fine layering captured by the well logs. There are ten such receivers in Layer 4, and the attenuation extracted from them is shown in Fig. 4.11. The reduced receiver separation leads to very large uncertainties. The ten usable receivers give three unphysical, though statistically plausible, intrinsic slopes (Fig. 4.11 right). I discarded the unphysical slopes when assessing the mean Q of Layer 4.

4.7.4 Mean intrinsic Q profile

As a final step in obtaining the mean absorption of the subsurface layers, the values of S from different receiver pairs were averaged by a weighted-least-squares procedure within each layer. The covariance matrix for the procedure has diagonal elements σ_{ii}^2 , given by eq. (4.13). The off-diagonal elements σ_{ij}^2 are non-zero for pairs i and j that have a common receiver, and are given by (Appendix G)

$$\sigma_{ij}^2 \approx \frac{1}{\Delta t_i \Delta t_j} \frac{\sigma_{A_0}^2}{n_f \sigma_f^2}, \quad (4.14)$$

where Δt_i is the time-separation in the i -th receiver pair, and $\sigma_{A_0}^2$ characterizes the uncertainty of the log-amplitude spectrum of the common receiver. It can be estimated by (Appendix G)

$$\sigma_{A_0}^2 = \frac{\text{median}(\Delta t^2 \sigma_e^2)_{\text{eff}}}{2} + \frac{\text{median}(\Delta t^2 \sigma_e^2)_{\text{sc}}}{2}, \quad (4.15)$$

where the subscripts 'eff' and 'sc' indicate estimation from the real and synthetic VSP respectively, σ_e is the standard deviation of the residuals [as in eqs. (4.10), (4.12)], and the median is taken over all pairs sharing the common receiver.

The mean-Q profile ($\bar{Q} = -27/\bar{S}$) resulting from this averaging procedure is shown in Fig. 4.12. Note that the error bars in Fig. 4.12 refer to the *mean* quality factor of each layer. They depend both on the variability of the quality factor inside each layer and on the data acquisition and inversion.

Not all estimates in Fig. 4.12 are the same. Shown by circles are estimates based on all available receiver pairs – they are purely data driven. Such an estimate for Layer 4 (using only 10 receivers) is not feasible because one third of the results correspond to unphysical Q values. I chose to discard them before computing the mean in Layer 4. The result is shown by a different symbol to indicate that this estimate of \bar{Q} is not like the others – it is conditioned by *a priori* knowledge about absorption (i.e., the intrinsic Q is positive). I also computed conditional estimates for Layers 3a and 3b by discarding outliers, even if physically plausible. The results (white crosses) turn out to be compatible with the unconditional estimates, but their error-bars (dashed in white) are smaller. In Layers 1 and 2 there were no obvious outliers.

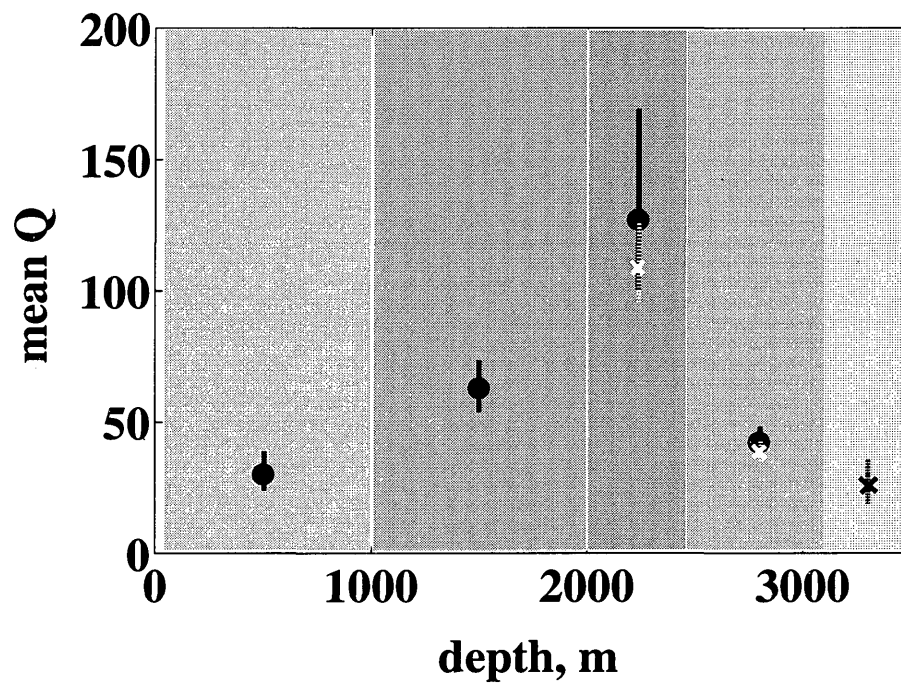


Figure 4.12. Mean intrinsic Q profile. The background shades visualize the layers, characterized by the mean Q . Circles indicate estimates derived from all available pairs. Crosses indicate conditional estimates, obtained by excluding outliers.

4.8 Discussion

The most remarkable feature of the intrinsic Q profile in Fig. 4.12 is that the absorption of each layer is clearly resolved (outside the error bars of its neighbors), despite that the data set was challenging⁷. A beneficial factor in obtaining such a result was the dense VSP coverage, providing many data points per layer. Another favorable factor is the geology, consisting of thick units with distinct properties and relatively low Q-factors (easier to assess than high Q-s). Last but not least, the reflection coefficient series was not very strong. The correlation between weak scattering and absorption resolution is clearly seen in Fig. 4.7. Compare, for example, the intrinsic attenuation obtained from pairs with separation 150-200 ms in Layers 3 and 2 (weak and strong reflectivity respectively) – the error bars are larger in the stronger reflectivity. The distinction between the absorption values in the top and bottom halves of Layer 3 would have been impossible in the presence of scattering as strong as that in Layer 2 – the absorption change would have been masked by the large variability of the absorption estimates.

The most uncertain slopes tend to come from pairs with a small separation. Again, this is largely due to scattering, rather than timing and positioning errors. If we had a purely transmission experiment (no reflections from below the receivers), the longer a pulse propagated through the scattering medium, the better the self-averaging in its amplitude spectrum would be. Shapiro & Zien (1993) showed that the standard deviation of the estimated scattering attenuation α is

$$\sigma_{\alpha} \propto \sqrt{\frac{\alpha}{L}}, \quad (4.16)$$

⁷Initial attempts to extract absorption from this particular VSP by feeding it to a commercial flow were unsuccessful.

where L is the distance traveled. As $L \rightarrow \infty$, σ_α diminishes and the spectral ratio of the output to the input pulse approaches its expected value, e.g., a straight line over a limited frequency band. The inability of the downgoing pulse to stabilize over a short path of propagation, especially in a strong reflectivity, is one of the reasons for the large fitting uncertainties in VSP spectral ratios. An additional reason is that reflections from below cause deviations from linearity in the spectral ratios that do not diminish as the receiver separation increases (they do not self-average). One way to reduce this uncertainty is to fit the spectral ratio over a large frequency band. However, this option is limited by the frequency range of the VSP – we need to assess the scattering as seen by the VSP, i.e., over a narrow frequency band. Another way to reduce the uncertainty caused by reflections from below is to separate the up- and down-going wavefields and apply the spectral-ratio method only to the downgoing part (Harris *et al.*, 1992).

To summarize, the uncertainties of all attenuation estimates are larger for pairs with a small separation, and in strong reflectivities. This could have been intuitively expected and has been noted in earlier studies (e.g., Spencer *et al.*, 1982).

It should be pointed out, however, that the scattering in a weak reflectivity can also play an important role in absorption estimation. For example, look at the effective attenuation in the almost homogeneous Layer 3a (Fig. 4.10, top left). Many of the slope estimates are positive (Q_{eff} is negative). Synthetic seismograms show that this is a scattering effect – after correcting for it, the intrinsic attenuation stands at about -0.25 dB/Hz/s (Fig. 4.10, top right). As an extra benefit from the thin-layering correction, the scatter (the deviation) of the attenuation estimates in Layer 3a has been reduced. This is easily seen for the set of dark data points – compare

their alignment before and after the scattering was subtracted. The consistency of the estimates suggests that, in terms of absorption, Layer 3a is quite homogeneous. The attenuation estimates from different receiver pairs, however, are not always made more consistent by the thin layering corrections – it depends both on the geology and the quality of the estimates. For instance, the scatter of the estimates is increased in Layer 3b, despite that the reflectivity strength in it is comparable to that in Layer 3a. Layer 3b is another illustration of how thin layering can be important even when the reflectivity is weak. The *effective* attenuation appears different for the top and bottom parts of Layer 3b (Fig. 4.10 left). However, the scattering corrections reconcile the results for the two sets of receiver pairs, and the *intrinsic* attenuation does not exhibit a systematic variation with depth (Fig. 4.10, bottom right).

The price of removing the bias caused by thin layering is increased uncertainty. The variance of S is essentially twice that of S_{eff} . Given the trade-off between bias and variability, is it worthwhile to correct for the scattering? The conventional way to answer this question is to look at the mean square error (sum of variance and squared bias) of the two absorption estimators. The mean square error (MSE) of the effective attenuation is

$$\text{MSE}(S_{\text{eff}}) = \text{Var}(S_{\text{eff}}) + S_{\text{sc}}^2, \quad (4.17)$$

while for the unbiased estimator S it is

$$\text{MSE}(S) = \text{Var}(S) = \text{Var}(S_{\text{eff}}) + \text{Var}(S_{\text{sc}}) \quad (4.18)$$

Since in most cases of slope fitting over a narrow frequency band $\text{std}(S_{\text{sc}}) > |S_{\text{sc}}|$,

	$ S_{sc}/S $
Layer 1	20%
Layer 2	30%
Layer 3a	70%
Layer 3b	20%
Layer 4	25%

Table 4.1. Scattering versus intrinsic attenuation – a median estimate over all receiver pairs in a given layer.

eqs. (4.17) and (4.18) give $MSE(S) > MSE(S_{\text{eff}})$; i.e., in a mean-square-error sense, the corrected slope S is worse than S_{eff} , at least for an individual receiver pair. For the average attenuation in a layer, it may happen that $MSE(\bar{S}) < MSE(\bar{S}_{\text{eff}})$ if the scattering compensation makes the estimates of S from different receiver pairs more consistent. In our example, this happens only in Layers 1 and 3a. So it seems that, even in terms of layer averages, the effective attenuation has a smaller MSE than the intrinsic attenuation. Unfortunately, this is not a green light to ignore the scattering. In some cases it is more important to have an unbiased estimate rather than a small variability. An obvious such case is when S_{eff} is positive (i.e., $Q_{\text{eff}} < 0$). Another is when the bias due to scattering is large compared to the intrinsic attenuation. Estimates of $|S_{sc}/S|$ are shown in Table 4.1. Note that the layer with the highest fraction of scattering (highest albedo) happens to be the almost homogeneous but low-absorbing Layer 3a.

Absorption uncertainties depend on many factors, but, if we are to summarize in coarse figures, we could say that an absorption estimate derived from a single receiver pair has an uncertainty $\sim 50\%$ (median over all receiver pairs in this study). To reduce it to about 10% , we have to average at least 25 independent estimates. With VSP receiver spacing of $\sim 10^1$ m, that corresponds to a typical absorption

resolution of $\sim 10^2$ m.

4.9 Conclusion

To characterize lithology or reservoir conditions from attenuation data, one must separate absorption from scattering effects and have an objective estimate of the absorption uncertainties. The price for removing the scattering is increased variability of the absorption estimates. It is worthwhile to pay if the apparent attenuation is large compared to the intrinsic attenuation. This may happen even when the scattering is weak. Therefore, scattering should not be neglected just because “the medium seems homogeneous” before its share in the effective attenuation has been assessed.

Incoherent scattering is the largest source of uncertainty. A fundamental way to reduce its influence is to have a VSP with a broader frequency band; additional improvement may be sought through wavefield separation. The next largest uncertainties are associated with positioning and timing errors in the synthetic and real VSP respectively. Ambient noise and tapering have a much smaller impact on the fitted slopes. Finally, the correlation between attenuation estimates from pairs with a common receiver must be taken into account when estimating the uncertainty of the mean quality factors of thick geological units.

Chapter 5

SEISMOGRAMS AND REFLECTIVITY – CAN WE SEE THE SUBSURFACE?

5.1 Introduction

In pursuit of higher resolution, we strive to compress the source signature and compensate for absorption in seismic data. Yet, we might not be able to see the reflection coefficient series r of the subsurface. Suppose we have a spike-like source and no absorption. Let us consider a zero-offset trace acquired over a horizontally layered medium, and compare that trace (synthetic seismogram) with the reflection coefficient series (called “reflectivity” for short). The two differ by the presence of transmission losses and multiples on the trace. Although an individual multiple is orders of magnitude smaller than a primary reflection, the number of possible multiples in the finely layered medium represented by r grows rapidly with time. Eventually all of the source energy is transferred to the multiples. While some short peg-leg multiples reinforce the primary reflections (O’Doherty & Anstey, 1971), other multiples obscure the primary reflections. This note investigates to what extent the earth reflectivity is visible on the trace. For that purpose two synthetic examples with a strong and a weak reflectivity are considered. The strong reflectivity is similar to that of Well 8 of Walden & Hosken (1985, 1986); its standard deviation is about 0.1. The weak reflectivity is simply the strong one, down-scaled by 50%. As we will see, multiples can dominate the trace and significantly deteriorate its correlation to the reflection

coefficient series even in a weak reflectivity.

5.2 Multiples take over

First, let us see how energy is distributed between primary and multiple reflections along the trace. To that end, three synthetic seismograms were computed from each reflectivity r – primary reflections only (y), with all multiples included (x), and with internal multiples only (x_0); x_0 is computed in the same way¹ as x except the earth’s surface reflection coefficient is set to 0 instead of -1. Fig. 5.1 shows that transmission losses at interfaces diminish primary reflections fast; primaries are virtually non-existent after 1 s in the stronger reflectivity. Their energy is transferred to internal and free-surface multiples. At late times, free-surface multiples dominate the trace. What a “late” or an “early” time is, depends on the reflectivity strength. A closer comparison between Fig. 5.1a and 5.1b shows that time runs four times slower in the twice weaker reflectivity. For example, internal multiples overtake primaries at about 250 ms in the strong reflectivity, and at 1 s in the weak one; they comprise 20% of the trace energy at 1 s in the strong reflectivity, and at 4 s in the weak one, etc. This observation agrees with the finding of Sheng *et al.* (1986) that scattering behavior is universal on a time-scale $\tau/[l(f)/v]$, where τ is the observation time, $l(f)$ is the frequency-dependent localization length, and v is the average velocity of the medium, the localization length in turn being inversely proportional to the square of the reflectivity strength (square of the relative impedance variation; Shapiro & Zien, 1993). Being aware of this time-scale relation between the strong- and weak-reflectivity cases facilitates their further comparison, and allows one to extrapolate

¹The synthetic seismograms are for plane waves at normal incidence and were computed by the time-domain reflectivity codes *sugoupillaud* and *sugoupillaudpo* freely distributed through SU (Cohen & Stockwell, 2002); see Appendix E.

the results from this study to other data.

Fig. 5.1 shows that multiples overtake the trace at times well before a typical exploration target. However, this does not necessarily mean that deeper reflectivity cannot be seen on the trace, because small-lag multiples are known to reinforce the primaries. Next, we investigate how visible the true earth is by comparing traces to reflectivity.

5.3 Correlation between traces and reflectivity

Fig. 5.2 shows the correlation coefficient between a set of time-windows on the traces x , x_0 , y and the same time-windows on the reflectivity series r . While the primaries-only seismogram correlates almost perfectly² with the reflection coefficient series, traces with multiples lose their correlation with r fast. For example, the correlation coefficient drops below 0.5 at about 0.5 s for trace with all multiples in the weak-reflectivity case. (Note that in terms of correlation, too, the time-scale for the twice weaker reflectivity is four times larger. That is why only figures for the strong-reflectivity case will be shown further.) The fast loss of correlation in Fig. 5.2 is alarming, but for practical purposes, it is a bit pessimistic, too, because the correlation was taken without band-limiting the data, i.e., including all frequencies up to the Nyquist. As Fig. 5.3 shows, the correlation drops faster at higher frequencies. Since much of the energy in r and x is carried by high frequencies (Chapter 2), the correlation coefficients in Fig. 5.2 probably underestimate those observed in practice with a lower-frequency seismic source. To get a more realistic estimate, the reflectivity series and all traces were band-limited to the low one-third of the original frequency

²This high correlation is locally valid, i.e., over a short time-window, in which the overall decay in y caused by transmission losses is small.

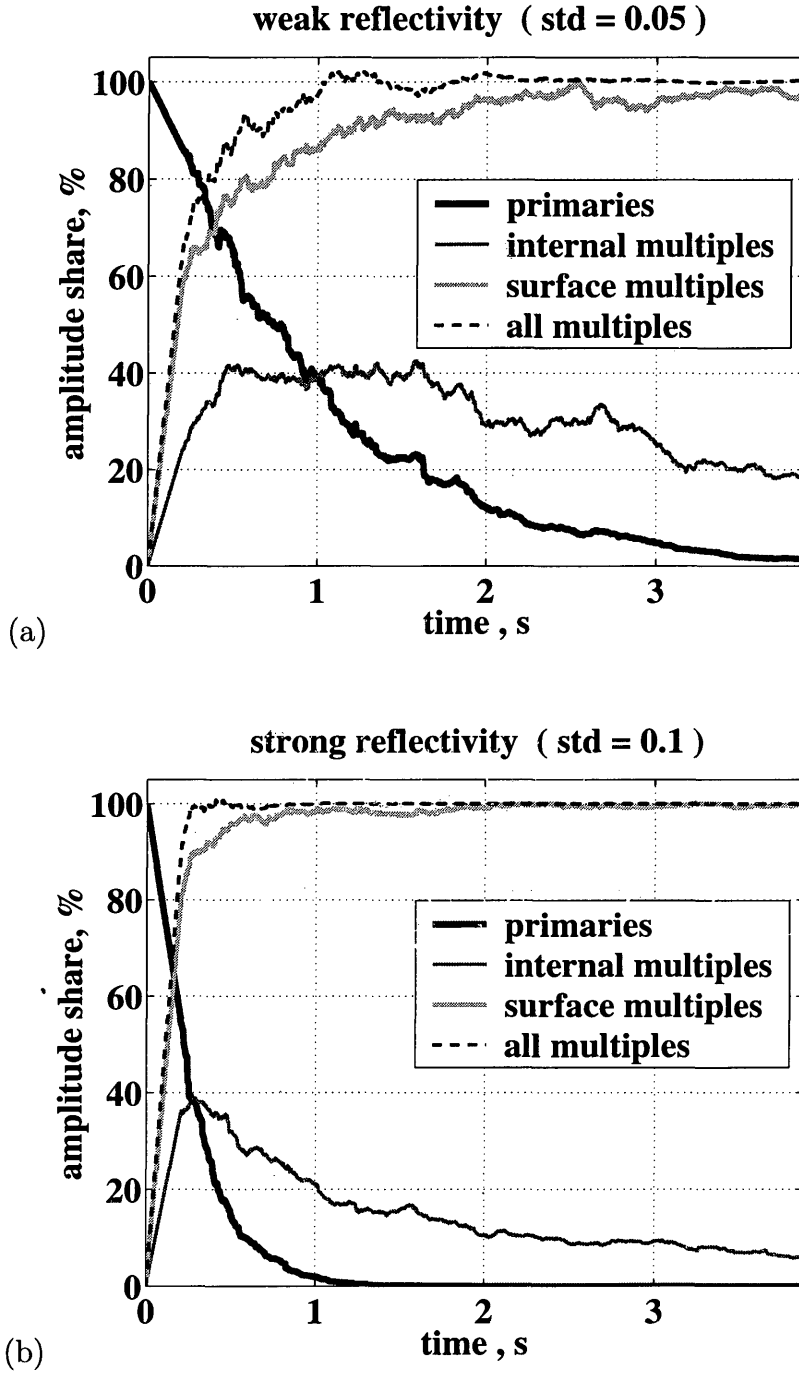


Figure 5.1. Share of primaries and multiples on the trace, computed as (from top to bottom of legend): $\text{std}(y)/\text{std}(x)$, $\text{std}(x_0 - y)/\text{std}(x)$, $\text{std}(x - x_0)/\text{std}(x)$, $\text{std}(x - y)/\text{std}(x)$. The sum of shares may exceed 100% because it does not take into account interference. (a) weak-reflectivity example; (b) strong-reflectivity example.

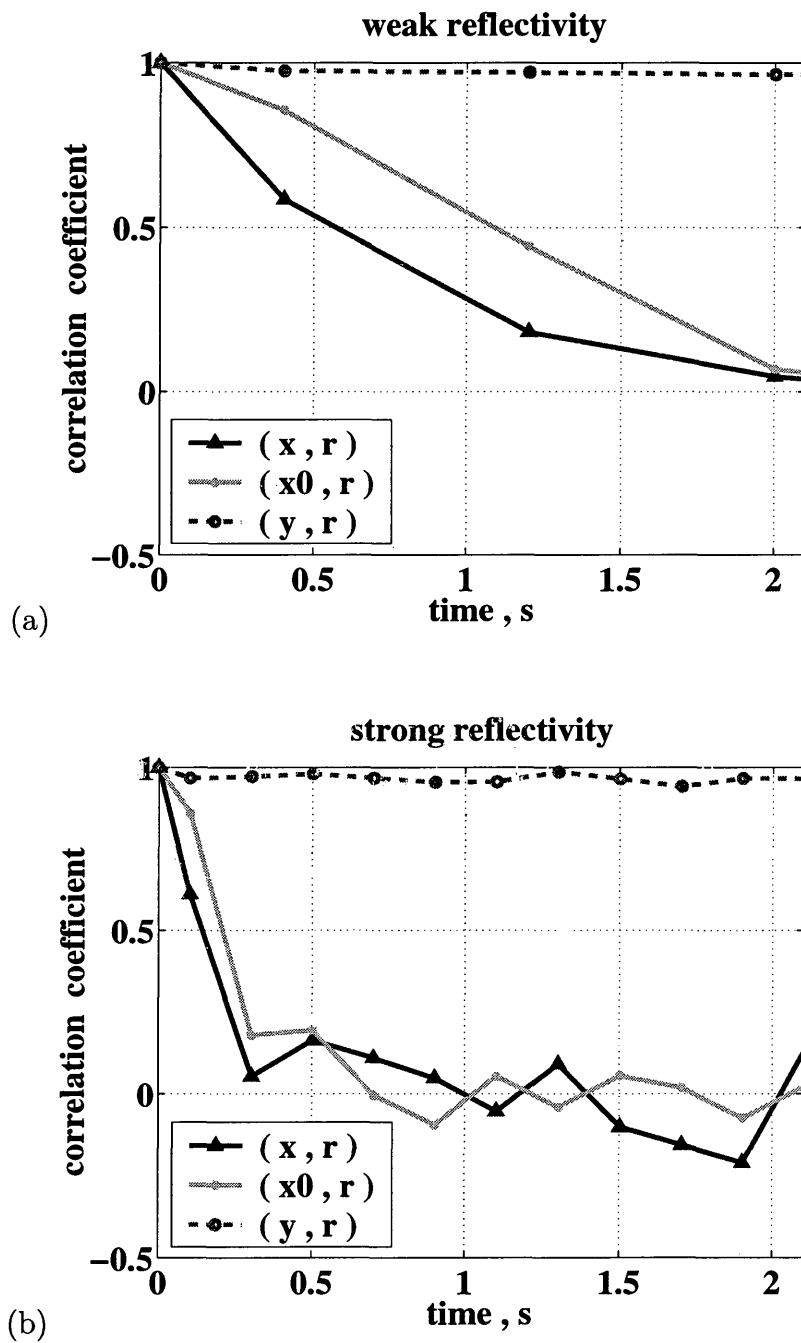


Figure 5.2. Zero-lag correlation between synthetic seismograms (x, x_0, y) and reflectivity (r) . Each data point is for a time window centered at that time, with length (a) 200 samples for the weak reflectivity, (b) 50 samples for the strong reflectivity.

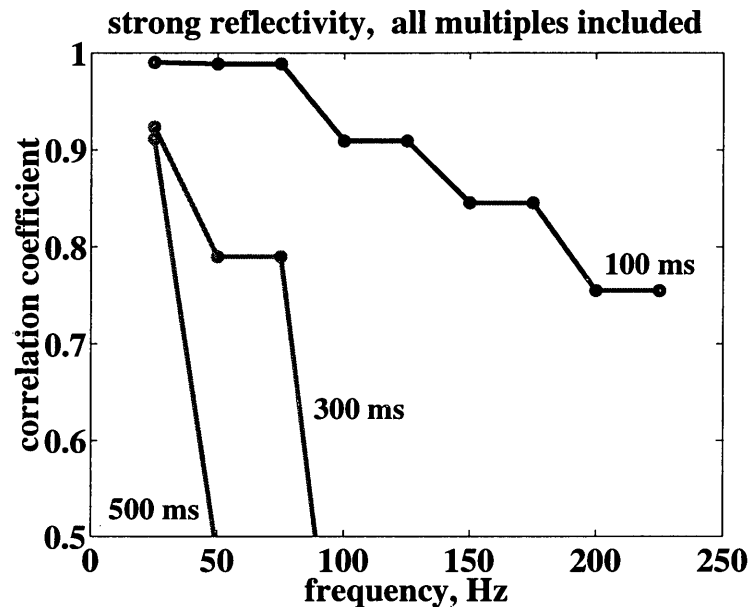


Figure 5.3. Zero-lag correlation between narrow band-pass filtered traces and reflectivity. The three curves are for time windows centered at 100, 300, and 500 ms, respectively. The picture is virtually the same in weak reflectivity for four-times later windows (0.4, 1.2, 2 s). In the absence of surface-related multiples, the trends are similar but the correlation is a bit higher at early times.

range (i.e., to 3-80 Hz). The corresponding correlation coefficients are shown by a gray dashed line in Fig. 5.4. They turn out higher, indeed, especially at early times; yet, the improvement is not large.

The correlation values considered so far were zero-lag; the fact that the trace may be a stretched version of the reflectivity due to dispersion or effective-velocity propagation Backus (1962) was not taken into account. Next, we allow for this possibility. To estimate the time-drift (velocity difference) between trace and reflectivity, each of them was narrow band-pass filtered, and for each frequency, the lag of the correlation maximum was found for a number of time windows. The purpose of the band-pass filtering was to facilitate cycle skipping detection; it is much more difficult to find a systematic time shift from the full-bandwidth trace because waveforms are

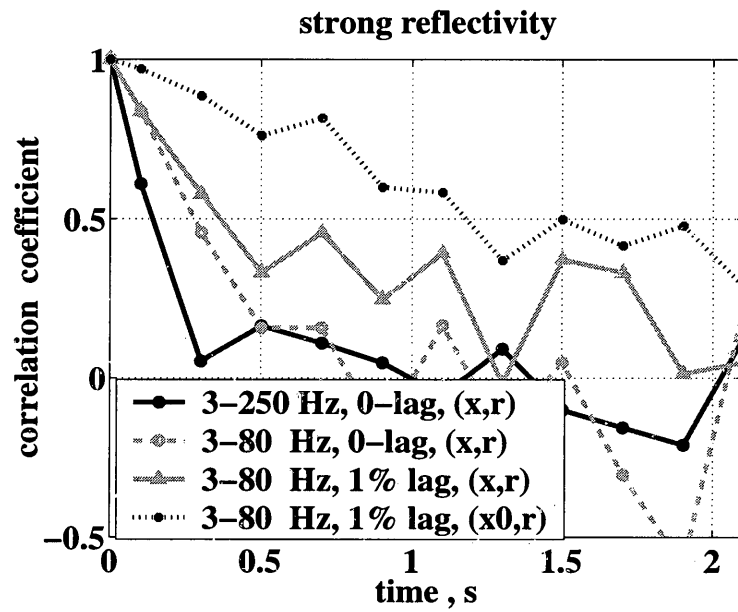


Figure 5.4. The decay in the correlation between trace and reflectivity (solid black line) is slower when: only low-frequencies are considered (dashed gray line), their lower effective velocity is taken into account (solid gray line), and free-surface multiples are removed (dotted black line).

very complicated and the maximum correlation occurs at rather erratic lags. Also, seeking the maximum correlation lag at different frequencies potentially allows us to detect dispersion. In our examples, however, dispersion was not observed – the estimated time lag was approximately the same at all frequencies. Its average value in the strong reflectivity case was 1 sample per a 100-sample increase of the window center time; i.e., the effective-medium velocity was 1% lower than the average velocity. Not surprisingly, in the weak reflectivity case, the time-lag was found to be four times smaller. Taking into account these seemingly small velocity discrepancies between trace and reflectivity improved significantly their correlation (solid gray line in Fig. 5.4). Yet, the correlation is not very high – it drops below 0.5 at about 0.5 s in the strong reflectivity. Further improvement may be sought through surface-multiple suppression (dotted black line in Fig. 5.4). However, this may not be easy, especially in land data acquired over finely layered stratigraphy. Moreover, even in the absence of surface-related multiples, the correlation between the trace and the reflectivity drops noticeably with time. Thus, it seems that the only way to see deep through the multiple-scattering fog is to develop fundamental understanding of the stratigraphic filter, and compensate for its action. A convolutional operator that accounts for the presence of multiples on the trace is derived and analyzed in Chapter 6.

5.4 Conclusions

The correlation between a seismic trace and the earth reflectivity decreases fast in the presence of multiples. At late times, the trace sees correctly only the low-frequency component of the reflectivity. In comparing the two, dispersion and medium averaging should be taken into account. The time scale of correlation loss is inversely proportional to the reflectivity variance. To achieve high resolution late in seismic

data, it is not enough to have a spike-wise source function and an accurate absorption compensation; we must learn to compensate for the filtering action of the small-scale heterogeneities in the earth, too.

Chapter 6

APPARENT ATTENUATION FROM SHORT-PERIOD MULTIPLES AND INTRINSIC ABSORPTION IN THE SEISMIC WAVELET MODEL¹

6.1 Introduction

Can one use a single *effective attenuation* operator in the convolutional model of the trace to account for both intrinsic absorption and the filtering action of thin, horizontal layering? Because the reflection coefficient series describing the subsurface is blue, i.e., rich in high frequencies over the seismic frequency band (Walden & Hosken, 1985; Saggaf & Robinson, 2000), the transmission response of the layered earth is dispersive and high-frequency deficient even without anelasticity (O'Doherty & Anstey, 1971). It is minimum phase, too (Sherwood & Trorey, 1965; Robinson & Treitel, 1977, 1978; Banik *et al.*, 1985). In this sense, the fine layering² in the earth acts similarly to absorption on the transmitted signal.

A seismic trace, however, is more complicated than the transmission response of a stack of layers; it results from a reflection experiment conducted over a half-space that is bounded by a free surface. Consequently, the question posed at the beginning of this section should be approached with care.

¹Submitted to GEOPHYSICS in a co-authorship with Douglas Hart, Regis University, and Scott MacKay, WesternGeco.

²Fine layering means thinner than a typical wavelength but not much thinner than the shortest wavelength in seismic records (Folstad & Schoenberg, 1992). We consider layers with a time thickness equal to the sampling interval in seismic data.

The intent of this paper is to investigate whether the intrinsic absorption and apparent attenuation operators can be combined for wavelet estimation and deconvolution. First, we derive a convolutional operator that accounts for short-period multiples and transmission losses at the interfaces in the earth. We then compare its spectral properties with those of intrinsic absorption. We focus on the phase spectrum and show that the apparent attenuation operator can be significantly non-minimum phase in media characterized by strong reflectivities. The deviation from the minimum-phase property is caused mainly by multiples from the earth's surface and is larger when the short-period multiples in the medium are strong.

6.2 Convolutional models for the seismic trace

Consider a horizontally-layered medium characterized by a reflection coefficient series, r . Let r_m denote its reflection impulse response. The sequence r_m includes transmission losses at interfaces and multiples. Next, let w_0 be a wavelet, which is defined in more detail below. A noise-free model of the seismic trace results from the convolution, $w_0 * r_m$. On the other hand, for signal processing purposes, one models the seismic trace as some wavelet, w , convolved with the earth's reflection coefficient series, r . The equivalence of the two models of the seismic trace can be expressed in the frequency domain as

$$WR = W_0R_m, \quad (6.1)$$

where the capital letters stand for the Fourier transforms of the respective time series. This equation implies that

$$W = W_0 \frac{R_m}{R}. \quad (6.2)$$

As an example, suppose the basic wavelet, W_0 , contains the source signature, S , the receiving instrumentation response, I , and the effect of anelasticity, Q . We can then write equation (6.2) as

$$W = SIQ \frac{R_m}{R}. \quad (6.3)$$

Thus, multiples and elastic transmission losses can be included in the wavelet model through the apparent attenuation operator, R_m/R . If this operator has the same properties as the intrinsic absorption operator, Q , namely:

- exponential decay with frequency,
- minimum phase,

short-period multiples and intrinsic absorption can be combined into an effective attenuation operator, Q_{eff} . This would allow us to model the seismic wavelet as simply

$$W = SIQ_{\text{eff}}, \quad (6.4)$$

where S and I are known, and Q_{eff} is measurable from the trace.

Although the amplitude decay with frequency of the apparent attenuation operator is not exactly exponential, it can be modeled as such reasonably well over a

limited frequency range (Appendix C).

The minimum-phase property is under investigation in this paper. We shall see that the apparent attenuation operator can be significantly non-minimum phase when the geology is characterized by a strong reflection coefficient series.

6.3 The operator R_m/R

The common assumption that the stratigraphic filter of the horizontally layered earth is minimum-phase rests on the fact that the transmission through a stack of thin layers is minimum phase (Sherwood & Trorey, 1965; Robinson & Treitel, 1977; Banik *et al.*, 1985). Therefore, to understand the phase of the operator R_m/R , it is useful to relate it to the transmission response of a stack of layers, which we will denote by M .

Below we discuss some weak-reflectivity approximations of R_m/R . Although our analysis is not limited to the weak-reflectivity case, these approximations are useful in predicting when the minimum-phase property of R_m/R might fail. For simplicity, we assume no anelastic absorption and that the reflection coefficient series is stationary, i.e., its spectrum does not change with depth.

6.3.1 Earth model without a free surface

Consider a surface seismic trace that is free of surface-related multiples. As illustrated in Figure 6.1, in a short time window starting at two-way time T , the elastic impulse response R_m is approximately

$$R_m \approx M^2 R. \quad (6.5)$$

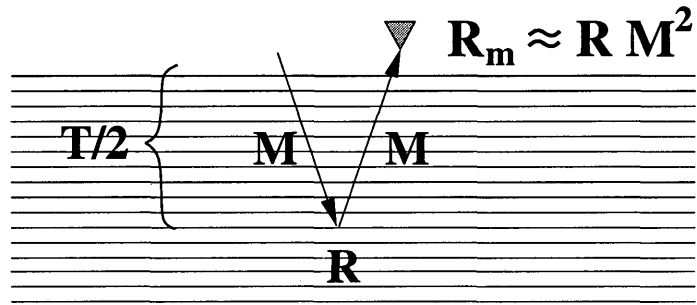


Figure 6.1. The reflection impulse response R_m of a layered half-space without a free surface: a weak-reflectivity approximation ignoring raypaths trapped in the shallow subsurface.

This can be seen as a convolution between the series of reflection coefficients describing the subsurface interval reached by the direct arrival at time $T/2$ and the two-way transmission filter of the overburden. Thus, without surface-related multiples, the operator R_m/R coincides with the two-way transmission response M^2 of the layered overburden, which is minimum-phase, with an amplitude spectrum given by O'Doherty and Anstey's formula:

$$|R_m/R| \approx e^{-|R|^2 T}, \quad (6.6)$$

where T is in dimensionless units (normalized by the time thickness of an individual layer, i.e., the sampling interval of the seismic data).

An underlying assumption in equations (6.5)–(6.6), is that most of the energy arriving at the surface at time T comes from the deepest horizon reached in one-way time $T/2$; i.e., raypaths trapped above the maximum depth of penetration are ignored. However, in strong reflectivities, the shallow raypaths may contribute significantly to the signal, especially at late times. In such cases equations (6.5)–(6.6) may become

inaccurate. Further violation of the minimum-phase property can be observed if too long a time window is used for spectral estimation. The reason is that R_m/R in equation (6.6) is not stationary – it loses predominantly high frequencies with time (hence the name “apparent attenuation” operator). Therefore, an estimate of R_m/R from a long time window includes averaging (summation) over different minimum-phase operators, the result of which is generally not minimum-phase. The robustness of the minimum-phase property is tested with a strong reflectivity and a long time window in the next section.

Showing that R_m/R is minimum phase without surface-related multiples is promising but insufficient. The earth surface (a free surface) has a strong influence on the seismic trace and must be considered.

6.3.2 Earth model with a free surface

Let $(R_m/R)_0$ denote the operator discussed above for the model without a free surface, and let $(R_m/R)_1$ be that for a model with a free surface. Then,

$$\left(\frac{R_m}{R}\right)_1 \approx 2 \left(\frac{R_m}{R}\right)_0 [1 + R(\omega) + R^2(\omega) + \dots] . \quad (6.7)$$

The factor of two accounts for the displacement doubling at the free surface. The terms proportional to powers of $R(\omega)$ in the brackets account for different orders of surface-related multiples. Since these terms have random phases, $(R_m/R)_1$ is not minimum-phase. However, the phase distortion will occur mainly at high frequencies where $|R|$ is large. At the low frequencies, containing most of the power of R_m/R , the phase of $(R_m/R)_1$ should be almost the same as that of $(R_m/R)_0$. On the other hand, the amplitude spectrum of $(R_m/R)_1$ is whiter than that of $(R_m/R)_0$, i.e., $|R_m/R|_1$ has

a smaller slope in dB/Hz than $|R_m/R|_0$. Indeed, as is seen from equations (6.6) and (6.7), surface-related multiples partially compensate for the high-frequency deficit in $|R_m/R|_0$. This whitening is more pronounced at low frequencies, where $R(\omega)$ is steeper, and in strong reflectivities, even though they are not well described by equations (6.6) and (6.7).

In summary, surface-related multiples do not alter significantly the phase of R_m/R , but they reduce the slope of its amplitude spectrum. Therefore, the minimum-phase equivalent of $|R_m/R|_1$ will underestimate the phase of the apparent attenuation operator. The error grows with time, because, while $|R_m/R|_1$ is stationary (Chapter 2), $|R_m/R|_0$ gets increasingly high-frequency deficient with time; i.e., over time, the minimum-phase equivalents of $|R_m/R|_0$ and $|R_m/R|_1$ become more different. To test the phase properties of the elastic stratigraphic filter, a strong-reflectivity example is considered below.

6.4 Strong-reflectivity example

6.4.1 Synthetic data

The synthetic reflectivity in this example is strong and blue, similar to the reflectivity measured in Well 8 from the papers of Walden and Hosken 1985; 1986. It has the following statistical properties:

- mean = -0.0002 , standard deviation ≈ 0.13 ;
- reflection-coefficient magnitudes are drawn from a Laplacian distribution;
- the reflectivity series is an ARMA(1,1) process with an autoregressive parameter $\theta = 0.9$ and a moving average parameter $\phi = 0.3$; this gives rise to the blue spectrum depicted in Figure 6.2.

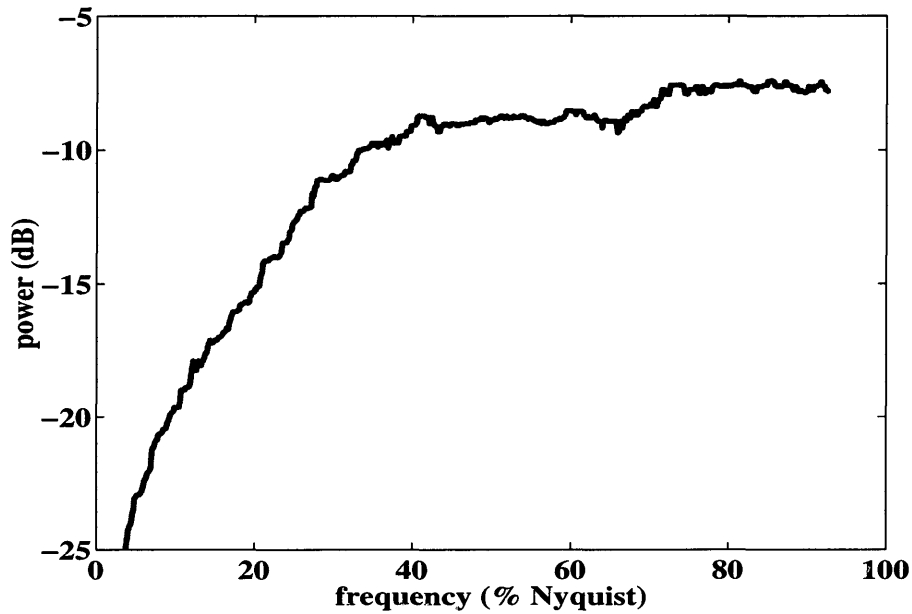


Figure 6.2. Power spectrum of the synthetic reflection coefficient series (average estimate over 100 realizations).

To enhance the reliability of the spectral analysis, 100 realizations of the reflection coefficient series were generated, 1024 samples each. Assuming that the medium is horizontally layered and non-absorbing, the corresponding 100 normal-incidence impulse responses were computed with and without surface-related multiples. Each synthetic seismogram was padded by zeroes to assure causality. The mean was removed and a 20% cosine taper applied before FFT. The resulting estimates of $R(\omega)$, $(R_m(\omega)/R(\omega))_1$, and $(R_m(\omega)/R(\omega))_0$ were averaged over the 100 realizations to reduce variability without smoothing over frequency³.

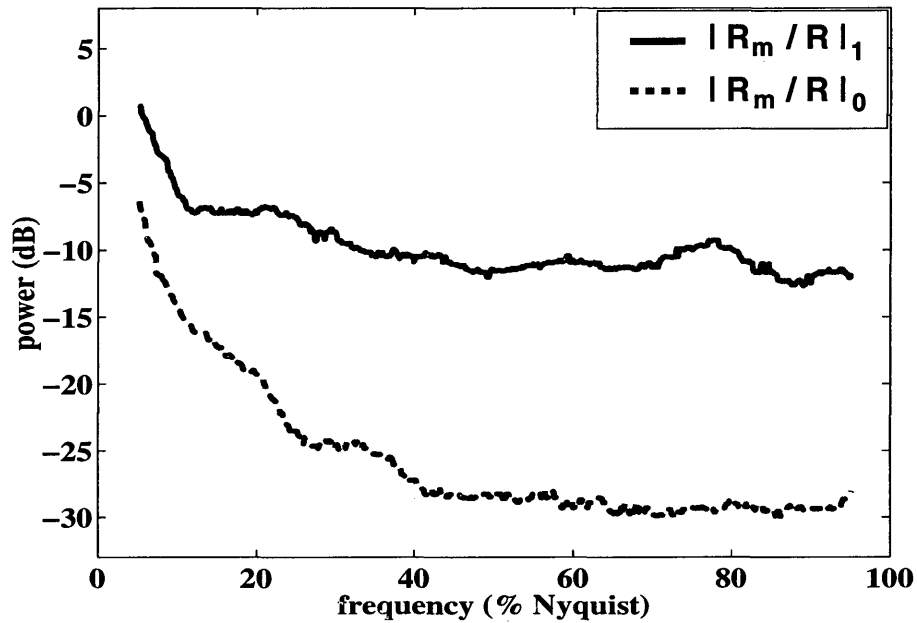


Figure 6.3. Power spectrum of R_m/R with (solid) and without (dashed) surface-related multiples.

6.4.2 Spectral properties test

Here we test the speculation from the previous section that while $(R_m/R)_0$ is approximately minimum-phase, $(R_m/R)_1$ is not because, surface-related multiples whiten the amplitude spectrum of the operator without altering its phase.

Let us first illustrate the free-surface influence on the operator. Figure 6.3 shows the amplitude spectrum of R_m/R with and without surface-related multiples. As expected, the slope of $|R_m/R|_1$ is smaller than that of $|R_m/R|_0$, most obviously so at low frequencies, where the frequency dependence of $R(\omega)$ is strongest. At the same time, the difference between the phase spectra of $(R_m/R)_1$ and $(R_m/R)_0$ at low frequencies is small (Figure 6.4); at higher frequencies it increases but can hardly affect

³Only for presentation purposes were the spectra in the figures smoothed by a 15%-of-series-length median filter.

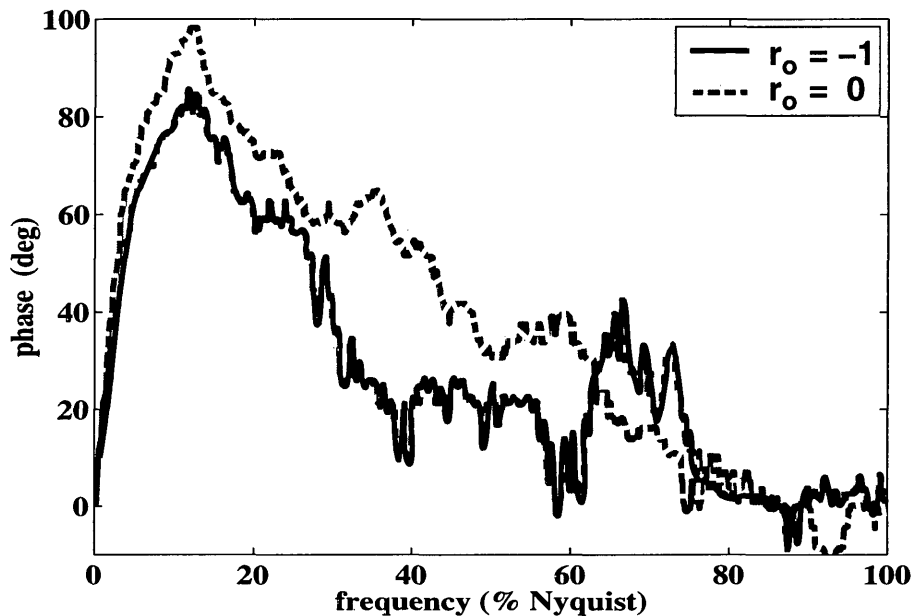


Figure 6.4. Phase spectrum of R_m/R with (solid) and without (dashed) surface-related multiples (reflection coefficient of the earth's surface, r_0 , set to -1 and 0 , respectively).

the wavelet, most of the power of which is at lower frequency. Near the Nyquist frequency, the phases of both $(R_m/R)_1$ and $(R_m/R)_0$ go to zero, which is a characteristic behavior of phase spectra that are Hilbert transforms of the logarithm of power spectra.

Now let us look at the minimum-phase⁴ property of R_m/R . As already explained, $(R_m/R)_0$ is expected to be minimum-phase in a weak reflectivity and over a small time window. The reflectivity in this example is about as strong as it ever gets, and the spectral estimates are based on a long time window (1024 samples) over which $(R_m/R)_0$ is not stationary. Nevertheless, the phase of $(R_m/R)_0$ is close to that of the minimum-phase equivalent derived from $|R_m/R|_0$ (Figure 6.5). In contrast, the

⁴Minimum-phase equivalents were computed by the inverse-of-inverse method, or, repeated Levinson recursion (Claerbout, 1985).

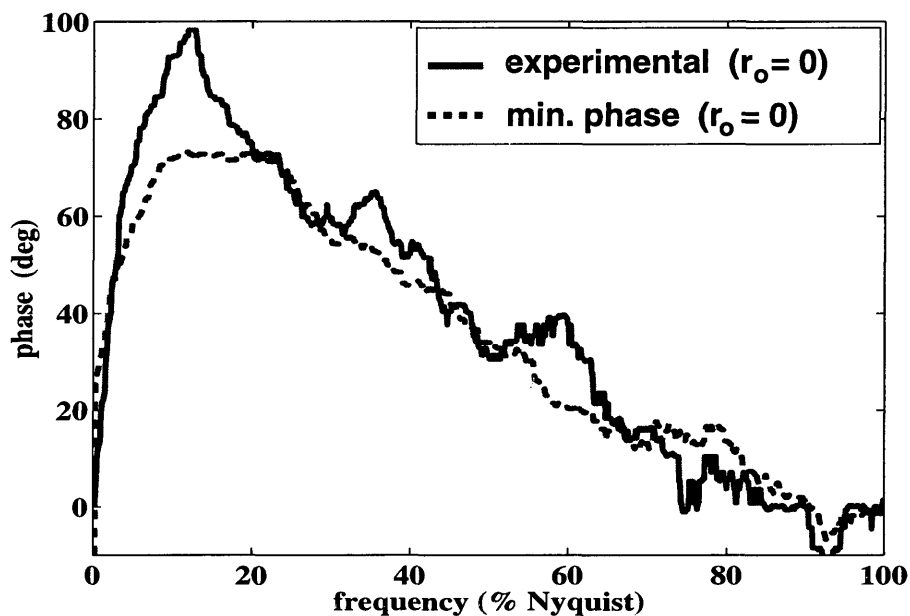


Figure 6.5. Phase spectrum of $(R_m/R)_0$ (solid) and minimum-phase spectrum (dashed) computed from $|R_m/R|_0$.

minimum-phase equivalent of $|R_m/R|_1$ does not match the true phase of $(R_m/R)_1$ (Figure 6.6). Therefore, in the presence of surface-related multiples (which is inevitable, especially in land data acquired over finely layered media), the conventional assumption that the stratigraphic filter is minimum-phase fails and causes an error of up to 45 degrees in the wavelet model (Figure 6.6). The largest error occurs over the low one-third of the spectrum which includes the frequency band of maximum trace power. Obviously, a better model for the stratigraphic filter phase is needed in strong non-white reflectivities.

6.5 Modeling the phase of the apparent attenuation operator using borehole data

If a reflection coefficient log or a regional stochastic model of it is available, one can compute the difference between the true phase of $(R_m/R)_1$ and the minimum phase equivalent of $|R_m/R|_1$ from synthetic seismograms. Adding this difference to the minimum-phase equivalent of the effective attenuation, measured on the seismic trace, would correct the phase of the wavelet derived under the assumption that the stratigraphic filter is minimum phase.

If instead of a reflection coefficient log a VSP is available, a phase correction can be derived from it, too. Suppose for a moment that the earth is non-absorbing. Then, using VSP first arrivals, one can measure the elastic transmission response M from the surface to a given depth. According to equations (6.5) and (6.6), $|R_m/R|_0 \approx |M|^2$. Knowing $|R_m/R|_0$, the phase of $(R_m/R)_1$ can be predicted based on two assumptions:

- $(R_m/R)_0$ is minimum-phase,
- phase of $(R_m/R)_1 \approx$ phase of $(R_m/R)_0$.

The numerical tests in the previous section suggest that these assumptions hold. Thus, it seems reasonable to try modeling the phase of $(R_m/R)_1$ through the minimum-phase equivalent of $|R_m/R|_0$. The result of such modeling is shown in Figure 6.7. The fit is obviously better than that in Figure 6.6. Most important is the improvement over the low frequencies, where the seismic signal is concentrated. The phase deviations at higher frequencies are a consequence of the random phase of R and the assumption that surface related multiples do not change the phase of R_m/R .

The fact that the real earth is absorbing does not impair the above scheme. Rather the phase of the elastic stratigraphic filter alone, the minimum-phase equiv-

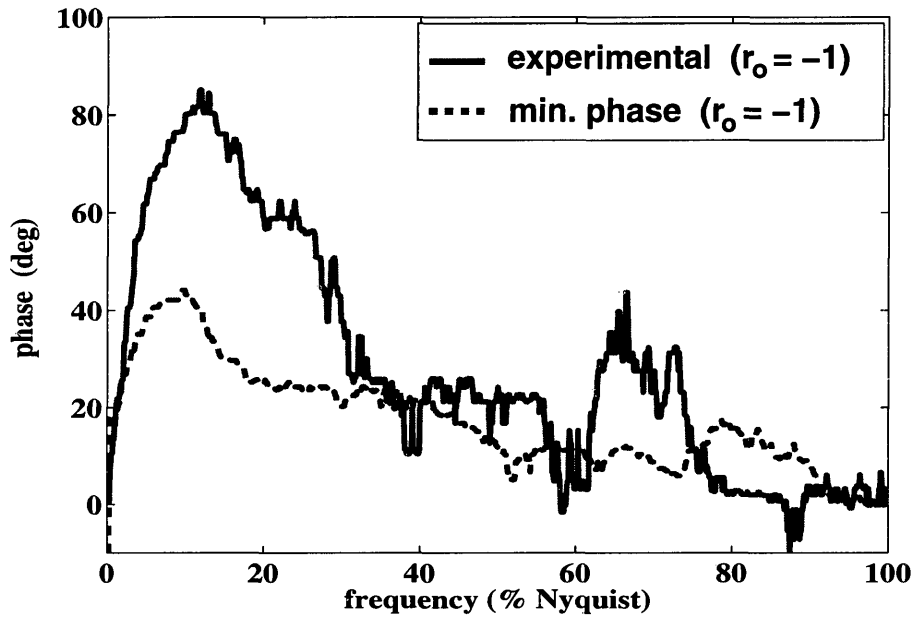


Figure 6.6. Phase spectrum of $(R_m/R)_1$ (solid) and minimum-phase spectrum (dashed) computed from $|R_m/R|_1$.

alent of the transmission response measured from a VSP (absorption and scattering together) predicts the phase of the effective attenuation operator, Q_{eff} , in surface seismic data. Note that this phase spectrum is to be combined with the amplitude spectrum $|Q_{\text{eff}}|$ measured from surface seismic data. The effective attenuation in surface data is generally smaller than that in VSP data because the high frequencies that are lost through scattering to the transmitted signal are present in the surface seismograms as reflected energy.

6.6 Discussion

Arguably, correcting the phase of $(R_m/R)_1$ is important only in strong non-white reflectivities (as in the example above), in which short-period multiples change noticeably the color of the trace spectrum. To determine the reflectivity range in which

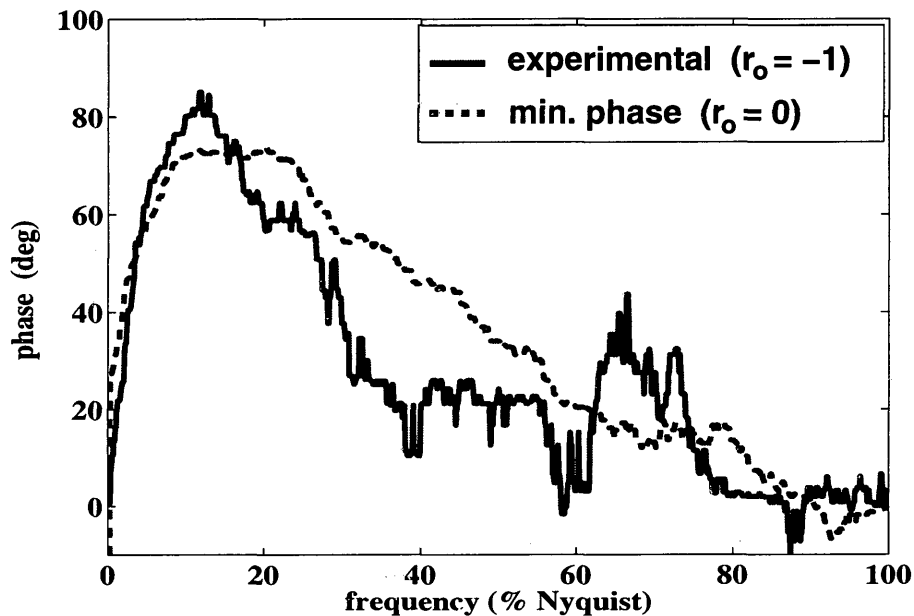


Figure 6.7. Phase spectrum of $(R_m/R)_1$ (solid) and minimum-phase spectrum (dashed) computed from $|R_m/R|_0$.

the phase error is important, we experimented with different strengths of a representative blue reflectivity. The frequency dependence, or color, of $R(\omega)$ is controlled by the difference between the auto-regressive and moving-average parameters in its ARMA(1,1) model. The larger $\theta - \phi$, the more blue the reflectivity spectrum. Analyzing a large collection of well logs, Saggaf & Robinson (2000) found that, on the average, $\theta = 0.69$, $\phi = 0.28$. Thus, a typically blue reflectivity is given by $\theta - \phi \approx 0.4$, compared to $\theta - \phi \approx 0.6$ for Well 8 of Walden and Hosken (1985, 1986), the parameters of which we used as an extreme example. For a reflectivity model with $\theta = 0.7$, $\phi = 0.3$, phase errors over the lower one-third of the spectrum are shown as a function of reflectivity strength in Figure 6.8. If we assume an error of less than 10° is negligible, the conventional assumption that the stratigraphic filter is minimum phase seems acceptable in reflectivities with standard deviations of up to 0.09 (solid

line in Figure 6.8); beyond that it deteriorates rapidly, the error reaching more than 40° for $\text{std}(r) = 0.12$. Modeling the phase of $(R_m/R)_1$ by the minimum-phase equivalent of $|R_m/R|_0$ reduces the error by a factor of two, e.g., to 17° at $\text{std}(r) = 0.12$ (thick dashed line in Figure 6.8). It does not eliminate the phase error completely because the minimum-phase property of $(R_m/R)_0$ deteriorates (dash-dot line) in strong reflectivities. This occurs when most of the energy emerging at the surface in the considered time window comes from the layers above the maximum depth of penetration. As expected, surface-related multiples have almost no influence on the phase spectrum of R_m/R at low frequencies (thin dash line).

The guidance on when the stratigraphic filter is minimum phase provided by Figure 6.8 should not be regarded as a rule of thumb because the properties of R_m/R are time dependent. The estimates in Figure 6.8 are for a time window of length 0.5 s, centered at time 0.5 s. In a later window, the minimum-phase property of $(R_m/R)_1$ can fail at a much weaker reflectivity (Figure 6.9). Ideally, one would judge whether the minimum-phase assumption is acceptable by computing $(R_m/R)_1$ from a reflectivity log (or a stochastic model of it) for the specific time window used for wavelet estimation or predictive deconvolution. Addressing the non-stationary aspect of the attenuation in the context of signal processing is beyond the scope of this paper.

The fundamental cause for the operator R_m/R to deviate from minimum phase is source-generated noise in the shallow subsurface. Surface-related multiples are a major component, but additional contributions can come from other strong shallow interfaces, such as the sea floor or the base of weathering. The stratigraphic filter remains minimum phase as long as the shallow multiples are weak compared to the deep primary reflections emerging at a given time.

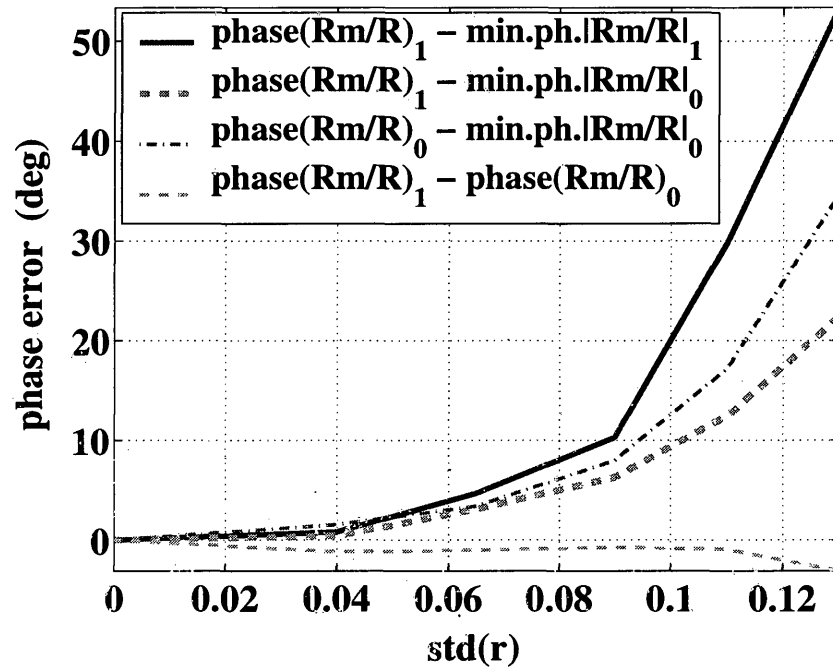


Figure 6.8. Typical phase properties of R_m/R as a function of reflectivity standard deviation: (solid) minimum-phase property in the presence of surface-related multiples; (dash-dot) minimum-phase property in the absence of surface-related multiples; (thick dash) modeling the phase of $(R_m/R)_1$ by the minimum-phase equivalent of $|R_m/R|_0$; (thin dash) influence of surface related multiples on the phase of R_m/R . All phase-error estimates are median over the low one-third of the spectrum ($f < \text{Nyquist}/3$), for a time window of 0.5 s centered at 0.5 s.

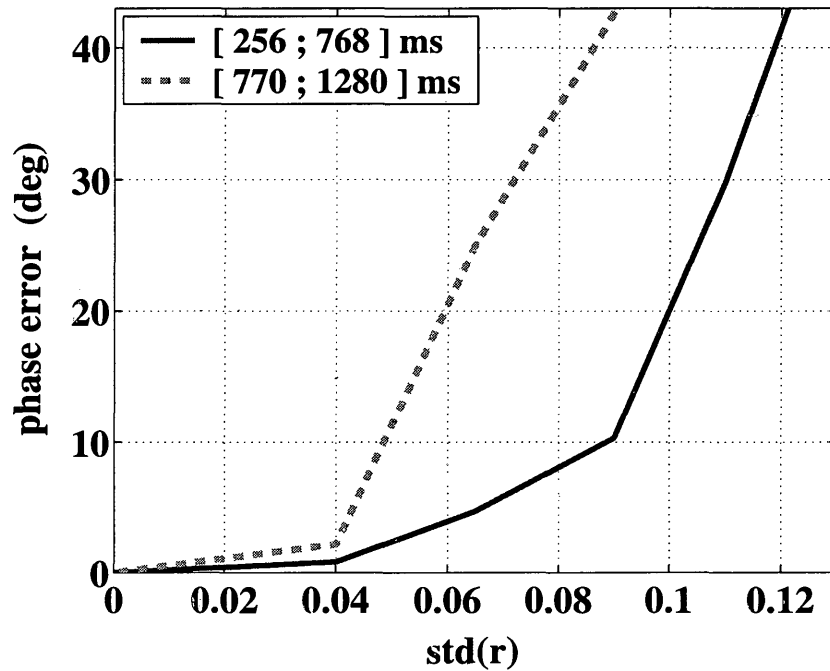


Figure 6.9. Minimum-phase property of $(R_m/R)_1$ in time windows centered at approximately 0.5 s (solid line; identical to that in Figure 6.8) and 1 s (dashed).

6.7 Conclusion

Short-period multiples can be included in the wavelet model through the apparent attenuation operator R_m/R . Often, apparent attenuation caused by short-period multiples and intrinsic absorption can be combined in a single effective attenuation operator for the purposes of signal processing. However, this cannot be done in finely layered media with large reflection coefficients. In such environments the apparent attenuation operator becomes significantly non-minimum phase. The minimum-phase equivalent of the observed effective attenuation underestimates the phase lag of the wavelet.

Chapter 7

CONCLUSION

This thesis takes a fresh look into an old problem. I hope it provides a better understanding and some interesting new insights into the multiple-scattering contribution to seismic exploration data. I come to three most basic conclusions. First, scattering can offset the loss of high-frequencies with time and depth; thus, contrary to popular belief, the effective attenuation measured from VSP and surface seismic data is not necessarily larger than the intrinsic absorption. Second, even-though it is difficult to separate absorption from scattering, their action along the seismic trace is not identical; therefore, it is not always possible to use an effective attenuation operator to account simultaneously for both in signal processing. Third, it is important to include the earth surface in attenuation studies. My work would be beneficial to the following areas:

- *Absorption estimation from surface seismic data*

In a homogeneously absorbing, stationary layered medium, spectral-ratio methods give accurate Q estimates, while absorption measurements directly from the trace spectrum may underestimate the intrinsic absorption. Suppressing free-surface multiples would not benefit absorption estimation in a homogeneously absorbing medium. Considerable further research is needed in mapping absorption *variations* in the presence of strong scattering.

- *Absorption estimation from VSP data*

While spectral ratios between early time windows characterize the medium between two VSP receivers, ratios between later arrivals are strongly influenced by the absorption properties of the shallow subsurface; thus, they do not provide a straightforward redundant measure of the absorption between the receivers. I also found that when reflectivity strength changes with depth, scattering can either cause a high-frequency loss larger than anelasticity, or on the contrary, it can over-compensate the anelastic loss and lead to a spectral ratio with a positive slope (negative effective Q).

- *Absorption error estimation for the purposes of reservoir characterization and lithology discrimination*

One must have a fair notion of the uncertainties in absorption data in order to make inferences from them about lithology or reservoir conditions. I proposed ways of quantifying the absorption errors introduced by different factors in VSP spectral ratios. Scattering is the largest source of uncertainty. It should not be neglected even if the medium seems homogeneous before its share in the effective attenuation has been assessed. The next largest uncertainties are associated with positioning and timing errors. Ambient noise and time windowing (when properly done) have a much smaller impact.

- *Signal processing in cyclic depositional environments*

We derived a convolutional operator accounting for short-period multiples and transmission losses along the trace. Comparing its properties to those of intrinsic absorption we found that when the scattering is weak, or even moderately strong, intrinsic and apparent attenuation can be combined into a single effective attenuation operator for the purposes of wavelet estimation and deconvolu-

tion. However, this cannot be done in strong reflectivities because the apparent attenuation operator becomes non-minimum phase.

- *Apparent attenuation modeling*

The software for synthetic seismogram generation developed in the course of my work is freely distributed through the Seismic Unix package (Cohen & Stockwell, 2002). The codes implement a time-domain reflectivity method. They are simple but flexible, and can be useful to other researchers.

REFERENCES

- Abercrombie, R. E. 1998. A Summary of Attenuation Measurements from Borehole Recordings of Earthquakes: The 10 Hz Transition Problem. *Pure and Applied Geophysics*, **153**, 475–487.
- Aki, K., & Chouet, B. 1975. Origin of Coda Waves: Source, Attenuation and Scattering Effects. *J. Geophys. Res.*, **80**, 3322–3342.
- Anstey, N. A., & O'Doherty, R. F. 2002a. Cycles, layers, and reflections: Part I. *The Leading Edge*, **21**(1), 44–51.
- Anstey, N. A., & O'Doherty, R. F. 2002b. Cycles, layers, and reflections: Part II. *The Leading Edge*, **21**(2), 152–158.
- Asch, M., Kohler, W., Papanicolaou, G., Postel, M., & White, B. 1991. Frequency Content of Randomly Scattered Signals. *SIAM Review*, **33**(4), 519–625.
- Backus, G. 1962. Long-wave Elastic Anisotropy Produced by Horizontal layering. *JGR*, **67**, 4427–4440.
- Banik, N.C., Lerche, I., & Shuey, R.T. 1985. Stratigraphic Filtering, Part I: Derivation of the O'Doherty-Anstey Formula. *Geophysics*, **50**, 2768–2774.
- Batzle, M., Han, D., & Castagna, J. 1996. Seismic Frequency Measurements of Velocity and Attenuation. *Pages 1687–1690 of: SEG Ann. Int. Mtg. Expanded Abstracts*, vol. 66. SEG. RP-1.3.

- Bianco, F., Castellano, M., Pezzo, E. Del, & Ibanez, J. M. 1999. Attenuation of short-period seismic waves at Mt. Vesuvius, Italy. *Geophys. J. Int.*, **138**(1), 67–76.
- Burridge, R., Papanicolaou, G., & White, B. 1988. One-dimensional wave propagation in a highly discontinuous layered medium. *Wave Motion*, **10**, 19–44.
- Burridge, R., de Hoop, M. V., Hsu, K., Le, L., & Norris, A. 1993. Waves in stratified viscoelastic media with microstructure. *J. Acoust. Soc. Am.*, **94**, 2884–2894.
- Castagna, J. P, Sun, S., & Siegfried, R. W. 2002. The use of spectral decomposition as a hydrocarbon indicator. *Gas Tips*, **8**(3), 24–27.
- Claerbout, J. F. 1985. *Fundamentals of geophysical data processing with applications to petroleum prospecting*. Blackwell Scientific Publications.
- Clark, R. A., Carter, A. J., Nevill, P. C., & Benson, P. M. 2001. Attenuation measurements from surface seismic data – azimuthal variation and time-lapse case studies. In: *EAGE Ann. Int. Mtg. Expanded Abstracts*, vol. 63. EAGE, Amsterdam, The Netherlands. L-28.
- Cohen, J. K., & Stockwell, Jr. J. W. 2002. *CWP/SU: Seismic Unix Release 36: a free package for seismic research and processing*. Colorado School of Mines.
- Dasgupta, R., & Clark, R. A. 1998. Estimation of Q from Surface Seismic Data. *Geophysics*, **63**, 2120–2128.
- De, G. S., Winterstein, D. F., & Meadows, M. A. 1994. Comparison of P- and S-wave velocities and Q's from VSP and sonic log data. *Geophysics*, **59**(10), 1512–1529.
- de Hoop, M. V., Chang, H. W., & Burridge, R. 1991a. The pseudo-primary field due to a point-source in a finely layered medium. *Geoph. J. Int.*, **104**, 489–506.

- de Hoop, M. V., Burridge, R., & Chang, H. W. 1991b. Wave propagation with tunneling in a highly discontinuous layered medium. *Wave Motion*, **13**, 307–327.
- Dolan, S.S., Bean, C.J., & Riollet, B. 1998. The Broad-Band Fractal Nature of Heterogeneity in the Upper Crust From Petrophysical Logs. *Geophys. J. Int.*, **132**, 489–507.
- Douma, H., & Roy-Chowdhury, K. 2001. Amplitude effects due to multiscale impedance contrasts and multiple scattering: implications for Ivrea-type continental lower crust. *Geoph. J. Int.*, **147**(2), 435–448.
- Folstad, P. G., & Schoenberg, M. 1992. Low frequency propagation through fine layering. *In: SEG Ann. Int. Mtg.: Expanded Abstracts*, vol. 62.
- Frankel, A., & Wennerberg, L. 1987. Energy-flux model of seismic coda: separation of scattering and intrinsic attenuation. *Bull. Seism. Soc. Am.*, **77**(4), 1223–1251.
- Ganley, D. C. 1981. A Method for Calculating Synthetic Seismograms Which Include the Effects of Absorption and Dispersion. *Geophysics*, **46**, 1100–1107.
- Goldberg, D., Kan, T. K., & Castagna, J. P. 1984. Attenuation measurements from sonic log waveforms. *Page paper NN of: 25th Ann. Logging Symp. Soc. Prof. Well Log Analysts*.
- Görich, U., & Müller, G. 1987. Apparent and intrinsic Q: The one-dimensional case. *J. Geophys.*, **61**, 46–54.
- Haase, A. B. 2000. Anelasticity and wavelet stretch. *Pages 2177–2179 of: SEG Ann. Int. Mtg. Expanded Abstracts*, vol. 70.

- Haase, A. B. 2001. Non-hyperbolic Moveout, Polar Anisotropy, and Anelasticity. *CSEG Recorder*, **2**, 10–17.
- Hackert, C. L., & Parra, J. O. 2002. Calibrating well-logs to VSP attributes: interval velocity and amplitude. *The Leading Edge*, **21**(1), 52–57.
- Hampson, D. 1991. AVO inversion: Theory and practice. *The Leading Edge*, **10**, 39–42.
- Haney, M., van Wijk, K., & Snieder, R. K. 2003. Radiative transfer in 1D, and the connection to the O'Doherty-Anstey formula. *Pages 25–36 of: CWP Project Review*. Center for Wave Phenomena, Colorado School of Mines.
- Harris, P. E., Kerner, C. C., & White, R. E. 1992. Multichannel estimation of frequency-dependent Q from VSP data. *In: EAEG Expanded Abstracts*, vol. 54.
- Hart, D. I., Hootman, B. W., & Jackson, A. R. 2001. Modeling the seismic wavelet using model-based wavelet processing. *SEG Ann. Int. Mtg. Expanded Abstracts*, **71**, 1823–1826.
- Hauge, P. 1981. Measurements of Attenuation from Vertical Seismic Profiles. *Geophysics*, **46**, 1548–1558.
- Hicks, G. J., & Pratt, R. G. 2001. Reflection waveform inversion using local descent methods: Estimating attenuation and velocity over a gas-sand deposit. *Geophysics*, **66**(2), 598–612.
- Hsu, K., & Burridge, R. 1991. Effects of averaging and sampling on the statistics of reflection coefficients. *Geophysics*, **56**, 50–58.

- Hubral, P., Treitel, S., & Gutowski, P. R. 1980. A sum autoregressive formula for the reflection response. *Geophysics*, **45**(11), 1697–1705.
- Ingram, J. D., Morris, C. F., MacKnight, E. E., & Parks, T. W. 1985. Direct phase determination of S-wave velocities from acoustic waveform logs. *Geophysics*, **50**, 1746–1755.
- Johnson, R. A., & Wichern, D. W. 2002. *Applied Multivariate Statistical Analysis*. 5 edn. Prentice Hall.
- Kan, T. K. 1981. Attenuation Measurements from Vertical Seismic Profiles. *In: SEG Ann. Intern. Mtg. Expanded Abstracts*, vol. 51.
- Kerner, C., & Harris, P. E. 1994. Scattering attenuation in sediments modeled by ARMA processes – validation of simple Q models. *Geophysics*, **59**(12), 1813–1826.
- Kjartansson, E. 1979. *Attenuation of Seismic Waves in Rocks and Applications in Energy Exploration*. Ph.D. thesis, Stanford, California.
- Klimentos, T., & McCann, C. 1990. Relationships between compressional wave attenuation, porosity, clay content, and permeability of sandstones. *Geophysics*, **55**, 998–1014.
- Lewicki, P., Burrige, R., & de Hoop, M. V. 1996. Beyond effective medium theory: pulse stabilization for multimode wave propagation in high-contrast layered media. *SIAM J. Appl. Math.*, **56**, 256–276.
- Lindsay, R., & Koughnet, R. Van. 2001. Sequential Backus Averaging: Upscaling well logs to seismic wavelengths. *The Leading Edge*, **20**, 188–191.

- Luh, P. C. 1993. Wavelet attenuation and bright-spot detection. *Pages 190–198 of: Castagna, J. P., & Backus, M. M. (eds), Offset-dependent reflectivity – theory and practice.* Investigations in Geophysics, no. 8. SEG.
- Marion, D., Mukerji, T., & Mavko, G. 1994. Scale Effects of Velocity Dispersion: From Ray to Effective Medium Theories in Stratified Media. *Geophysics*, **59**(10), 1613–1619.
- Martini, F., Bean, C. J., Dolan, S., & Marsan, D. 2001. Seismic image quality beneath strongly scattering structures and implications for lower crustal imaging: numerical simulations. *Geophys. J. Int.*, **145**(2), 423–435.
- Mavko, G. M., & Nur, A. 1979. Wave Attenuation in Partially Saturated Rocks. *Geophysics*, **44**, 161–178.
- Mavko, G. M., Kjartansson, E., & Winkler, K. 1979. Seismic Wave Attenuation in Rocks. *Rev. of Geophys. and Space Physics*, **17**, 1155–1164.
- Menke, W. 1983. A formula for the apparent attenuation of acoustic waves in randomly layered media. *Geophys. J. Res. Astr. Soc.*, **75**, 541–544.
- Mitchell, B. J., & Romanowicz, B. (eds). 1999. *Q of the Earth: Global, Regional, and Laboratory Studies.* Birkhauser Verlag.
- Moos, D. 1984. A case study of vertical seismic profiling in fractured crystalline rock. *Advances in Geophysical Data Processing*, **1**, 9–37.
- Müller, T. M., & Shapiro, S. A. 2000. Most probable seismic pulses in single realizations of two- and three-dimensional random media. *Geophys. J. Int.*, **144**(1), 83–95.

- O'Doherty, R. F., & Anstey, N. A. 1971. Reflections on Amplitudes. *Geophys. Pros.*, **19**, 430–458.
- Pan, C. 1998. Spectral ringing suppression and optimal windowing for attenuation and Q measurements. *Geophysics*, **63**(2), 632–636.
- Papanicolaou, G. C., & Lewicki, P. 1994. Reflection of waveforms by randomly layered media. *Wave Motion*, **20**, 245–266.
- Patton, S. W. 1988. Robust and least-squares estimation of acoustic attenuation from well-log data. *Geophysics*, **53**(9), 1225–1232.
- Pramanik, A. G., Singh, V., Dubey, A. K., Painuly, P. K., & Sinha, D. P. 2000. Estimation of Q from Borehole Data and Its Application to Enhance Surface Seismic Resolution: A Case Study. *Pages 2013–2016 of: SEG Ann. Int. Mtg. Expanded Abstracts*, vol. 70.
- Quan, Y., & Harris, J. M. 1997. Seismic attenuation tomography using the frequency shift method. *Geophysics*, **62**, 895–905.
- Raikes, S. A., & White, R. E. 1984. Measurements of earth attenuation from down-hole and surface seismic recordings. *Geophys. Pros.*, **32**, 892–919.
- Resnick, J. R., Lerche, I., & Shuey, R. T. 1986. Reflection, Transmission, and the Generalized Primary Wave. *Geophys. J. Int.*, **87**(2), 349–377.
- Richards, P. G., & Menke, W. 1983. The Apparent Attenuation of a Scattering Medium. *Bull. Seismol. Soc. Am.*, **73**, 1005–1021.
- Robinson, E. A. 1983. *Multichannel Time Series Analysis with Digital Computer Programs*. 2 edn. Goose Pond Press.

- Robinson, E. A. 2001. Inversion of a seismic transmission response. *Geophysics*, **66**(4), 1235–1239.
- Robinson, E. A., & Treitel, S. 1977. The spectral function of a layered system and determination of the waveform at depth. *Geophys. Prosp.*, **25**, 434–459.
- Robinson, E. A., & Treitel, S. 1978. The fine structure of the normal incidence synthetic seismogram. *Geophys. J. RAS*, **53**, 289–309.
- Roecker, S. W., Tucker, B., King, J., & Hatzfeld, D. 1982. Estimation of Q in Central Asia as a Function of Frequency and Depth Using the Coda of Locally Recorded Earthquakes. *Bull. Seismol. Soc. Am.*, **72**, 129–149.
- Saggaf, M. M., & Robinson, E. A. 2000. A United Framework for the Deconvolution of Traces of Nonwhite Reflectivity. *Geophysics*, **65**, 1660–1676.
- Sams, M., & Goldberg, D. 1990. The validity of Q estimates from borehole data using spectral ratios. *Geophysics*, **55**(1), 97–101.
- Sato, H. 1984. Attenuation and Envelope Formation of Three-component Seismograms of Small Local Earthquakes in Randomly Inhomogeneous Lithosphere. *J. Geophys. Res.*, **89**, 1221–1241.
- Scales, J. A. 1993. On the use of localization theory to characterize elastic wave propagation in randomly stratified 1-D media. *Geophysics*, **58**, 177–179.
- Scales, J. A., & van Vleck, E. S. 1997. Lyapunov exponents and localization in randomly layered media. *J. of Comput. Physics*, **133**, 27–42.
- Scales, J. A., & van Wijk, K. 1999. Multiple scattering attenuation and anisotropy of ultrasonic surface waves. *App. Phys. Lett.*, **74**, 3899–3901.

- Schoenberger, M., & Levin, F. K. 1974. Apparent Attenuation due to Intrabed Multiples. *Geophysics*, **39**, 278–291.
- Schoenberger, M., & Levin, F. K. 1978. Apparent Attenuation due to Intrabed Multiples, II. *Geophysics*, **43**, 730–737.
- Schoenberger, M., & Levin, F. K. 1979. The Effect of Subsurface Sampling on 1D Synthetic Seismograms. *Geophysics*, **44**, 1813–1829.
- Shapiro, S. A., & Hubral, P. 1996. Elastic waves in finely layered sediments: The equivalent medium and generalized O’Doherty-Anstey formulas. *Geophysics*, **61**(5), 1282–1300.
- Shapiro, S. A., & Zien, H. 1992. Transmission of wavefields through finely layered media: attenuation, velocity, fluctuations. *Pages 820–823 of: SEG Ann. Int. Mtg. Expanded Abstracts.*
- Shapiro, S. A., & Zien, H. 1993. The O’Doherty-Anstey formula and localization of seismic waves. *Geophysics*, **58**(5), 736–740.
- Shapiro, S. A., Hubral, P., & Zien, H. 1994a. Frequency-dependent anisotropy of scalar waves in a multilayered medium. *J. Seis. Expl.*, **3**(1), 37–52.
- Shapiro, S. A., Zien, H., & Hubral, P. 1994b. A generalized O’Doherty-Anstey formula for waves in finely layered media. *Geophysics*, **59**(11), 1750–1762.
- Sheng, P., White, B., Zhang, Z. Q., & Papanicolaou, G. 1986. Multiple scattering noise in one dimension: Universality through localization length scaling. *Phys. Rev. Lett.*, **57**, 1000–1003.

- Sherwood, J. W. C., & Trorey, A. W. 1965. Minimum-phase and related properties of the response of a horizontally stratified absorptive earth to plane acoustic waves. *Geophysics*, **30**, 191–197.
- Sollie, R., & Mittet, R. 1994. Prestack Depth Migration: Sensitivity to the Macro Absorption Model. *Pages 1422–1425 of: Ann. Intern. Mtg. Expanded Abstracts*, vol. 64. SEG.
- Sollie, R., Millet, R., & Hokstad, K. 1994. Pre-stack depth migration with compensation for absorption. *Page paper H031 of: 56th Ann. Conf. EAGE, Extended Abstracts*.
- Solna, K. 2001. Estimation of pulse shaping for well logs. *Geophysics*, **66**(5), 1605–1611.
- Spencer, T. W., Sonnad, J. R., & Butler, T. M. 1982. Seismic Q – Stratigraphy or Dissipation. *Geophysics*, **47**, 16–24.
- Spetzler, J., & Snieder, R. 2001. The effect of small-scale heterogeneity on the arrival time of waves. *Geophys. J. Int.*, **145**(3), 786–796.
- Sun, S., & Castagna, J. 2000. Attenuation Estimation from Vertical Seismic Profile Data. *Pages 1787–1790 of: 70-th Ann. Intern. Mtg. of SEG -- Expanded Abstracts*, vol. 70. SEG.
- Swan, H. W. 1991. Amplitude-versus-offset measurement errors in a finely layered medium. *Geophysics*, **56**(1), 41–49.
- Thomson, D. J. 1982. Spectrum estimation and harmonic analysis. *Proc. IEEE*, **70**, 1055–1096.

Tonn, R. 1991. The Determination of the Seismic Quality Factor Q from VSP Data: A comparison of Different Computational Methods. *Geophys. Pros.*, **39**, 1–27.

Treitel, S., & Robinson, E. A. 1966. Seismic wave propagation in layered media in terms of communication theory. *Geophysics*, **31**, 17–32.

van der Baan, M. 2001. Acoustic wave propagation in one-dimensional random media: the wave localization approach. *Geophys. J. Int.*, **145**(3), 631–646.

van Wijk, K. 2003. *Surface wave multiple scattering in the laboratory*. Ph.D. thesis, Colorado School of Mines.

Walden, A. T. 1990. Improved low-frequency decay estimation using the multitaper spectral analysis method. *Geophys. Prosp.*, **38**, 61–86.

Walden, A. T. 1993. Simulation of Realistic Synthetic Reflection Sequences. *Geophys. Pros.*, **41**, 313–321.

Walden, A. T., & Hosken, J. W. J. 1985. An Investigation of the Spectral Properties of Primary Reflection Coefficients. *Geophys. Pros.*, **33**, 400–435.

Walden, A. T., & Hosken, J. W. J. 1986. The Nature of Non-Gaussianity of Primary Reflection Coefficients and Its Significance for Deconvolution. *Geophys. Pros.*, **34**, 1038–1066.

Walden, A. T., & Hosken, J. W. J. 1988a. Tutorial: Choosing the Average Interval when Calculating Primary Reflection Coefficients from Well Logs. *Geophys. Pros.*, **36**, 799–824.

Walden, A. T., & Hosken, J. W. J. 1988b. Tutorial: Choosing the Averaging Interval

when Calculating Primary Reflection Coefficients from Well Logs. *Geophys. Pros.*, **36**, 799–824.

Walden, A. T., & Nunn, K. R. 1988. Correcting for Coloured Primary Reflectivity in Deconvolution. *Geophys. Pros.*, **36**, 282–297.

Wegler, U., & Lühr, B.-G. 2001. Scattering behaviour at Merapi volcano (Java) revealed from an active seismic experiment. *Geophys. J. Int.*, **145**(3), 579–592.

White, B., Sheng, P., Zhang, Z.Q., & Papanicolaou, G. 1987. Wave localization characteristics in time domain. *Phys. Rev. Lett.*, **59**, 1918–1921.

White, B., Sheng, P., & Nair, B. 1990. Localization and backscattering spectrum of seismic waves in stratified lithology. *Geophysics*, **55**(9), 1158–1165.

White, R. E. 1992. The accuracy of estimating Q from seismic data. *Geophysics*, **57**(11), 1508–1511.

Widmaier, M., Shapiro, S. A., & Hubral, P. 1994. Kirchhoff migration/inversion in thinly-layered media. *In: 56th Meeting, Expanded Abstracts*. EAEG. Paper H026.

Winkler, K., & Nur, A. 1979. Pore Fluid and Seismic Attenuation in Rocks. *Geophys. Res. Letters*, **6**, 1–4.

Wu, R. S., & Aki, K. 1988. Multiple scattering and energy transfer of seismic waves – separation of scattering effect from intrinsic attenuation II. Application of the theory to Hindu Kush Region. *Pure and Applied Geophysics*, **128**(1/2).

Zhang, C., & Ulrych, T. J. 2002. Estimation of quality factors from CMP records. *Geophysics*, **67**(5), 1542–1547.

APPENDIX A

WEAK-REFLECTIVITY APPROXIMATIONS TO THE REFLECTION/TRANSMISSION RESPONSE OF A LAYERED MEDIUM

In this appendix I give some useful weak-reflectivity approximations to the impulse response of a horizontally layered elastic medium for plane waves at normal incidence.

- *Transmission through a stack of layers (Figure A.1):*

Near the direct arrival time T , the transmission response p_0 is minimum-phase (Sherwood & Trorey, 1965; Treitel & Robinson, 1966), with an amplitude spectrum given by O'Doherty & Anstey (1971)'s formula

$$|p_0| = e^{-R^2(\omega)T}, \quad (\text{A.1})$$

where $R^2(\omega)$ is the reflectivity power spectrum, and T is in dimensionless units (normalized by the one-way traveltime thickness of an individual thin layer).

- *Reflector r below a stack of layers (Figure A.2):*

In a small window after the two-way traveltime to the reflector, the reflection impulse response p is

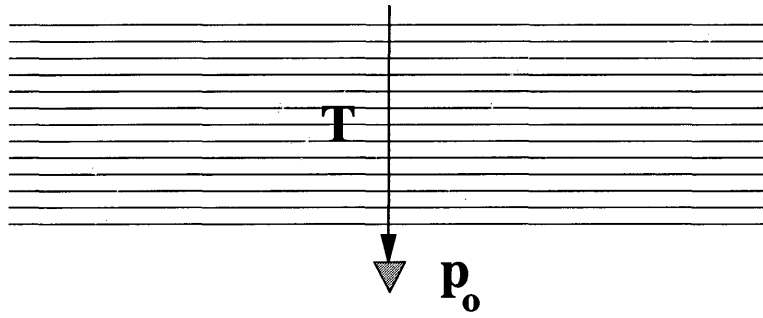


Figure A.1. Transmission through a stack of layers

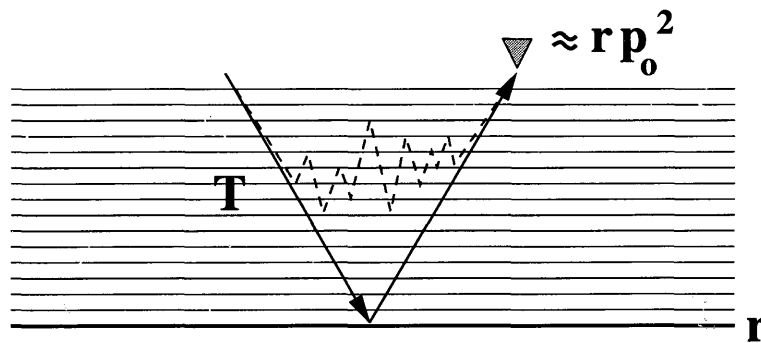


Figure A.2. Two-way transmission through a stack of layers: raypaths trapped in the shallow subsurface (dash-line) are ignored.

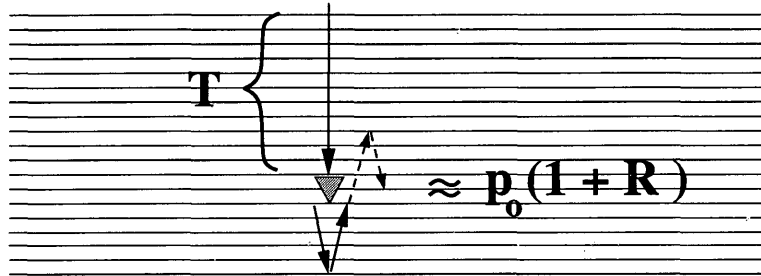


Figure A.3. Signal in a buried receiver shortly after the first arrival: direct arrival and primary reflections from below; multiples of the reflections from below (dash-line) are ignored, as well as changes in the downgoing pulse over the considered short time interval.

$$p \approx r p_0^2, \quad (\text{A.2})$$

where p_0 is the one-way transmission response already defined. Equation (A.2) is approximate because it assumes that most of the energy arriving at time $2T$ comes from the depth reached by the ballistic arrival in that time; i.e., contributions from raypaths trapped in the shallower regions are ignored (a reasonable assumption for weak reflectivity, but it worsens with time).

- *Buried receiver (Figure A.3):*

Near the time T of the direct arrival, the impulse response p in a buried receiver can be seen as a sum of the down-going pulse, filtered by the overburden, and its reflections from immediately below the receiver, i.e.,

$$p \approx p_0(1 + R(\omega)), \quad (\text{A.3})$$

This approximation ignores multiples of reflections from below the receiver as well as time changes in the downgoing pulse over the considered time window. It is consistent with the results of Banik *et al.* (1985) obtained through mean-field theory. Namely, their equations (17) and (25) state that

$$p = p_0 + \delta p, \quad (\text{A.4})$$

where p_0 is the same as above, and

$$\frac{\delta p}{p_0} = \sum_{l=-\infty}^n r_l + \sum_{l=n}^{\infty} r_l \exp [i \omega 2(l - n) \Delta T], \quad (\text{A.5})$$

where n is the index of the receiver layer and ΔT is the time-thickness of an individual layer. The first sum in eq. (A.5) is over the interfaces above the receiver and goes to zero because the reflectivity series is zero-mean. The second sum is over the reflection coefficients below the receiver, and is in fact, their Fourier transform. Therefore,

$$\frac{\delta p}{p_0} \approx R(\omega), \quad (\text{A.6})$$

which, combined with eq. (A.4) gives eq. (A.3).

- *Surface seismogram without surface-related multiples (earth model with an absorbing surface) (Figure A.4):*

In a small time window starting at time $2T$, the reflection impulse response

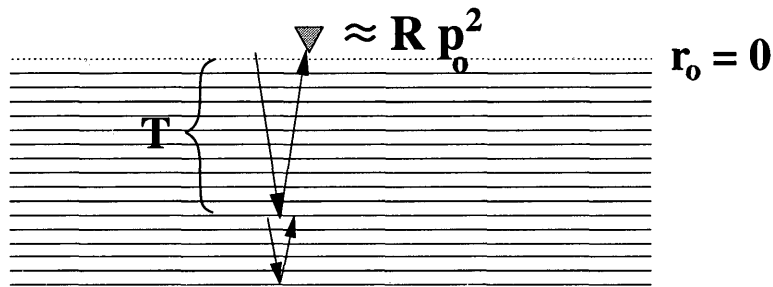


Figure A.4. Signal in a surface receiver (earth surface omitted)

can be modelled as a convolution between the reflection coefficient series at the depth reached in time T and the two-way transmission response of the overburden, i.e.,

$$p \approx R(\omega) p_0^2 \quad (\text{A.7})$$

This is an approximation as in the previous two cases; i.e., it ignores raypaths trapped in the overburden, as well as changes in the down-going pulse that generates the primary reflections over the considered (small) time window.

- *Surface seismogram with surface-related multiples (earth model with a free surface) (Figure A.5):*

In a small time window starting at time $2T$, the up-going impulse response has the form

$$p \approx R(\omega) p_0^2 \left[1 + R(\omega) + R^2(\omega) + \dots + R^{N(T)}(\omega) \right] \quad (\text{A.8})$$

The terms proportional to powers of $R(\omega)$ in the brackets account for surface-

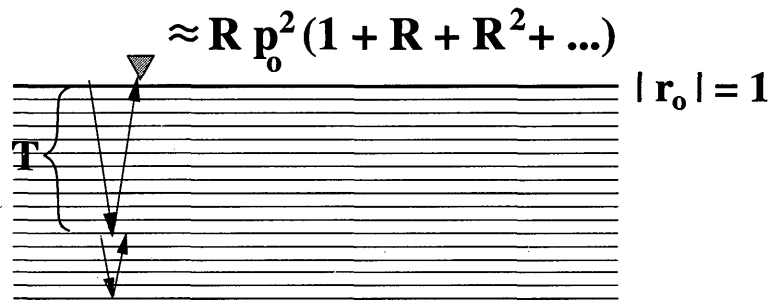


Figure A.5. Signal in a surface receiver (earth surface accounted for)

related multiples of different orders. For a discrete (layered) medium, the highest possible order N increases with time.

APPENDIX B

FROM PLANE WAVES AT NORMAL INCIDENCE TO POINT SOURCE AND OFFSET RECEIVERS

Through a rigorous mathematical derivation, Asch *et al.* (1991) obtained expressions for the spectrum of the reflection impulse response for a point source and offset receivers. Here I show that, when expressed in terms of χ (distance traveled in localization length units), their results are structurally identical to the plane-wave expressions given by White *et al.* (1990) (Chapter 2), multiplied by a geometrical spreading factor $1/4\pi(vt)^2$. This can be verified by a direct substitution in eqs. (2.2)-(2.4), or (2.5)-(2.6). Suppose the seismic source is an impulse vertical point force with a power spectrum

$$|S(f)|^2 = \frac{1}{4\pi v^2} \frac{1}{\xi^2}, \quad (\text{B.1})$$

where ξ is the acoustic impedance, defined by

$$\xi = \frac{\rho v}{\sin \theta} \quad (\text{B.2})$$

The division by ξ^2 appears in the power spectrum when one goes from a pressure field to a velocity field (all expressions and synthetic seismograms in Chapter 2 are for the velocity field). With such a source term, eq. (2.5) can be rewritten for a point source

and offset receivers as

$$P_1^*(t, f, \theta) = \frac{1}{4\pi(vt)^2} \frac{1}{4\pi v^2} \frac{1}{\xi^2} \frac{4v \sin \theta}{l(f, \theta)} \quad (\text{B.3})$$

$$= \frac{1}{(2\pi)^2} \frac{\sin \theta}{v(vt)^2 \xi^2 l(f, \theta)} \quad (\text{B.4})$$

where, in (B.3), the vertical distance traveled in localization length units [χ in eq. (2.5)] has been generalized to oblique propagation through eq. (2.7). Eq. (B.4) coincides with eq. 3.163 in Asch *et al.* (1991)¹. To simplify eq. (B.4) to (2.10), $l(f, \theta) \approx c_2 \sin^2 \theta / f^2$ (eq. 2.9) was assumed; such a low-frequency approximation is used in Asch *et al.* (1991), too.

In a similar manner eq. (2.6) can be rewritten for a point source and offset receivers as

$$P_0^*(t, f, \theta) = \frac{1}{4\pi(vt)^2} \frac{1}{4\pi v^2} \frac{1}{\xi^2} \frac{\frac{v \sin \theta}{l(f, \theta)}}{\left(1 + \frac{t v \sin \theta}{l(f, \theta)}\right)^2} \quad (\text{B.5})$$

This coincides with eq. 3.79 in Asch *et al.* (1991) for $r_0 = 0$, except for the lack of $1/\xi^2$ in their expression which is for pressure rather than velocity. Again, the

¹In Asch *et al.* (1991), $l(f, \theta)$ denotes localization *depth* (although they call it length) – it is a quantity, twice smaller than here. Thus, their equation has an extra 2 in the denominator. Also, in Asch *et al.* (1991), v is the background, or mean, velocity in the layered medium, while in White *et al.* (1990) it is the effective (low-frequency) velocity. However, since both studies assume a constant-density medium, these two velocities are equal (Shapiro *et al.*, 1994b).

low-frequency approximation of $l(f, \theta)$ (eq. 2.9) was used in simplifying eq. (B.5) to (2.11).

APPENDIX C

POWER SPECTRUM OF THE ELASTIC STRATIGRAPHIC FILTER

The operator R_m/R is a novelty for wavelet modeling and deconvolution, but in fact, its amplitude properties have been investigated in apparent attenuation studies. For example, Schoenberger & Levin (1974) computed synthetic seismograms with different orders of intrabed multiples (for a model without a free surface) and compared them to a seismogram containing only primary reflections. The primary reflection seismogram differs from the reflection coefficient series r only by transmission losses, which Schoenberger & Levin showed to be frequency-independent. Thus, the ratio between the amplitude spectra of synthetic seismograms with and without intrabed multiples is equivalent to $|R_m/R|$ up to a scaling factor. Schoenberger & Levin showed that the presence of intrabed multiples leads to apparent attenuation, i.e., that $|R_m/R|$ is high-frequency deficient. Strictly speaking, its decay with frequency is not linear on a semi-log scale. It tends to whiten, or level off, at high frequencies (Figure 6.3). This effect may or may not be seen in seismic data, depending on the frequency band of the signal, the length of the time window for spectral estimation, geology, presence of surface-related multiples, background noise, etc. Usually $|R_m/R|$ can be approximated by a straight line over the limited frequency band of a seismic source. In fact, should the whitening of $|R_m/R|$ at high frequencies is observable, it may be beneficial. It may allow us to separate absorption from scattering effects. The absorption can be evaluated from the slope of the trace spectrum over the band in which $|R_m/R|$ is approximately frequency-independent. One could either man-

ually divide the trace spectrum into two regions with different slopes and fit them separately for the effective and intrinsic Q , or attempt to fit a trace model of the kind

$$X(\omega) = \sigma_s W_s e^{-\frac{\omega t}{2q_i}} e^{-\frac{\omega t}{2q_a} H(\omega_c - \omega)} e^{-\frac{\omega_c t}{2q_a} H(\omega - \omega_c)} + \sigma_n W_n \quad (\text{C.1})$$

where $X(\omega)$ is the power spectrum of the trace, σ_s and σ_n are constants defining signal and noise levels, W_s accounts for source and receiver signatures, W_n for non-white background noise (Hart *et al.*, 2001), q_i is the quality factor corresponding to intrinsic absorption, q_a corresponds to apparent attenuation (short-period multiples), ω_c is the corner frequency above which R_m/R is white (or can be considered as such given the variability of the spectral estimate), and H is the Heaviside step-function. The attenuation at low frequencies ($\omega < \omega_c$) can be described by an effective quality factor given by

$$\frac{1}{q_{\text{eff}}} = \frac{1}{q_i} + \frac{1}{q_a}, \quad (\text{C.2})$$

while the attenuation at high frequencies ($\omega > \omega_c$) is caused, presumably, by intrinsic absorption and described by q_i .

APPENDIX D

GENERATING SYNTHETIC REFLECTIVITIES

A time-domain synthetic reflectivity $\{r_i\}$ can be modelled as an ARMA(1,1) process (Walden & Hosken, 1985) with an autoregressive parameter θ ($0 < \theta < 1$) and a moving average parameter ϕ ($0 < \phi < 1$, $\phi < \theta$), i.e.,

$$r_i = \phi r_{i-1} + a_i - \theta a_{i-1}, \quad (\text{D.1})$$

where $\{a_i\}$ is an independent and identically distributed (*iid*) innovation sequence. The larger the difference between θ and ϕ , the steeper with frequency (more blue) is the power spectrum of the reflectivity. These two parameters define the *correlation* between the samples in the time-domain reflectivity $\{r_i\}$.

The *amplitudes* of the reflection coefficients follow a mixture of two Laplace distributions with a mixing proportion parameter p ($0 \leq p \leq 1$ being the proportion of the first distribution) and scaling parameters λ_1 and λ_2 , respectively (Walden & Hosken, 1986). These three quantities define the variance σ_r^2 and the kurtosis K_r of the reflectivity series ($K_r > 6$, as found out by Walden & Hosken by analyzing well-logs from various locations).

To generate a time series $\{r_i\}$ with the desired correlation, variance, and kurtosis, the innovation sequence $\{a_i\}$ in eq. (D.1) is drawn from a mixed Laplace distribution with variance σ_a^2 and kurtosis K_a such that

$$\sigma_a^2 = \frac{1 - \phi^2}{1 + \theta^2 - 2\phi\theta} \sigma_r^2, \quad (\text{D.2})$$

$$K_a = \left[K_r - 6 \frac{(\phi - \theta)^2 (1 - \phi^4) + \phi^2 (\phi - \theta)^4}{[1 - \phi^2 + (\phi - \theta)^2]^2 (1 + \phi^2)} \right] \frac{[1 - \phi^2 + (\phi - \theta)^2]^2 (1 + \phi^2)}{[1 - \phi^4 + (\phi - \theta)^4] (1 - \phi^2)} \quad (\text{D.3})$$

The connection between the variance σ^2 and the kurtosis K of a Laplace mixture, and the distribution parameters p , λ_1 , λ_2 is

$$\sigma^2 = 2 \left(p \lambda_1^2 + (1 - p) \lambda_2^2 \right), \quad (\text{D.4})$$

$$K = 6 \frac{p \lambda_1^4 + (1 - p) \lambda_2^4}{p \lambda_1^2 + (1 - p) \lambda_2^2} \quad (\text{D.5})$$

Given the desired variance and kurtosis for the sequence $\{a_i\}$ [eqs. (D.2),(D.3)], the relationships (D.4)–(D.5) are insufficient to determine p_a , λ_{a1} , λ_{a2} (three unknowns). As an additional constraint, one may require that $\lambda_{r1}/\lambda_{r2} = \lambda_{a1}/\lambda_{a2}$. It has been observed that in most cases $\lambda_{r2} \approx 3\lambda_{r1}$ (Walden & Hosken, 1986). Even with this restriction, however, equations (D.4) and (D.5) have two plausible solutions for $\{p_a, \lambda_{a1}, \lambda_{a2}\}$ (because of the powers at which λ_1 and λ_2 appear in eqs. (D.4)–(D.5)). Typically, one of the solutions is close to the reflectivity parameters $\{p_r, \lambda_{r1}, \lambda_{r2}\}$; that is the solution I chose.

Once the parameters $\{p_a, \lambda_{a1}, \lambda_{a2}\}$ have been chosen, two *iid* sequences $\{a1_i\}$ and $\{a2_i\}$ are drawn from Laplace distributions with mean zero and scale parameters

λ_{a1} and λ_{a2} respectively. Also, a “flag” sequence $\{b_i\}$ is drawn from a Bernoulli distribution with mean p_a . When $b_i = 1$, $a_i = a1_i$; when $b_i = 0$, $a_i = a2_i$. Constructing such an innovation sequence $\{a_i\}$ is easily done, for example, in *Mathematica*.

Having $\{a_i\}$, θ and ϕ , we are almost ready to construct the reflectivity $\{r_i\}$ from eq. (D.1). We only need an initial value r_1 for the reflectivity. Walden (1993) proved that an almost immediate stationarity of the generated reflectivity is provided by the initial conditions:

$$r_1 = \sigma_r e_1 \tag{D.6}$$

and

$$a_1 = \frac{\sigma_a^2}{\sigma_r} e_1 + \sqrt{\sigma_a^2 - \frac{\sigma_a^4}{\sigma_r^2}} e_2, \tag{D.7}$$

where e_1 and e_2 are drawn from a mixed Laplace distribution with variance one and mean zero. As the innovations $\{a_i\}$ are independent, the first value a_1 can be simply set to (D.7).

Since the synthetic reflectivity $\{r_i\}$ was generated with a zero mean, a DC-component \bar{r} can eventually be added to it. The mean \bar{r} of a reflection coefficient log is usually very small (i.e., $\bar{r} \ll \sigma_r$).

The generated reflection coefficients should be checked for physical feasibility (occasionally $|r_i| \leq 1$ might be violated, especially when σ_r^2 is large). I clipped values with magnitude above 0.4.

APPENDIX E

CODES FOR 1-D SEISMOGRAMS GENERATION –

sugoupillaud, sugoupillaudpo

This appendix describes the codes for synthetic seismogram generation that were developed as part of this thesis. One of them, *sugoupillaud*, computes the full (all multiples included) 1D impulse response of a lossless horizontally layered medium. The other, *sugoupillaudpo*, computes only primary reflections. Both codes were included in the Seismic Unix (SU) free software package (Cohen & Stockwell, 2002). The basics of the two codes are given below. For further details see the code self-documentation.

- *Earth model*

The earth is modelled as a non-absorbing Goupillaud-type layered medium, i.e., as a stack of horizontal layers of equal time-thickness. Below the layers is a homogeneous half-space.

Such a medium is fully described by a set of reflection coefficients, r_0, r_1, \dots, r_n , where r_0 refers to the earth surface, and r_i - to the i -th subsurface interface.

Thick layers can be simulated by setting some coefficients $r_i = 0$.

Reflection coefficient series can be extracted from sonic and density logs as shown by Walden & Hosken (1988a).

- *Input*

The input consists of one or more reflection coefficient series in a SU format, i.e.,

binary floats with a SU header. The sampling interval specified in the header is interpreted by the code as two-way travelttime thickness of the layers.

- *Wavefield*

Normal incidence of plane waves is assumed. The wavefield can be either of a vector type, e.g., displacement/velocity/acceleration, or a scalar, e.g., pressure.

- *Source*

The source is a unit spike at time zero. It can be placed at any depth (at the top of any layer). A surface source (at the top of the first layer, just below the earth surface) produces a downgoing spike of amplitude 1 both for vector and scalar fields. In contrast, a buried source acts differently for vector and scalar fields and produces two spikes – downgoing and upgoing. For vector fields, the downgoing spike is of amplitude 1 while the upgoing spike is of amplitude -1. For scalar fields both spikes are of amplitude 1.

- *Receiver*

The receiver can be placed at any depth (at the top of any layer).

- *Output from sugoupillaud*

The output from *sugoupillaud* is the time-domain 1D impulse response, including all possible multiples. The sampling interval of the output is equal to that of the input reflectivity series (two-way travelttime thickness of the layers).

The computations are performed through z-transforms. Useful references are: Treitel & Robinson (1966); Robinson (1983), Chapters 3 and 1; Claerbout (1985), Chapter 8; and Ganley (1981).

- *Output from sugoupillaudpo*

The output from *sugoupillaudpo* is the time-domain 1D impulse response, including only primary reflections from interfaces both below and above the source and the receiver.

APPENDIX F

REFLECTIVITY LOG FOR MODELING THE SCATTERING EFFECTS

In Chapter 4, I assessed the share of scattering in the spectral ratio slopes extracted from the real VSP from synthetic seismograms. To compute them, a non-absorbing Goupillaud model was used, i.e., an earth model, consisting of perfectly elastic horizontal layers of equal time thickness. The reflection coefficient (RC) series defining such a model is computed from sonic and density logs. After converting it to the time domain and interpolating to the nearest uniform time-grid, one may anti-alias filter and resample to the VSP rate (e.g., 2 ms two-way time). I did not resample because the computation of the synthetic seismograms from the full reflectivity log was fast enough; later, I used only the low-frequency part of the synthetic spectra to evaluate scattering.

The well logs span only the 600-3500 m interval. To fill in the missing reflectivity of the upper 600 m, I assumed that the top sequence present in the reflectivity log (600-1000 m) extends up to the surface. I combined its amplitude spectrum with a random phase spectrum, drawn from a uniform distribution $U[-\pi, \pi]$, and inverse-Fourier transformed to the time domain to create a synthetic RC with which to append the real log. The magnitudes of the synthetic reflection coefficients do not follow a mixed Laplace distribution as the real ones do (Walden & Hosken, 1986). However, this does not matter in the apparent attenuation estimation which, in my experience, depends mainly on the power spectrum of the RC series.

In the same manner the reflectivity log was extended below the borehole bottom using the power spectrum of the reflection coefficient log in Layer 4 (3100-3500 m). This was needed because the deepest VSP receivers feel the medium below the borehole; to predict the scattering effects in them, we need a model of the reflectivity below the borehole.

Finally, the near-surface sandstone layer was added by putting a reflection coefficient of -0.45 at 15 ms one-way traveltime below the earth surface. The time thickness of the sandstone was determined from notches in the spectra of the VSP traces. The choice of the reflection coefficient magnitude was a bit arbitrary. The main consideration was that it should be large compared to the other coefficients in order to create such strong notches. An additional requirement was that it be consistent with the VSP and well-log data. Continuing the sonic log trend up to the sandstone base suggests a sub-sandstone velocity of roughly 3400 m/s. Then, a reflection coefficient of -0.45 can be explained by a 20 m thick sandstone with velocity 1300 m/s, which is a plausible model. Tests with slightly different values led to virtually identical estimates of S_{sc} . Similarly, the synthetic spectral ratios are not sensitive to the earth's surface reflection coefficient. For a free surface, it is appropriately set to -1 (as seen from above by the displacement field). However, given that the thin sandstone layer is expected to have a very low quality factor, it may be more appropriate to model the earth as bounded by a semi-absorbing surface with a smaller reflection coefficient. In general, it is important to account for the earth's surface in apparent attenuation studies (Chapter 2). However, the spectral ratios between *early* windows on VSP traces are an exception in that they are not sensitive to the properties of the near surface (Chapter 3).

APPENDIX G

COVARIANCE OF SLOPE ESTIMATES FROM PAIRS WITH A COMMON RECEIVER

Suppose two spectral ratios, y_1, y_2 , are based on a common receiver, i.e.,

$$y_1(f) = \frac{1}{\Delta t_1} [P_1(f) - P(f)] \tag{G.1}$$

$$y_2(f) = \frac{1}{\Delta t_2} [P_2(f) - P(f)]$$

where P, P_1 and P_2 are log-amplitude spectra, measured at frequencies f_1, \dots, f_n , and $\Delta t_{1,2}$ is the time-separation in the corresponding receiver pair. The covariance between the two spectral ratios caused by the common receiver is

$$\text{Cov}(y_1, y_2) = \frac{1}{\Delta t_1 \Delta t_2} \text{Var} [P(f)] \tag{G.2}$$

Suppose that the amplitude spectra of all traces have equally large uncertainties. Then, as seen from (G.1), the variability of the common receiver spectrum can be estimated, for example, by

$$\text{Var} [P(f)] = \text{median}_i \frac{\sigma_{y_i}^2 (\Delta t_i)^2}{2}, \tag{G.3}$$

where the median is taken over all ratios containing the spectrum $P(f)$, and $\sigma_{y_i}^2$ is the variance of the residuals of the best linear fit of spectral ratio y_i [i.e., $\sigma_{y_i}^2 \approx \text{Var}(y_i)$].

The correlation between the spectral ratios caused by the common receiver propagates in the fitted slopes s_i of $y_i(f)$. As is known from statistical analysis (e.g., Johnson & Wichern, 2002),

$$\text{Cov}(s_1, s_2) \approx \frac{\text{Cov}(y_1, y_2)}{n \sigma_f^2} \quad (\text{G.4})$$

where σ_f is the standard deviation of the frequencies over which the spectral ratios were fit. Eq. (G.4) is strictly valid for data with Gaussian noise, while the fitting residuals seems to have a distribution that is sharper than a Gaussian; hence the approximate sign.

Substituting (G.2) in (G.3), and (G.3) in (G.4), we get

$$\text{Cov}(s_1, s_2) \approx \frac{1}{2n \sigma_f^2} \frac{\text{median}(\sigma_{y_i}^2 (\Delta t_i)^2)}{\Delta t_1 \Delta t_2} \quad (\text{G.5})$$

This equation is applied separately to the real and synthetic VSP to get the off-diagonal elements of the covariance matrix needed when averaging slopes within a macro-layer (Chapter 4).